NASA Technical Paper 1362

The NASA-Ames Research Center Stratospheric Aerosol Model

I. Physical Processes and Computational Analogs

R. P. Turco, P. Hamill, O. B. Toon,
R. C. Whitten, and C. S. Kiang

APRIL 1979

NASA

NASA Technical Paper 1362

The NASA-Ames Research Center Stratospheric Aerosol Model

I. Physical Processes and Computational Analogs

R. P. Turco
R and D Associates
Marina del Rey, California

P. Hamill, O. B. Toon, R. C. Whitten
Ames Research Center
Moffett Field, California

C. S. Kiang
National Center for Atmospheric Research
Boulder, Colorado

National Aeronautics
and Space Administration

**Scientific and Technical
Information Office**

1979

BLanK
Page

SYMBOLS[1]

D, $D(z)$	eddy diffusion coefficient, $cm^2\ sec^{-1}$
f, $f(r,z,t)$	average core volume fraction of the aerosol droplets $n(r,z,t)$
g_{ik}^{ℓ}	droplet growth rate, $\mu m\ sec^{-1}$
g_H	droplet growth rate due to water vapor equilibrium, $\mu m\ sec^{-1}$
g_{oa}	droplet growth "kernel" for H_2SO_4-H_2O condensation, $\mu m\ cm^3\ sec^{-1}\ molecule^{-1}$
h	altitude grid spacing, 2×10^5 cm
i,j	discrete analog of particle size
k	discrete analog of altitude
$K(r,r')$	coagulation kernel for particles of radii r and r', $cm^3\ particle^{-1}\ sec^{-1}$
Kn	Knudsen number
K_{ijk}	coagulation kernel for particles of sizes i and j at altitude level k, $cm^3\ particle^{-1}\ sec^{-1}$
ℓ	discrete analog of time
L_a	sulfuric acid vapor loss rate due to condensation on particles, sec^{-1}
m_ν	molecular mass of species ν, g
M_ν	molecular weight of species ν, amu
n, $n(r)$, $n(r,z)$, $n(r,z,t)$	aerosol droplet size distribution, particles $cm^{-3}\ \mu m^{-1}$
$n_{B\nu}$	boundary concentration for species ν, molecules cm^{-3}
n_i, n_{ik}, n_{ik}^{ℓ}	concentration of aerosol droplets of size i, particles cm^{-3}

[1] In the text some units have been modified for consistency in certain expressions.

n_M	total concentration of air molecules, molecules cm^{-3}
n_ν	concentration of the gaseous species ν, molecules cm^{-3} (ν = a for H_2SO_4, ν = H for H_2O)
n_ν^o	equilibrium vapor concentration (vapor pressure) of species ν over an aerosol droplet, molecules cm^{-3}
$\hat{n}$, $\hat{n}(r)$, $\hat{n}(r,z)$, $\hat{n}(r,z,t)$	condensation nuclei size distribution, particles cm^{-3} μm^{-1}
$\hat{n}_i$, $\hat{n}_{ik}$, $\hat{n}_{ik}^{\ell}$	concentration of condensation nuclei of size i, particles cm^{-3}
$\mathcal{N}_A$	Avogadro's number (6.02×10^{23} molecules $mole^{-1}$)
$\hat{P}$	condensation nuclei production rate from evaporating droplets, particles cm^{-3} μm^{-1} sec^{-1}
P_a	sulfuric acid vapor production rate, molecules cm^{-3} sec^{-1}
r, r_i	particle radius, μm
R_N	heterogeneous heteromolecular nucleation rate, sec^{-1}
R_W	aerosol droplet rainout rate, sec^{-1}
t	time, sec
T	air temperature, K
u, u(r,z,t)	total core volume of the droplets n(r,z,t), μm^3 cm^{-3} μm^{-1}
u_i, u_{ik}^{ℓ}	total core volume of the droplets n_{ik}^{ℓ}, μm^3 cm^{-3}
v_B	boundary recombination velocity, cm sec^{-1}
v_S, $v_S(r,z)$	particle gravitational sedimentation velocity, cm sec^{-1}
V, V_i	particle volume, μm^3
γ_k^{ℓ}	total particle volume per unit volume of air at height k and time ℓ, μm^3 cm^{-3}
W	weight fraction of sulfuric acid in aqueous solution
z	altitude, cm
α	sticking coefficient for H_2SO_4 molecules on aerosol droplets

γ, $\gamma(z)$	atmospheric stratification factor
ε, $\varepsilon(r,z,t)$	total core volume second moment of the droplets $n(r,z,t)$, $\mu m^6\ cm^{-3}\ \mu m^{-1}$
ε_i, ε_{ik}^{ℓ}	total core volume second moment of the droplets n_{ik}^{ℓ}, $\mu m^6\ cm^{-3}$
$\eta(v,w,t)$	size distribution of droplets according to their volume, v, and their core volume w, particles $cm^{-3}\ \mu m^{-6}$
θ_{ij}	double counting factor for coagulation terms (θ = 1, $i \neq j$; 1/2, $i = j$)
μ, $\mu(r,z)$	aerosol stratification factor
ρ	aqueous sulfuric acid solution density, g cm^{-3}
ρ_c	aerosol droplet core density, g cm^{-3}
$\bar{\rho}$	average aerosol particle density, g cm^{-3}
τ	numerical time step, sec
τ_o	characteristic coagulation time, sec
τ_{ik}^{ℓ}	growth time of droplets from size i to size i + 1, sec
$\tau_{ik}^{H\ell}$	water vapor growth time for droplets from size i to size i + 1, sec
ϕ_D	vertical particle diffusion flux, particles $cm^{-2}\ \mu m^{-1}\ sec^{-1}$
ϕ_S	vertical particle sedimentation flux, particles $cm^{-2}\ \mu m^{-1}\ sec^{-1}$
ϕ_{SD}	total vertical particle flux due to sedimentation and diffusion, particles $cm^{-2}\ \mu m^{-1}\ sec^{-1}$
ϕ_{SD}^{u}	vertical droplet core volume flux, $\mu m^3\ cm^{-2}\ \mu m^{-1}\ sec^{-1}$
$\phi_{i,k}^{SD}$	vertical flux of particles of size i at altitude k, particles $cm^{-2}\ sec^{-1}$

THE NASA-AMES RESEARCH CENTER STRATOSPHERIC AEROSOL MODEL

I. PHYSICAL PROCESSES AND COMPUTATIONAL ANALOGS

R. P. Turco
R and D Associates

O. B. Toon
Ames Research Center

P. Hamill*
Ames Research Center

R. C. Whitten
Ames Research Center

C. S. Kiang†
National Center for Atmospheric Research

SUMMARY

A time-dependent one-dimensional model of the stratospheric sulfate aerosol layer is presented. In constructing the model, a wide range of basic physical and chemical processes are incorporated in order to avoid predetermining or biasing the model predictions. The simulation, which extends from the surface to an altitude of 58 km, includes the troposphere as a source of gases and condensation nuclei and as a sink for aerosol droplets. The size distribution of aerosol particles is resolved into 25 categories with particle radii increasing geometrically from 0.01 to 2.56 μm such that particle volume doubles between categories. In the model, sulfur gases reaching the stratosphere are oxidized by a series of photochemical reactions into sulfuric acid vapor. At certain heights this results in a supersaturated H_2SO_4-H_2O gas mixture with the consequent deposition of aqueous sulfuric acid solution on the surfaces of condensation nuclei. The newly formed solution droplets grow by heteromolecular heterogeneous condensation of acid and water vapors; the droplets also undergo Brownian coagulation, settle under the influence of gravity, and diffuse in the vertical direction. Below the tropopause, particles are washed from the air by rainfall. A set of continuity equations is derived which describes the temporal and spatial variations of aerosol droplets and condensation nuclei concentrations in air as well as the sizes of cores in droplets; numerical techniques to solve these equations accurately and efficiently are also developed. Calculations illustrate the behavior and precision of the computer algorithms. The model correctly predicts many of the observed properties of the sulfate layer, including its height, density, composition, and particle size spectra.

INTRODUCTION

The stratospheric sulfate layer is a highly dispersed aerosol of sulfuric acid-water solution droplets which is usually found between altitudes of 15 and 30 km. The layer was discovered by Junge and his coworkers nearly two decades ago (ref. 1) and since then has been a subject of considerable interest to climatologists and atmospheric scientists. This interest has been stimulated by recent suggestions that the aerosol may exert an important

*Now at Systems and Applied Sciences Corporation, Hampton, Virginia 23666.
†Now at Georgia Institute of Technology, Atlanta, Georgia 30332.

influence on the climate of Earth (refs. 2-4) as well as being responsible for brilliant sunsets and some rather unusual optical phenomena (ref. 5). Additionally, there is concern that anthropogenic perturbations of the layer due to increased sulfur loading of the stratosphere or the injection of particulate matter at high altitudes could possibly affect the climate or catalyze heterogeneous chemical interactions that affect global ozone abundances (ref. 6). As a consequence, there has been a fairly concerted effort to study the layer, both experimentally and theoretically, and to develop analytical tools to evaluate the effect of perturbations on the layer. In this paper we describe a time-dependent one-dimensional model that accurately simulates many of the observed properties of the stratospheric aerosol layer and may be useful as a predictive device.

Because of the large number of observational studies that have been carried out since its discovery, the characteristics of the sulfate layer are relatively well-defined. Many investigators have used balloon-borne diffusion chambers (refs. 1 and 7) and optical particle counters (refs. 8-11) to analyze the aerosol particles. Other experiments have utilized high-flying aircraft equipped with wire impactors or filters to collect particle samples (refs. 12-15). Sunlight scattered by the layer has been detected from satellites (ref. 16) and the layer has been extensively probed with laser light using lidar techniques (refs. 17 and 18). The results of these experiments have led to a quite comprehensive and consistent picture of the aerosol layer.

In the sulfate layer, the height of the maximum in the number mixing ratio of large aerosol particles (radii greater than about 0.15 μm) usually lies between 20 and 25 km and appears to be closely related to the altitude of the tropopause (ref. 8). The aerosol mass mixing ratio is also peaked between 20 and 25 km in the stratosphere. The sulfate layer exhibits seasonal, latitudinal, and short-time scale variability and can be greatly enhanced following major volcanic activity (ref. 19). Aerosol particle size distributions fall off rapidly for particle radii greater than 0.1 μm, and the ratio of the concentrations of particles with radii greater than 0.15 μm to those greater than 0.25 μm is about three to five in the layer. Unlike the mixing ratio of large particles, the number mixing ratio of total particles falls off rapidly above the tropopause.

A model of the stratospheric sulfate aerosol should reproduce the general characteristics of the aerosol layer indicated above. In the past, aerosol models have, for the most part, been developed to investigate specific aerosol properties. Junge et al. (ref. 1) first used a one-dimensional diffusion model with particle sedimentation and coagulation to explain the observed rapid decrease of the total aerosol particle mixing ratio above the tropopause. Friedlander (ref. 20) formulated a detailed model of particle coagulation and applied it to the prediction of stratospheric aerosol size distributions. Later, Martell (ref. 21) utilized a model similar to Junge's to study the transport and coagulation of Aitken (small) particles in the lower atmosphere.

Over the past decade, a large number of aerosol models dealing principally with aerosol transport has been published. For example, Hunten

(ref. 22) used a one-dimensional diffusion-sedimentation model for a monodispersed aerosol to estimate the residence times of particles in the stratosphere. Hoffmann et al. (ref. 23) employed a similar model, but for several different particle sizes, to calculate the stratospheric accumulation of aluminum oxide particles emitted by Space Shuttle booster engines. Cadle et al. (refs. 24 and 25) investigated the global dispersion of aerosol particles following volcanic activity using a two-dimensional model with particle sedimentation and parameterized meridional transport.

Some recent aerosol models have treated aerosol physics in more detail. Kritz (ref. 26) presented a novel and detailed treatment of aerosol growth and coagulation and investigated the development of stratospheric particle size distributions by these processes. Burgmeier and Blifford (ref. 27) constructed a "box" model for the stratospheric aerosol, which includes particle coagulation and growth (by absorption of sulfur dioxide molecules). They used their model to study aerosol "aging" — that is, the short-time evolution of different initial particle size distributions. Rosen and Hofmann (refs. 28 and 29) extended their earlier work (ref. 23) to account for particle coagulation and growth, and they reestimated the effect of Space Shuttle operations on the stratospheric aerosol layer.

Photochemical theories involving atmospheric sulfur constituents have developed in parallel with the physical aerosol models. Junge et al. (ref. 1) first suggested that the large aerosol particles observed in the stratosphere might be formed by the condensation and reaction of vaporous sulfur compounds. Subsequently, Scott et al. (ref. 30) and Friend et al. (ref. 31), among others, introduced chemical reaction mechanisms by which sulfur dioxide molecules absorbed by aerosol droplets could be oxidized into sulfate. Other workers have proposed gas phase reaction sequences that can convert sulfur oxides into sulfuric acid vapor (e.g., refs. 15, 32, and 33) which readily condenses on aerosol particles (e.g., ref. 34). Using one-dimensional transport models, Harrison and Larson (ref. 35), Harker (ref. 36), and Crutzen (ref. 33) have all studied atmospheric gas phase sulfur chemistry and have found that sulfate can be produced in the lower stratosphere at a rate fast enough to maintain the observed aerosol layer.

In the remainder of this report, we construct a new time-dependent one-dimensional model of the stratospheric sulfate layer. In our model, we have attempted to combine all of the important features of aerosol physics and sulfur photochemistry found in earlier models. In addition, we have adopted the most recent theories for the nucleation and growth of aerosol droplets as well as some newer measurements of the abundances and reactivities of sulfur compounds in air. We have also introduced a treatment of aerosol cores that describes their accumulation and evolution in stratospheric solution droplets; the analysis of core size and composition can be a valuable theoretical and diagnostic tool for understanding the aerosol layer. Our model is a comprehensive, interactive gas-particle simulation of the stratospheric aerosol.

In the second section of this paper, Physical Chemistry of Atmospheric Sulfur, we consider the sources and sinks of atmospheric sulfur compounds, their photochemical interactions in air, and the relation of gaseous sulfur

chemistry to the formation of sulfuric acid solution droplets. The physical aerosol processes that are incorporated into our model are discussed in the third section, Physical Aerosol Processes, and some related parameter values are tabulated in appendix A. The continuity equations for aerosol particles and condensation nuclei and for the cores within the aerosol droplets are derived in the fourth section, The Aerosol Continuity Equation, and in appendix B. Our treatment of coagulation and of particle growth by condensation is also outlined in the third and fourth sections and in appendix B. In the fifth section, A Numerical Representation of the Aerosol Continuity Equations, and appendix C, we establish the finite difference equations in one (vertical) direction and solve them to obtain time-dependent aerosol particle distributions. In the sixth section, Model Validations and Simulations, we present the results of model validation tests and briefly compare our model predictions of aerosol properties with stratospheric observations. Tables 2-4 summarize most of the important sources of uncertainty (chemical, physical, and numerical) for our model calculations. Finally, conclusions about the potential applications of our aerosol model are given in the seventh section.

In a companion publication (ref. 37) hereafter referred to as NASA TP-1363, we make a more detailed comparison of our model predictions with aerosol observational data. In NASA TP-1363, we also present a comprehensive sensitivity analysis showing areas where our aerosol model is most uncertain and suggest new observations that might help to resolve important questions about the origin of the stratospheric aerosol layer.

PHYSICAL CHEMISTRY OF ATMOSPHERIC SULFUR

Gaseous sulfur compounds have an important role in the formation and maintenance of the stratospheric aerosol layer. One goal of our aerosol model is to investigate the interactions of sulfur gases with aerosol particles. Accordingly, we need to determine the abundances and distributions of volatile sulfur constituents in the environment. In this section we discuss the known sources, sinks, and concentrations of atmospheric sulfur-bearing molecules and outline the stratospheric photochemistry applicable to these species. The aeronomical model, which we use to compute the concentrations of sulfur compounds in air, is also described. Finally, we present and discuss typical vertical distributions of the sulfur constituents as predicted by our model.

Sulfur Compounds in the Atmosphere

Sulfur gases can be introduced into the atmosphere in several different forms by a host of sources. For example, industry releases copious amounts of sulfur dioxide (SO_2), and smaller amounts of hydrogen sulfide (H_2S), carbon disulfide (CS_2), and carbonyl sulfide (OCS) into the environment (refs. 38-40). Sulfur oxides, including sulfuric acid vapor, can be generated in automotive engine exhaust systems. Hydrogen sulfide is a by-product of the decay of vegetable matter (ref. 41). Dimethyl sulfide, $(CH_3)_2S$, may be produced in the Earth's oceans (refs. 42 and 43), and carbon disulfide has been

found dissolved there (ref. 44). Volcanic eruptions also inject sulfurous compounds into the air (e.g., ref. 45). These and a few other natural and anthropogenic sources probably account for most of the sulfur input to the atmosphere (ref. 41).

Sulfur dioxide and hydrogen sulfide molecules can react in air with O, O_2, O_3, and OH (ref. 46), leading to H_2SO_4 and other stable sulfates (ref. 47). At low altitudes, water soluble gases like SO_2, H_2S, and H_2SO_4 can be washed out of the atmosphere by rainfall (refs. 48 and 49); SO_2 and H_2S absorbed in hydrometeors can react in solution with dissolved O_2 and O_3 as well as with other substances to form soluble and insoluble sulfated compounds (refs. 38, 47, and 50). Near the ground, sulfur gases can be removed on plant and mineral surfaces or be dissolved in the seas (refs. 41 and 47). The sulfur compounds containing H-C bonds are probably attached by hydroxyl radicals in the troposphere, eventually forming soluble sulfur oxides.

Sulfur dioxide and hydrogen sulfide gases have been detected at low altitudes, but they exhibit a wide range of concentrations with sea-level values usually less than a few parts per billion by volume (ppbv) and often very much less (refs. 41, 47, 51, and 52); and the effects of meteorology, urban pollution, and gas analysis techniques on these measured concentrations are unknown, however.

Based on sulfur mass balance calculations, the tropospheric residence time for SO_2 has been estimated to be only a few days (refs. 41 and 53). Hydrogen sulfide, because of its extreme reactivity, is estimated to have an atmospheric lifetime much less than a day (refs. 47 and 54). Likewise, sulfuric acid vapor and dimethyl sulfide are also expected to have very short low altitude residence times. Nevertheless, Jaeschke et al. (ref. 55) have observed about 0.05 ppbv of SO_2 in the upper troposphere and lower stratosphere. The altitude-dependence of the tropospheric SO_2 mixing ratio observed in reference 55 appears to be consistent with the estimates by Friend (ref. 41) and Levy (ref. 53) of the tropospheric lifetime of SO_2.

Carbonyl sulfide has been measured near the ground over a wide geographical range. Hanst et al. (ref. 56) found about 0.2-0.3 ppbv of OCS in air; A. Bandy (private communication, 1977) detected about 0.47 ± 0.05 ppbv; and Sandalls and Penkett (ref. 57) observed about 0.51 ± 0.05 ppbv. Disregarding the Hanst measurement, which has a large experimental uncertainty associated with it, OCS appears to have a very uniform concentration of about 0.5 ppbv throughout the lower troposphere (according to the authors of ref. 57, a large fraction of their reported OCS variability may actually have resulted from their gas analysis procedure). Unlike most other sulfur gases, OCS is expected to have a long tropospheric lifetime, possibly a year or more.

Carbon disulfide is a less inert chemical than OCS, but it may still have some aeronomical significance because of its possible oxidation to OCS (ref. 58). Sandalls and Penkett (ref. 57) measured an average CS_2 concentration of about 0.10 ppbv near the surface, with a very large variability (±50%).

By contrast with observations in the lower troposphere, indications are that, except for OCS and SO_2, sulfur molecule concentrations in the upper troposphere are very low (refs. 55 and 59).

Because of the apparent instability of most of the dominant sulfur compounds in air, and the corresponding failure to detect large amounts of them at high altitudes, it seems that only a small fraction of the total quantity of these substances which are emitted at the ground actually reach the stratosphere and thus influence the aerosol layer. Accordingly, in the present model, we consider only SO_2 and OCS as gaseous sources of sulfur for aerosol particles.

To simulate the small percentage of the surface emission of SO_2 that is transported to the lower stratosphere, we have adjusted its ground mixing ratio to about 0.6 ppbv and allowed the SO_2 molecules to diffuse upward through the tropopause. After depletion by rainout and chemical oxidation, the SO_2 abundance near the tropopause is about 0.05 ppbv, in agreement with the high-altitude measurement of reference 55. There are several mechanisms by which sulfur dioxide may be directly injected into the stratosphere, including deposition by aircraft engines and volcanic eruptions (ref. 45). However, for the purpose of establishing the ambient properties of the aerosol layer, we have not included sulfur gas injection in our present calculations.

As we have already mentioned, OCS originates in biological, volcanic, and industrial processes (refs. 40 and 60) and is transported upward into the stratosphere, much like the halocarbons $CFCl_3$ and CF_2Cl_2 (ref. 61), where it can be photochemically transformed into SO_2 in situ (ref. 33). To determine the quantity of sulfur dioxide that is generated by OCS photolysis, we have adopted a tropospheric OCS concentration of 0.47 ppbv and the OCS transport and photolysis rates to be discussed shortly.

The total weight of sulfate leaving the stratosphere in aerosol has been estimated by Lazrus and Gandrud (ref. 14) to be equivalent to 1.2×10^5 metric tons of SO_2 per year and by Hofmann et al. (ref. 8) to be about 2.5 times greater (1×10^5 metric tons of SO_2 annually is equal to about 6.5×10^6 SO_2 molecules per square centimeter column per second, globally averaged). The mass of SO_2 that diffuses into the stratosphere through the tropopause in our model is almost 2×10^5 metric tons yearly for our assumed SO_2 concentrations and vertical diffusion coefficients (which will be discussed later in this section). However, most of this SO_2 is converted into particle sulfate just above the tropopause level and is removed rapidly from the stratosphere as particulate matter. At a distance a few kilometers above the tropopause, the upward diffusive flux of tropospheric sulfur dioxide is greatly reduced, and the downward flux of aerosol sulfate is due primarily to OCS decomposition at higher altitudes (equivalent to about 9×10^4 metric tons of SO_2 per year).

The Photochemistry of Sulfur Compounds

Sulfur dioxide, carbonyl sulfide, and other sulfur gases that reach the stratosphere can be photochemically oxidized into sulfuric acid vapor.

Table 1 presents a set of photochemical reactions by which OCS molecules are transformed into H_2SO_4 molecules; these are the sulfur reactions used in our model.

Since OCS is a very stable compound, its aeronomy is quite limited. In fact, besides its source at the ground, only photolysis and transport are thought to influence its distribution in the upper atmosphere (ref. 33). The OCS photoabsorption coefficients have been measured (refs. 70 and 71). The observed absorption spectrum, illustrated in figure 1, when combined with the solar fluxes of Ackerman (ref. 76), leads to the daily averaged OCS photodissociation rates given in table 1.

According to reference 77, the OCS ultraviolet photolytic process is

$$OCS + h\nu \rightarrow S + CO \qquad (1)$$

where the sulfur atom can be electronically excited. We do not distinguish between the different states of the product sulfur atom here since its degree of excitation does not affect our results.

Carbonyl sulfide reacts very slowly with oxygen atoms in the atmosphere (see reaction R10 in table 1). In our model, less than 10% of the OCS reaching the stratosphere is decomposed by this reaction. The reaction of OCS with excited oxygen atoms, $O(^1D)$, is even less important; although the rate coefficient is probably large ($\sim 10^{-10}$ cm^3 sec^{-1}), $O(^1D)$ concentrations are extremely small in the stratosphere (<100 atoms cm^{-3}). The reaction of OCS with OH is, likewise, negligible; in a recent experiment (ref. 78), an upper limit of 7×10^{-15} cm^3 sec^{-1} was placed on the room temperature rate constant. We have not considered other possible (tropospheric) loss processes for OCS in this study because our aim here is simply to determine the stratospheric distribution of OCS when its tropospheric mixing fraction is known.

Carbon disulfide will be decomposed in the atmosphere by processes analogous to, but much faster than, those for OCS (e.g., ref. 40). Tropospheric CS_2 concentrations are lower and more uncertain than those of OCS. Moreover, the fraction of CS_2 reaching the stratosphere is probably much less than that of OCS. Accordingly, in this report we have omitted CS_2 as an active stratospheric sulfur constituent, recognizing that its role in forming the sulfate aerosol layer may need to be evaluated later.

The sulfur atoms generated during OCS photodecomposition react rapidly with molecular oxygen to form SO. Sulfur monoxide is, in turn, rapidly oxidized into SO_2. There are three reactions (R5, R6, and R7) that further oxidize SO_2, and each has been proposed at one time or another as an important mechanism leading to stratospheric H_2SO_4 production. Except for reaction (R7) these processes are all quite slow, having time constants ranging from months to years; the rate of SO_2 oxidation by reaction (R7) is dominant by at least one order of magnitude throughout the lower stratosphere.

The sulfur radical HSO_3 formed by reaction (R7) can react with O_2 to produce HSO_5, which can react in turn with nitrogen oxides to yield compounds such as $HOSO_2ONO$ and $HOSO_2ONO_2$ (ref. 79). Because the photochemistry of these

latter species is not well known, we have not been able to include them in our model. However, it is interesting to note that Farlow et al. (ref. 80) have recently detected small amounts of similar nitrogen-bearing sulfate compounds in stratospheric aerosol samples.

As a radical in air, HSO_3 is likely to be quickly transformed into a more stable H_2SO_4 molecular configuration. Therefore, it is reasonable to assume that the sequence of reactions leading from HSO_3 to H_2SO_4 does not limit the overall rate of conversion of SO_2 into sulfuric acid vapor. We have proposed reaction (R8) — which may actually occur in the atmosphere, although at a slower rate than the direct oxidation of HSO_3 by O_2 — followed by reaction (R9) as a substitute for a more complex HSO_3-to-H_2SO_4 reaction sequence (also see ref. 81). In fact, detailed reaction schemes have been suggested; some result in H_2SO_4 formation and some do not, but none of them is supported by rate constant data (refs. 32 and 82). Graedel (ref. 83) has considered several HSO_x radicals in an analysis of the role of sulfur oxides in photochemical smog and has roughly estimated rate constants for a hypothetical series of HSO_x reactions. However, regarding the importance of these species to aerosol formation, Graedel's work is not conclusive and, in addition, his proposed reaction scheme cannot be realistically applied under stratospheric conditions. For these reasons we have chosen to defer consideration of any additional sulfur radical reactions until more chemical rate information is available.

In our model, all of the reactions we have discussed so far lead to the creation of sulfur trioxide, SO_3, which in turn rapidly combines with H_2O to form sulfuric acid vapor (reaction R9). Considering that stratospheric water vapor concentrations are about 3-6 ppmv (ref. 84), it is doubtful that SO_3 has any other significant aeronomical interactions. For example, its photolysis rate would have to exceed 0.1 sec^{-1} to compete with reaction (R9) anywhere within the aerosol layer. There is still some doubt about the mechanism of the reaction between SO_3 and H_2O; it may be a heterogeneously catalyzed process. Accordingly, the role of SO_3 as a precursor of sulfuric acid vapor might be exaggerated in our reaction scheme. Until an alternative gas-phase sulfur oxidation mechanism is verified experimentally, however, the reactions in table 1 are sufficient for our purposes.

Stratospheric sulfuric acid molecules generated by SO_3 hydration can diffuse to high altitudes and be photodissociated, presumably forming SO_2 in one or more photochemical steps; they can diffuse to the troposphere and be filtered from the air by rainfall, or they can interact in situ with aerosol particles. H_2SO_4 absorption coefficients in the ultraviolet spectrum are unavailable. We have arbitrarily adopted HCl absorption cross sections (ref. 75) for H_2SO_4 even though H_2SO_4 binds hydrogen atoms more tightly than HCl. Obviously, a measurement of the H_2SO_4 ultraviolet absorption coefficient is needed. But even so, the photolytic lifetime of sulfuric acid vapor below 50 km is probably long enough (several months or more) that chemical, aerosol, and transport processes can control its concentration in the stratosphere. Photodissociation will be more important at higher altitudes. In this case, when H_2SO_4 is being fragmented by energetic photons, it is probably a reasonable approximation (ignoring other possible dissociation products) to assume that the initial step in the photodecomposition releases SO_2.

In the mesosphere, where the radiation environment is more intense, the SO_2 can be further reduced to SO or S.

The gas phase reactions of H_2SO_4 molecules with the atoms and radicals normally found in the atmosphere have not been studied experimentally. Although it is possible that H_2SO_4 could react with O, Cl, and OH in the middle and upper stratospheres, no rate constant data are available for these interactions. The H_2SO_4 photolysis rate is quite small throughout the stratosphere (see table 1 for the values corresponding to our assumed H_2SO_4 dissociation cross sections). Accordingly, even a very slow reaction — most probably one with OH — could affect the H_2SO_4 abundance in the upper stratosphere. On the other hand, such a reaction would not materially affect our predictions for the aerosol layer because at the higher altitudes where a slow radical reaction might be important, the aerosol layer is already quite evanescent.

Molecular rainout and washout processes are difficult either to describe or model realistically. Tropospheric hydrometeor ensembles have a significant function as filters of sulfur gases migrating from surface sources to the stratosphere. In this work, we have, by necessity, only partially treated the problem of the tropospheric sulfate balance and the possible leakage of biospheric sulfur to the stratosphere. The usual aeronomic approximation for the precipitation removal of a gaseous species is to specify a decreasing rainout rate with increasing altitude such that the resulting average atmospheric residence time corresponds roughly to one deduced using global mass budget arguments. For SO_2 we have adopted a lifetime against washout (plus rainout) of about 3 days at the surface; the rate of SO_4 washout (or the inverse of the SO_2 washout lifetime) is assumed to decrease linearly with increasing height above sea level to 0 at 13 km (see table 1). Presently, there are insufficient data to evaluate the tropospheric residence time of H_2SO_4 against heterogeneous removal; we have therefore assigned it a washout lifetime of 0.5 day at ground level and a washout profile similar to that for SO_2. The radical HSO_3 is assumed to be washed from the air at the same rate as H_2SO_4. (Later, we will consider tropospheric precipitation as a sink for downward diffusing aerosol droplets as well.)

The interaction of sulfuric acid vapor with stratospheric aerosol droplets is discussed in detail in the next section. H_2SO_4 condensation on and evaporation from aerosol particles are taken into account in our photochemical model. However, we have not included the heterogeneous interaction of other gaseous species with aerosol particles. Friend et al. (ref. 31) have pointed out that SO_2 could react directly with sulfuric acid-water droplets to produce additional dissolved sulfates; the process would require the presence in solution of a buffering agent such as ammonium ions. Recently, Eggleton and Penkett (ref. 85) observed that SO_2 can be readily oxidized in aqueous solution by hydrogen peroxide and to a lesser degree by ozone; the rate of oxidation is sensitive to the solution composition, however.

The inclusion of heterogeneous SO_2 oxidation mechanisms in a model would obviously increase the rate at which sulfur gases are converted into aerosol particles. In NASA TP-1363, however, we have varied this conversion rate to show that it does not greatly affect the aerosol layer.

HSO_3 and other sulfur radicals might also condense or react on aerosol surfaces before they can be oxidized into H_2SO_4 by gas phase reactions or might nucleate to form new aerosols. Unfortunately, nothing is presently known about the interaction of these species with stratospheric particles. In a test, we allowed HSO_3 to condense on aerosol particles at the same rate as H_2SO_4, and we assumed that HSO_3 reacts instantaneously in solution to form H_2SO_4. As expected, the concentrations of both HSO_3 and H_2SO_4 (whose precursor is HSO_3) are reduced. However, the observable characteristics of the aerosol layer are essentially unaltered (neglecting possible effects on aerosol nucleation mechanisms).

According to the previous discussion, it is reasonable to omit a detailed treatment of heterogeneous interactions from our present aerosol model while more suitable theories describing these interactions are being developed. All of the processes involving gaseous sulfur compounds that are included in our model are summarized in figure 2.

The Aeronomical Model

We have used a one-dimensional model to calculate the atmospheric concentrations of the sulfur constituents S, SO, SO_2, SO_3, HSO_3, H_2SO_4, and OCS. The model includes the photoreaction scheme in table 1, augmented by the interaction of sulfuric acid vapor with aerosol particles. We have assumed that the vertical transport of gaseous species occurs by eddy diffusion processes. Our technique for solving the related time-dependent one-dimensional species continuity equations is identical to a method we developed for a much larger aeronomical system (e.g., refs. 86-90). Summarizing our technique, we solve the species continuity equations at 30 equally spaced grid points between 0 and 58 km with a numerical finite difference formulation that is fully implicit in the transport terms and partially implicit in the photochemical terms for greater stability. (Implicit, in the numerical sense, means evaluation at the end of a computational time step. Implicit variables are therefore quantities to be calculated during that step. Explicit variables are evaluated at the beginning of the step and are known).

We define a family of sulfur constituents, denoted as SO_x, which consists of all the sulfur species listed above except OCS. The photochemical reactions that affect SO_x include only those processes which give a net production or loss of sulfur in the SO_x family. Using the net SO_x chemistry, we compute the concentration of SO_x independently of the individual species concentrations. The SO_x abundance is then compared to the summation of the family species concentrations to estimate the cumulative error in the latter solutions and is used to correct those solutions if necessary (see ref. 87 for more details of this scheme).

In our model, we also average the rate of each photochemical process diurnally to account for the effects of nighttime reactions on species abundances (ref. 90). In most respects, the aeronomical model used in this study is a simplified version of our more complete atmospheric model.

We have simulated vertical atmospheric transport in our model by the use of an "eddy" diffusion process. Our assumed eddy diffusion coefficient, shown in figure 3 and discussed in detail in reference 89, results in a very stable air layer near the tropopause which acts as a narrow escape valve for subsiding stratospheric gases and as an efficient barrier to rising tropospheric gases. Since the photochemical lifetime of SO_2 is not very long in the sulfate layer, we expect that SO_2 injected or produced above the tropopause will not be extensively redistributed before it reacts and will almost always be chemically consumed near the altitude where it is added.

We have selected the diffusion profile shown in figure 3 because reference 91 has shown that it gives an excellent representation of the observed time-decay of excess stratospheric carbon-14 following atmospheric nuclear bomb tests. Our eddy diffusion coefficient also satisfies a second criterion: in an aeronomical model it leads to methane and nitrous oxide molecule concentrations in the upper stratosphere that are close to measured values (e.g., refs. 89 and 92). Nonetheless, since there are large variabilities and uncertainties in atmospheric transport rates, the diffusion coefficients adopted here are certainly not unique.

The actual mechanisms by which tropospheric gases and particles are transported into the stratosphere may be more closely related to injection than to diffusion. Such injection can occur — in an equivalent sense — during thundercloud penetration, tropopause folding, and vertical convection at the intertropical convergence zone. Horizontal advection would subsequently distribute the injected material zonally and meridionally. Obviously, we cannot simulate the hydrodynamics of multidimensional transport with a one-dimensional model. However, we can roughly simulate the globally averaged mass transfer rates between the stratosphere and troposphere. More detailed studies of the meteorology of the stratospheric aerosol layer will have to wait the development of two- and three-dimensional dynamic models that can also accurately treat gaseous photochemistry and particle microphysics.

In the present model, we utilize fixed profiles for O, O_3, OH, HO_2, and NO_2; these profiles are illustrated in figure 4. The data, for the most part, are taken from our large atmospheric simulation above 10 km (recent unpublished calculations) and are extrapolated to the appropriate ground level abundances (e.g., ref. 93). A standard midlatitude ozone profile constructed by Krueger and Minzner (ref. 94) has been adopted here. The tropospheric water vapor concentrations are derived from a study of midlatitude humidity by Sissenwine et al. (ref. 95). Neutral atmospheric densities and temperatures are taken from the U. S. Standard Atmosphere (ref. 96) for midlatitude spring/fall conditions.

We have performed interactive aerosol-gas calculations with our more complete aeronomical model and found that, except for the sulfur compounds, none of the air constituents is significantly affected by the presence of aerosol particles. However, we have not yet treated potentially important radiative and chemical feedback effects arising from the optical and catalytic properties of the aerosol (e.g., ref. 6), and we have also ignored solution reactions within the liquid droplets. Some of these problems will be addressed in subsequent papers.

The lower boundary condition in our photochemical model is specified in terms of a fixed boundary concentration, n_{B_α} (molecules cm^{-3}) for each species, α, at the ground. A flux necessary to maintain this concentration is established at the boundary according to the relation,

$$\phi = v_B(n_{B_\alpha} - n_\alpha) \tag{2}$$

where ϕ is the flux (molecules cm^{-2} sec^{-1}); v_B is the boundary velocity, taken to be 1 cm sec^{-1}; and n_α (molecules cm^{-3}) is the instantaneous species abundance. Boundary condition (2) implies that within the model boundary layer, counterbalancing surface fluxes seek to maintain $n_\alpha \approx n_{B_\alpha}$. The actual processes that generate these surface fluxes (emission, absorption, and recombination) are not specified, but are implied. Except for SO_2 and OCS, whose boundary concentrations are taken to be 1.3 ppbv and 0.47 ppbv, respectively, each sulfur gas is assumed to have $n_B = 0$. (For SO_2, a value of n_B of 1.3 ppbv leads to a surface concentration of 0.6 ppbv in our model.) At the upper boundary of the model (which is near the stratopause), a null flux is assumed for each of the sulfur compounds, ignoring a possible small contribution of meteoric sulfur to the sulfate layer (ref. 97). Our boundary conditions are reasonable approximations for a model of the stratospheric aerosol layer.

Predicted Profiles for the Gaseous Sulfur Constituents

Figure 5 gives our model predictions of typical atmospheric distributions of the dominant sulfur gases, including the effects of aerosols. The number mixing ratio of OCS is constant in the troposphere — which is indicative of a long lifetime in this region — then falls off uniformly above the tropopause to maintain an upward flux of molecules and decreases rapidly above 25 km where it is photolyzed by sunlight.

The sulfur dioxide mixing ratio falls off sharply above the ground due to washout, which diminishes its abundance to about 0.05 ppbv at the tropopause. In the lower stratosphere, SO_2 decreases even more precipitously, being trapped and oxidized at these heights. At first, this result might seem to contradict the recent observation in reference 55 of a nearly constant SO_2 mixing fraction for several kilometers above the tropopause level. However, these researchers have pointed out that their measurements were made near a tropopause break, and they believe that their data were actually taken in upper tropospheric air freshly transported into the stratosphere. Since the oxidation time of SO_2 in the lower stratosphere is about a week, SO_2 transported there would remain intact for some time. Above the aerosol layer, SO_2 concentrations increase in the region where OCS is photolyzed and again at higher altitudes where H_2SO_4 is photodissociated.

Sulfuric acid vapor has an interesting distribution in that its lowest concentrations occur in the vicinity of the aerosol layer. Obviously the aerosol particles absorb H_2SO_4, significantly affecting its local abundance.

This result suggests that aerosol models that do not include interactive gas-particle processes for H_2SO_4 are probably quite inaccurate in their predictions for the sulfate layer.

The H_2SO_4 mixing fraction increases sharply near the top of the aerosol layer (at about 30 km) due to the evaporation of the acid solution droplets that rise into this region of warmer, drier air. Notice, however, that the total mixing ratio of gaseous sulfur above the aerosol layer (where it is primarily H_2SO_4) is smaller by a factor of 2 to 3 than that near the tropopause (where it is predominantly OCS). The gravitational sedimentation of aerosol particles effectively acts to reduce the total amount of sulfur in the upper stratosphere.

The sulfur radical HSO_3 has a vertical distribution similar to that of H_2SO_4; in fact, it has a larger abundance than H_2SO_4 over much of the stratosphere.

The predicted sulfur gas distributions shown in figure 5 are not unique. They depend on the assumed model boundary conditions, eddy diffusion profile, photochemical rate coefficients, nonsulfurous minor constituent concentrations, and aerosol abundances; they might also depend to some extent on heterogeneous physical and chemical processes not yet included in our model. Accordingly, the species mixing ratios given in figure 5 should only be interpreted as representative values corresponding to a specific set of aeronomical parameters.

PHYSICAL AEROSOL PROCESSES

Stratospheric aerosol particles can be formed and existing ones can grow in an environment that is saturated with sulfuric acid vapor. Aerosol particles can also undergo dynamical motions and interact with each other. In this section, we discuss some of the important microphysical processes for particles residing in the upper atmosphere, that is, nucleation, condensation, evaporation, coagulation, sedimentation, and diffusion, and we describe how each process is incorporated into our model.

Aerosol Droplet Nucleation

We assume that stratospheric aerosol particles are aqueous sulfuric acid solution droplets which are formed in situ by the heterogeneous heteromolecular nucleation of H_2SO_4 and H_2O vapors onto condensation nuclei or Aitken particles. Reference 98 has shown that the stratospheric nucleation rates for homogeneous nucleation or nucleation onto molecular ions are much smaller than those for the heterogeneous process. Recent experiments (ref. 99) have detected undissolved granules in about 30% of the aerosol droplets collected in the stratosphere over a wide geographic range; moreover, most of the other droplets, when evaporated, left behind a crystalline matrix suggestive of dissolved core materials. These observations lend credence to the hypothesis

that heterogeneous heteromolecular nucleation dominates aerosol formation in the ambient stratosphere. Nevertheless, the possibility exists that large ions composed of a charged core surrounded by a cluster of polar molecules such as H_2O, HNO_3, and H_2SO_4 may be formed in the stratosphere. Some of these ions might reach a critical size during their lifetime and grow rapidly into small aerosol particles (Castleman, private communication). It is also possible that the recombination of large clustered positive and negative ions might lead to larger neutral clusters which might act as condensation nuclei. We hope to investigate some of these alternative nucleation processes in future work.

Physically, the heterogeneous heteromolecular nucleation of stratospheric Aitken nuclei takes place when sulfuric acid and water vapors can combine to "wet" the particle surfaces. Under stratospheric conditions, the newly formed particles would consist of the core nucleus surrounded by a (probably impure) sulfuric acid-water solution of between 70 and 80% H_2SO_4 by weight, which is the range of sulfuric acid concentrations generally found in stratospheric aerosol particles (ref. 100).

Because very little is known about heteromolecular heterogeneous nucleation, we have parameterized it by assuming that all Aitken particles that are mixed into a region where H_2SO_4 vapor is supersaturated will be nucleated in 10^6 sec. In NASA TP-1363, we show that this arbitrary choice of nucleation time does not significantly affect our model results.

Stratospheric condensation nuclei are assumed to have a tropospheric origin, presumably by atmospheric transport which is simulated in our model by eddy diffusion (e.g., see a recent review of stratospheric Aitken nuclei in ref. 101). Condensation nuclei may also be deposited above the tropopause by volcanic activity, aircraft traffic, and meteoritic ablation, but these latter sources have not been incorporated into the ambient model being discussed here.

In determining the concentrations of condensation nuclei in the atmosphere, we fix their total number density and size distribution at the ground. The number density selected is 1200 cm^{-3} and the size distribution varies as r^{-4} for nuclei larger than 0.01 μm radius, r being the particle radius (0.01 μm is the smallest particle size in the model). The total particle concentration at the ground has been adjusted to give a total of a few hundred condensation nuclei and droplets near the tropopause, as has been observed. The r^{-4} condensation nuclei size distribution is quite different from the observed size distribution for stratospheric aerosol droplets (ref. 102). We chose the r^{-4} distribution because it simultaneously yields the measured values of the number of condensation nuclei and their total mass at the tropopause level. We have used several other condensation nuclei size spectra in our model to determine their influence on the predicted aerosol size distribution; our findings are given in NASA TP-1363.

Aerosol Growth by Molecular Condensation

Once sulfuric acid-water solution aerosol droplets are nucleated, they can grow by heteromolecular condensation of H_2SO_4 and H_2O vapors. The growth of sulfuric acid solution droplets by heteromolecular condensation has been discussed in references 34, 103, and 104, to which the reader is referred for details. These workers have shown that the growth rate of such a droplet is controlled by the rate at which sulfuric acid molecules impinge upon it. The fluxes of H_2SO_4 and H_2O vapors to the droplet are balanced so that the droplet is always in equilibrium with the water vapor in the environment; that is, the H_2O vapor pressure of the droplet is always equal to the local partial pressure of H_2O. At a given temperature, the water vapor equilibrium uniquely determines the weight percentage of H_2SO_4 in the solution and, consequently, the H_2SO_4 vapor pressure over the droplet (see ref. 105). If the partial pressure of H_2SO_4 in the surrounding air is greater than its vapor pressure, some of the sulfuric acid molecules incident on the droplet are absorbed; otherwise, sulfuric acid molecules are evaporated from the droplet. The droplet absorbs or evaporates just enough water vapor, essentially instantaneously, to maintain a constant weight percentage of H_2SO_4 in solution.

Under these conditions, the growth equation for the droplet is

$$g \equiv \frac{dr}{dt} = \frac{m_a D_a (n_a - n_a^\circ)}{r\rho W(1 + \lambda_a Kn_a)} \times 10^8 \qquad (3)$$

$$= g_{oa}(n_a - n_a^\circ)$$

where g is the growth rate ($\mu m\ sec^{-1}$); m_a is the mass (g) of an H_2SO_4 molecule; r is the droplet radius (μm); ρ is the droplet solution density ($g\ cm^{-3}$); W is the H_2SO_4 weight fraction of the solution (we use the terms "weight fraction" and "weight percentage" interchangeably; a fraction is always implied in our equations); n_a is the H_2SO_4 vapor concentration (molecules cm^{-3}) near the droplet; and n_a° is the equilibrium H_2SO_2 vapor concentration (molecules cm^{-3}) over the droplet. (Note that in our calculations, vapor pressures have been converted to equivalent molecular concentrations per cubic centimeter using the ideal gas law.) The factor of 10^8 in equation (3) is required to convert centimeters to microns. D_a is a diffusion coefficient ($cm^2\ sec^{-1}$) for sulfuric acid molecules in air (ref. 106) which depends on the mean collision diameter of H_2SO_4 molecules with air molecules (taken to be 4.3×10^{-8} cm in this work). The Knudsen number for sulfuric acid vapor diffusion is given by

$$Kn_a = \ell_a / r \qquad (4)$$

where ℓ_a is the H_2SO_4 molecular free path in air (μm). The parameter λ_a is given by

$$\lambda_a = \frac{1.33 + (0.71/Kn_a)}{1 + (1/Kn_a)} + \frac{4(1 - \alpha_a)}{3\alpha_a} \tag{5}$$

where α_a is the H_2SO_4 sticking coefficient, which is usually assumed to be unity. Note that for large Knudsen numbers, or long molecular free paths, g is roughly proportional to α. Hence, the sticking coefficient is an important parameter determining the high-altitude growth rate of solution droplets. We discuss the effect of uncertainties in the sticking coefficient more thoroughly in NASA TP-1363.

Several assumptions are implicit in the derivation of equation (3). The effect of dissolved impurities (core material) on the H_2O and H_2SO_4 vapor pressures over the droplet is ignored. There are presently very little data available to evaluate this effect. In addition, the influence on the temperature of the droplet of the latent heat released by vapor condensation is not compensated in the growth equation. However, we would expect that stratospheric particles are in close thermal equilibrium with their surroundings. Another interaction left essentially untreated is the clustering of water vapor to the H_2SO_4 molecules as they diffuse toward the aerosol droplet. To account for this process, an effective cluster diffusion coefficient D_a^c would replace D_a in equation (3), and the form of growth equation would be modified somewhat (ref. 107). If only one or two water molecules, which are small and light, are attached, however, the clustering effect is unimportant.

According to the preceding analysis of the behavior of H_2SO_4-H_2O droplets in air, we can calculate a fixed set of acid-water solution properties at each height in our model in the following manner. At a given altitude, we evaluate the equilibrium vapor pressure of water over an H_2SO_4-H_2O solution mixture using the empirical relation (ref. 108)

$$\tilde{P}_h^\circ(W) = (T_o/T)^{C_1(W)} \exp\left(\sum_{\xi=2}^{5} C_\xi(W) T^{\xi-3}\right) \tag{6}$$

where $\tilde{P}_h^\circ$ is the H_2O vapor pressure over a flat sulfuric acid solution having an H_2SO_4 weight percentage W; T_o is a reference temperature equal to 298.15 K; and T is the local air temperature (K). The constants C(W) are tabulated in reference 108 for a discrete set of H_2SO_4 weight percentages W. We selected 30 values of W between 10 and 98% for our model; to obtain vapor pressures at intermediate weight percentages, we perform a logarithmic interpolation between adjacent tabulated vapor pressure values. At a given height in the model, the equilibrium weight percentage of H_2SO_4 in solution W is determined by matching the calculated H_2O vapor pressure $\tilde{P}_h^\circ(W)$ to the known H_2O partial pressure in the air at the height. Using this value of W, the sulfuric acid equilibrium vapor pressure $\tilde{P}_a^\circ(W)$ is evaluated by an equation similar to equation (6), but with the set of constants C(W) appropriate for H_2SO_4 (also tabulated in ref. 108). For the same value of W, the H_2SO_4-H_2O solution density, ρ(g cm^{-3}), is obtained from data at 273 K tabulated in reference 109. Finally, the vapor pressure of H_2SO_4 is corrected for the sphericity of the droplets using the Kelvin relation.

We have omitted several small effects from the preceding analysis. We have not accounted for the Kelvin effect on the H_2O vapor pressure over small droplets. Also, in calculating the Kelvin effect, we have ignored the dependence of the solution free-surface energy (assumed to be 83 ergs cm^{-2}) on the solution temperature and composition, and we have not considered the possible effects of surface enrichment or volume contraction. Finally, we have not extrapolated the acid solution densities below their known 273 K values.

In the stratosphere, the growth equation gives a negative value for dr/dt when the H_2SO_4 concentration is less than the saturated value n_a°; this corresponds to droplet evaporation. During the evaporation process, molecules must escape the free-surface barrier of the droplet, and one might logically postulate an "evaporation coefficient" β which is the counterpart of α for condensation. There are no data for α or β for H_2SO_4 condensation. Nominally, we set $\alpha = \beta = 1$ for aerosol droplets (ref. 110), and in NASA TP-1363 we study the effect of these parameters on our model results.

Aerosol Droplet Cores

Solution droplets may evaporate to their cores in our model. Accordingly, we need to distinguish between activated cores — which have a thin coating of acid solution and can grow freely by condensation, as can droplets — and condensation nuclei, which require a certain nucleation time before they can grow (activated cores are equivalent to droplets in our model). To do this, we must specify a deactivation time for the activated cores which are present in an unsaturated environment, that is, a delay time before they become condensation nuclei again. We have arbitrarily assumed a zero deactivation time for such cores. As a result, the rate of release of condensation nuclei from evaporating particles is only limited by the rate at which droplets evaporate to their cores.

Monitoring the droplet cores in a model is necessary for several reasons. First, the size of the cores limits the volume of solution which can evaporate from a droplet. Therefore, cores must be considered if one hopes to properly conserve the total mass of sulfate in gases and particles.

Cores also modify the average density of a particle, and the density is a factor which influences the rates of particle sedimentation and coagulation. If we define f as the fraction of the total droplet volume that is occupied by core material, then the average particle density is

$$\bar{\rho} = f\rho_c + (1 - f)\rho \tag{7}$$

where ρ_c is the core density (assumed to be 1.67 gm cm^{-3}, as for ammonium sulfate). In all our computations of particle settling velocities and coagulation kernels, we use average droplet densities $\bar{\rho}$ corresponding to an ambient distribution of aerosol droplet cores which is predicted by our model. The average particle densities will change during a perturbation of the ambient aerosol layer, but since ρ_c is close to ρ anyway, these density

changes can usually be ignored (i.e., sedimentation and coagulation rates are not significantly altered by small variations in $\bar{\rho}$).

To properly evaluate the effect that cores have on aerosol processes, we must know the size distribution of the cores within the aerosol droplets. In our model we determine the core size distribution using only the first two core volume moments. For the cores residing in a collection of droplets of a specific size at a given height, we calculate the total core volume and core volume squared for those droplets. Our subsequent use of these core volume moments to derive the core size distribution is explained in appendix B. Although our treatment of droplet cores is an approximate one, we show later that it accurately determines core size spectra.

When a droplet contains several cores — because of coagulation — they will probably coalesce to a large degree. Therefore, we would expect to see a substantial difference between the size distribution of the cores from which a collection of aerosol droplets is formed and the size distribution of the cores within the droplets themselves. In NASA TP-1363 we discuss in detail the evolution of aerosol core size spectra.

Water Vapor Growth

As mentioned earlier, an H_2SO_4-H_2O solution droplet comes into equilibrium with its surroundings by absorbing or evaporating water molecules so rapidly that only a negligible amount of H_2SO_4 is simultaneously transferred with the environment. Now imagine a single solution droplet that changes altitude. The environmental conditions (temperature, H_2O partial pressure, etc.) affecting its equilibrium H_2SO_4 weight percentage and its density also change. The droplet absorbs or evaporates water vapor in such a way that three quantities are conserved: the number of particles (unity, of course), the acid mass of the particle, and the core mass of the particle. Combining these three constraints, it can be demonstrated that the particle moves along a trajectory in an r-z space, where z is the altitude, such that

$$\frac{dr}{dz} = -\frac{r}{3}\left[1 - f_o\left(\frac{r_o}{r}\right)^3\right]\frac{d}{dz}\,\ell n(\rho W) \tag{8}$$

where f_o is the droplet core volume fraction at a reference droplet radius, r_o. We refer to the change in the size of an aerosol droplet due to a change in its height as water vapor growth. In the stratosphere, the product ρW is relatively constant over a wide altitude range (e.g., see the data in table 5 of appendix A). Accordingly, the water vapor growth process is of rather limited importance to the stratospheric aerosol.

Particle Coagulation

Coagulation is another important particle growth mechanism which is included in our model. Considering a discrete set of particle sizes, the

change in the concentration n_i of particles of radius r_i due to collisions with particles of radius r_j is (ref. 111)

$$\frac{dn_i}{dt} = \frac{dn_j}{dt} = -K_{ij} n_i n_j \tag{9}$$

Here, K_{ij} is the coagulation kernel ($cm^3\ sec^{-1}$) for particles of sizes r_i and r_j. The expression for K_{ij} which we have adopted is taken from reference 111. It might be pointed out that K_{ij} is a function of the diameter of the air molecules, which is assumed to be 3.65×10^{-8} cm, and the kinematic viscosity of air, which is evaluated using Sutherland's equation (ref. 112).

In our model we consider the coagulation of aerosol droplets with each other, and with condensation nuclei, but we ignore self-coagulation of the bare condensation cores because of the low probability of their colliding and sticking together. A bare nucleus colliding with and adhering to a solution droplet is assumed to form a larger droplet. Our aerosol coagulation scheme is fully developed in the following two sections and in appendix B. Another coagulation process, coalescence, in which larger particles "run into" smaller particles due to a difference in their terminal fall velocities, is not important and is neglected in our model.

Particle Transport by Sedimentation and Diffusion

The sedimentation of aerosol particles is treated by evaluating the terminal fall velocity according to the Stokes-Cunningham formula (refs. 111 and 113).

The rate of vertical diffusion of particles and gases by atmospheric mixing is usually derived from the phenomenological relation

$$\phi_D = -D n_M \frac{\partial}{\partial z}\left(\frac{n}{n_M}\right) \tag{10}$$

where ϕ_D is the diffusive flux (particles $cm^{-2}\ sec^{-1}$), D is the eddy diffusion coefficient ($cm^2\ sec^{-1}$) already discussed in the second section of this paper, Physical Chemistry of Atmospheric Sulfur, n_M is the air density (molecules cm^{-3}), and n is the number density of the diffusing species (number cm^{-3}). Equation (10) states that when particles are uniformly mixed in air, their net diffusive flux is zero. We define an "exponentially" increasing atmospheric structure parameter

$$\gamma \equiv \frac{n_M(\text{ref})}{n_M} \tag{11}$$

where n_M(ref) is the air concentration at a reference height. Then equation (10) can be written

$$\phi_d = -\frac{D}{\gamma}\frac{\partial}{\partial z}(\gamma n) \tag{12}$$

Eddy diffusion is the standard parametric approximation for describing the vertical movement of stratospheric gas constituents in one-dimensional models. The concept should also apply to particle motions, provided the particles are small enough. For large particles, eddy diffusion may be inappropriate; gravitational sedimentation is probably the dominant transport mode in this case. Here, all sizes of particles are assumed to diffuse under the influence of the same diffusion coefficient, the same one used for gases (see fig. 3). We do not expect this to lead to significant errors in the predicted transport rates of the aerosol particles.

Aerosol Removal by Washout and Rainout

Liquid aerosol droplets can probably be washed from the air very efficiently by rainfall. We include tropospheric aerosol washout and rainout in our model with a removal rate, R_w, of about 1 day^{-1} at the ground, decreasing linearly with height (as for the gaseous species) to zero at the tropopause; that is, we take

$$R_W = \begin{cases} 1.2 \times 10^{-5}(1 - z/z_T)\ sec^{-1}, & z \leq z_T \\ 0, & z > z_T \end{cases} \tag{13}$$

where z_T (km) is the tropopause altitude. For a uniformly mixed tropospheric aerosol, equation (13) results in an average lifetime against washout and rainout of about 2-3 days. We do not include the washout of condensation nuclei in our model because we are not attempting to model tropospheric aerosols. In fact, the most important property of condensation nuclei for our present purpose is their total concentration at the tropopause. In NASA TP-1363 we study the influence of different tropospheric rainout rates on the stratospheric aerosol layer.

Aerosol Parameter Values

We have tabulated the values of several of the physical aerosol parameters used in our model in appendix A. The vapor pressures, growth rates, coagulation kernels, and sedimentation velocities given in appendix A were calculated using the equations that are referred to in this section and that are incorporated into our model. The uncertainties associated with these aerosol parameters are briefly reviewed later in table 3.

In summary, figure 6 depicts, schematically, most of the particle and gas mechanisms that are treated in our model. While our simulation is not an exhaustive one, we believe that it is sufficiently detailed to give an accurate representation of the natural aerosol. In the following two sections we describe how the aerosol processes delineated above, and shown in figure 6, are utilized in our model.

THE AEROSOL CONTINUITY EQUATION

The quantitative effects of chemical and physical processes on aerosol particle concentrations can be calculated with a particle continuity equation. In this formulation, the rate of change of the particle concentration is calculated as the sum of the rates of change due to each individual process. The particle mechanisms which are included in our calculations are nucleation, condensation, coagulation, sedimentation, diffusion, and washout. Corresponding to these processes, we have the following continuity equation to solve:

$$\frac{\partial n}{\partial t} = \frac{\partial n}{\partial t}\Big)_{\text{nuc.}} + \frac{\partial n}{\partial t}\Big)_{\substack{\text{growth} \\ \text{or evap.}}} + \frac{\partial n}{\partial t}\Big)_{\text{coag.}} + \frac{\partial n}{\partial t}\Big)_{\text{sed.}}$$

$$+ \frac{\partial n}{\partial t}\Big)_{\text{diff.}} + \frac{\partial n}{\partial t}\Big)_{\text{washout}} \tag{14}$$

where n is the particle concentration (defined below).

Various types of aerosol continuity equations have been published before, but none of them are directly analogous to equation (14). Accordingly, in this section we derive the continuity equations that are required for our model.

Aerosol Variables

In our model we distinguish between sulfuric acid solution droplets and bare condensation nuclei. We define the size distribution of the droplets as $n(r,z,t)$, where ndr is the number of droplets per unit volume of air at height z and whose radii lie in the range r to $r + dr$ at time t; the units of n are particles $cm^{-3}\ \mu m^{-1}$. The size distribution of the condensation nuclei is defined as $\hat{n}(r,z,t)$ and has the same interpretation and units as n.

In our model we also need to calculate the first two droplet core volume moments; these moments are used to determine the core size spectrum, which in turn affects the rates of certain aerosol processes. We denote the total volume of the cores in the droplet $n(r,z,t)$ as $u(r,z,t)$ with the units $\mu m^3\ cm^{-3}\ \mu m^{-1}$; u is therefore the summation of n droplet core volumes. Because we do not explicitly distinguish between the sizes of the cores in individual droplets, we could assume that each droplet has an average size core whose fractional volume is

$$f(r,z,t) = u(r,z,t)/Vn(r,z,t) \tag{15}$$

where V is the volume (μm^3) of a particle (either a droplet or a nucleus) of radius r.

The second core volume moment of the droplets $n(r,z,t)$ is denoted by $\varepsilon(r,z,t)$ and has the units, $\mu m^6\ cm^{-3}\ \mu m^{-1}$; ε is the summation of the squares of n droplet core volumes. In our model ε is used to estimate the variance, or width, of the core size distribution.

In the following subsection, we derive the continuity equation for the aerosol droplet number density n by developing the corresponding set of rate terms for equation (14). Because the continuity equation for $\hat{n}$ is very much like that for n, fewer details of its derivation are given. The continuity equations for u and ε are obtained by taking the appropriate core volume moments of the continuity equation for aerosol droplets having cores of a specific size (see appendix B). Certain terms in the droplet continuity equation commute with the core volume moment operators and, as a result, the corresponding rate expressions for n, u, and ε all have the same form; these "commutative" terms are discussed below. However, the terms for droplet coagulation, water vapor growth, and evaporation are more involved, and their treatment is given in appendix B. For the most part, the continuity equations for n, $\hat{n}$, u, and ε have very similar structures, which simplifies their presentation here.

Many of the quantities that describe physical aerosol processes depend on particle size because of weight, drag, and surface tension factors and on altitude because of air temperature, density, and trace gas composition effects. With this in mind, we do not specifically write out the r and z variables in expressions except where clarity demands it.

The Rate Terms in the Aerosol Continuity Equations

Heterogeneous heteromolecular nucleation converts bare condensation nuclei into solution droplets in situ at a rate which is easily seen to be

$$\left.\begin{aligned}
\frac{\partial n}{\partial t}\Big)_{nuc.} &= R_N \hat{n} \\
\frac{\partial \hat{n}}{\partial t}\Big)_{nuc.} &= -R_N \hat{n} \\
\frac{\partial u}{\partial t}\Big)_{nuc.} &= R_N \hat{n} V \\
\frac{\partial \varepsilon}{\partial t}\Big)_{nuc.} &= R_N \hat{n} V^2
\end{aligned}\right\} \qquad (16)$$

where R_N is the local nucleation coefficient (sec^{-1}). Heteromolecular nucleation should not affect the total number of particles (droplets plus nuclei), and equations (16) fulfill this requirement.

The aerosol processes of growth, sedimentation, and diffusion can be analyzed by considering the related flux of particles they generate in an r-z space; mathematically, the corresponding rate of change of the particle concentration due to each process is then the negative divergence of the local flux for that process. If we consider aerosol droplet growth by heteromolecular condensation, the growth rate, $g = dr/dt$, from equation (3), can be interpreted as a radial "velocity" which produces a radial particle flux,

$$\phi_g = gn \tag{17}$$

ϕ_g represents the number of particles per cubic centimeter of air which are growing to size r each second. Therefore, the change in ϕ_g over a small radial size interval represents the rate of accumulation or depletion of particles in that size interval, or more precisely,

$$\left.\frac{\partial n}{\partial t}\right)_{\text{growth}} = -\frac{\partial}{\partial r}(gn) \tag{18}$$

The growth process also generates radial fluxes of droplet core volume and core volume second moment. It is easy to see, however, that cores will be affected by growth as follows, for example,

$$\left.\frac{\partial u}{\partial t}\right)_{\text{growth}} = -\frac{\partial}{\partial r}(gu) \tag{19}$$

When the sulfuric acid supersaturation ratio n_a/n_a° is less than unity, the growth rate g is negative and droplets will evaporate. The extent of the evaporation is limited by the cores in the droplets. As we already mentioned, once a droplet evaporates to its core, we assume that it is instantaneously deactivated into a condensation nucleus. Hence, in an evaporative environment, there is a net production of condensation nuclei,

$$\left.\frac{\partial \hat{n}}{\partial t}\right)_{\text{evap.}} \equiv \hat{P} \tag{20}$$

The details of the calculation of $\hat{P}$ are given in appendix B.

The evolution of an ensemble of coagulating particles has been studied in detail many times (e.g., refs. 26, 111, and 114). The rate of change of the concentration of particles of radius r due to coagulation can be expressed as the difference between two integrals over the particle size distribution: one integral represents the production rate of particles of size r by the coagulation of two smaller particles, and the second integral represents the loss rate of particles of size r by their coagulation with other particles. The coagulation integrals are well known and are not reproduced here. In appendix B, however, we do give the coagulation integrals for droplets with cores when the core size spectrum is resolved.

In our model, aerosol particles are transported by gravitational sedimentation and vertical diffusion. The sedimentation flux (particles cm^{-2} sec^{-1} μm^{-1}) is

$$\phi_S = -v_S n \tag{21}$$

where v_S is the settling velocity (cm sec^{-1}); we use the same value of v_S for all particles (droplets or nuclei) of the same size. For diffusive transport, the particle flux ϕ_D is given by equation (12). The particle flux equations apply equally to condensation nuclei and acid solution droplets.

The rate of change of particle concentration due to transport is given by the corresponding flux divergence; for example,

$$\left.\frac{\partial n}{\partial t}\right)_{\text{sed. + diff.}} = -\frac{\partial}{\partial z}(\phi_S + \phi_D) \tag{22}$$

Often, when the divergence of the sedimentation flux is evaluated in a model using standard finite-difference techniques, "numerical" or artificial diffusion errors can occur. To help eliminate this problem, we have combined the diffusion and sedimentation fluxes given by equations (12) and (21) into a single composite diffusion flux. For this purpose we define the particle scaling factor

$$\mu(r,z) \equiv \exp\left[\int_0^z \frac{v_S(r,z')}{D(z')}\,dz'\right] \tag{23}$$

where D is the diffusion coefficient (cm^2 sec^{-1}). Then, it is easy to show that

$$\phi_{SD} = \phi_S + \phi_D = -\frac{D}{\gamma\mu}\frac{\partial}{\partial z}(\gamma\mu n) \tag{24}$$

and

$$\left.\frac{\partial n}{\partial t}\right)_{\text{sed. + diff.}} = -\frac{\partial}{\partial z}\phi_{SD} \tag{25}$$

where γ is defined by equation (11).

Since we have assumed that particle transport is independent of particle composition, we can readily demonstrate that the droplet core volume flux is

$$\phi^u_{SD} = -\frac{D}{\gamma\mu}\frac{\partial}{\partial z}(\gamma\mu u) \tag{26}$$

and that a similar relation holds for ε.

Droplet water vapor growth occurs with vertical particle displacements. Because the vertical diffusion process can, phenomenologically, transport cores and droplets at different rates, and because the resulting fractional expansion of each droplet is a function of its core size, the water vapor growth term is quite complex. Using equation (8), the following expression is, however, derived in appendix B:

$$\left.\frac{\partial n}{\partial t}\right)_{\substack{H_2O \\ growth}} = -\frac{\partial}{\partial r}\left\{-\frac{r}{3}\left[\frac{d}{dz}\,\ell n(\rho W)\right]\left[\phi_{SD} - \frac{\phi^u_{SD}}{V}\right]\right\} \tag{27}$$

The corresponding water vapor growth equations for u and ε are also deduced in appendix B.

Using equations (15) and (24), we can reorganize equation (27) into a more useful form; thus, we write

$$\left.\frac{\partial n}{\partial t}\right)_{\substack{H_2O \\ growth}} = -\frac{\partial}{\partial r}\,(g_H n) \tag{28}$$

with

$$g_H = \frac{r}{3}\,(1 - f)D\left[\frac{d}{dz}\,\ell n(\rho W)\right]\frac{\partial}{\partial z}\,\ell n[\gamma\mu(1 - f)n] \tag{29}$$

Expressions similar to equations (28) and (29) can be derived for u and ε as well.

The rates of tropospheric washout of droplets and their cores are simply

$$\begin{aligned}\left.\frac{\partial n}{\partial t}\right)_{washout} &= -R_W n \\ \left.\frac{\partial u}{\partial t}\right)_{washout} &= -R_W u\end{aligned} \tag{30}$$

Consolidating all of the rate terms we have just discussed, we can write out the aerosol droplet and condensation nuclei continuity equations:

$$\frac{\partial n}{\partial t} = R_N\hat{n} - R_W n - \frac{\partial}{\partial r}[(g + g_H)n] + \left.\frac{\partial n}{\partial t}\right)_{coag.} - \frac{\partial}{\partial z}\left[-\frac{D}{\gamma\mu}\,\frac{\partial}{\partial z}\,(\gamma\mu n)\right] \tag{31}$$

and

$$\frac{\partial \hat{n}}{\partial t} = \hat{P} - R_N\hat{n} + \left.\frac{\partial \hat{n}}{\partial t}\right)_{coag.} - \frac{\partial}{\partial z}\left[-\frac{D}{\gamma\mu}\,\frac{\partial}{\partial z}\,(\gamma\mu\hat{n})\right] \tag{32}$$

The continuity equations for u and ε have the same general form as equation (31).

The Gas-Particle Interaction

The growth and evaporation of aerosol droplets can affect the concentrations of the sulfurous gases in the air surrounding the droplets. In our model we specifically account for the interaction of H_2SO_4 vapor with aerosol droplets. The rate at which H_2SO_4 molecules condense on and evaporate from droplet surfaces is determined by the particle growth rate and the total particle surface area available. At any altitude, the net rate at which acid molecules are condensing onto existing particles is

$$\frac{dn_a}{dt} = 1\times10^{-12}\ \rho W \frac{\mathcal{N}_A}{M_a} \int_o^\infty 4\pi r^2 g n\ dr \tag{33}$$

where n_a is the sulfuric acid vapor concentration; $\mathcal{N}_A$ is Avogadro's number; and M_a is the molecular weight of H_2SO_4 (the factor 10^{-12} is needed to convert units from μm^3 to cm^3). Using the droplet growth rate g from equation (3), we can rearrange equation (33) into

$$\left.\frac{dn_a}{dt}\right)_{aerosol} = P_a - n_a L_a \tag{34}$$

with

$$\begin{aligned} P_a &= 1\times10^{-12}\ \rho W \frac{\mathcal{N}_A}{M_a} \int_o^\infty 4\pi r^2 g_{oa} n_a^\circ n\ dr \\ L_a &= 1\times10^{-12}\ \rho W \frac{\mathcal{N}_A}{M_a} \int_o^\infty 4\pi r^2 g_{oa} n\ dr \end{aligned} \tag{35}$$

P_a and L_a are the sulfuric acid vapor production (molecules cm^{-3} sec^{-1}) and loss (sec^{-1}) rates, respectively, due to aerosols. P_a and L_a are included as factors in the H_2SO_4 vapor continuity equation used to calculate its concentration in air. Our method of solving the continuity equations for the gaseous species has already been outlined in the second section of this paper, Physical Chemistry of Atmospheric Sulfur.

Sulfuric acid vapor condensation on particles, as expressed by equations (34) and (35), provides a sensitive feedback mechanism which can moderate the overall growth rate of stratospheric aerosol droplets. For example, if a large number of particles is added to the stratosphere, the H_2SO_4 vapor concentration will be depleted and particle growth will be slowed. On the other hand, if the H_2SO_4 concentration is raised significantly, the existing

particles will grow rapidly and decrease the H_2SO_4 partial pressure. In each case, the impact of the perturbation on the aerosol layer is reduced by the gas-particle interaction. This interaction is, therefore, an important feature of our model.

A NUMERICAL REPRESENTATION OF THE AEROSOL CONTINUITY EQUATIONS

Introductory Comments

We wish to recast the aerosol continuity equations into discrete finite-difference relations suitable for computer analysis. The altitude grid adopted for the aerosol calculation is the same one used for the photochemical analysis; that is, there are 30 equally spaced altitude levels between 0 and 58 km, with a grid separation h of 2 km.

Natural aerosol particles usually have diameters spanning several orders of magnitude. It is therefore logical, in an approximate model such as ours, to utilize a set of geometrically increasing particle size categories such as the ones shown in figure 7 (see ref. 26). In this arrangement, particle volume doubles from one size category to the next — that is, $V_2 = 2V_1$, $V_3 = 2V_2$, etc. — and the corresponding volume intervals, or bins, associated with each size are two-thirds of the category volume. These bin relationships are indicated in figure 7. For comparison, a "classical" equal-width bin structure is also shown in figure 7. Obviously, it takes many more classical bins to cover the same size range as a set of geometrical bins. For our model, we have selected 25 particle sizes corresponding to particle *radii* between 0.01 μm and 2.56 μm. With the bin boundaries defined in figure 7, the equivalent *radial* interval for each bin is

$$\Delta r_i = \frac{r_i(2^{1/3} - 1)2^{1/3}}{3^{1/3}} \tag{36}$$

where r_i is the radius for the ith size category. Accounting for the bin widths, the total aerosol size range that we treat extends from about 0.009 to 2.9 μm radius.

In our model, time is divided into discrete steps of τ seconds; τ is automatically increased or decreased during a computation according to the maximum rate of change among the gaseous species and aerosol particle concentrations; the same τ value is used in both the aerosol and gas phase segments of the model. In numerical form, the functional dependence of a variable on r, z, or t is replaced by the subscripts i, k, or superscript ℓ, respectively. Our solution scheme only requires that information be stored for two times, t and $t + \tau$, or equivalently, ℓ and $\ell + 1$; variables evaluated at $\ell + 1$ are, by a previous definition, implicit ones. Our plan here is to utilize numerical "implicitness" wherever possible to achieve stability in our solutions, while still making the necessary adjustments to satisfy the conservation requirements imposed by the physics.

Analogous to the definitions of n, $\hat{n}$, u, and ε in the fourth section, The Aerosol Continuity Equation, we call n_{ik}^{ℓ}, $\hat{n}_{ik}^{\ell}$, u_{ik}^{ℓ}, and ε_{ik}^{ℓ} the solution droplet concentration (particles cm^{-3}), condensation nuclei concentrations (particles cm^{-3}), droplet core volume (μm^3 cm^{-3}), and core volume second moment (μm^6 cm^{-3}), respectively, in the radial (or volume) size interval i at altitude level k at time ℓ. Hence, for the size-altitude bin (i,k), n_{ik}^{ℓ} is a size-integrated, height-averaged, instantaneous value of $n(r,z,t)$, while u_{ik}^{ℓ} and ε_{ik}^{ℓ} are the corresponding (total) core volume moments for the droplets in that bin.

In the following development we limit our discussion, for the most part, to the continuity equation for the aerosol droplets, recognizing that there is a set of parallel relations for the condensation nuclei and the core volume moments.

The Numerical Treatment of Particle Growth

To obtain numerical solutions of the aerosol continuity equations, we utilize a "discrete" particle formulation for droplet growth and coagulation. The discrete approximation assumes that all of the particles in a given size bin have the same volume and physical properties; that is, that the particle distribution consists of a series of sharp spikes at the bin centers (in volume coordinates). To display the equivalent continuous particle size spectrum, the total number of particles in a bin can be uniformly spread across the bin.

We have also investigated two other numerical approaches. In one, the particles in a bin are assigned a specific size distribution (e.g., uniform apportionment across a bin), and particle growth (and coagulation) rates are computed from the integro-differential expressions for these processes by insertion of the fixed size distribution. In the second approach, the particle size spectrum is assumed to be continuous over the entire particle size range of interest, and the radial derivatives and integrals are calculated using differencing and quadrature schemes appropriate for a grid of points centered in the size bins; in this case, only the size distribution values at the grid points are computed.

For droplet growth, we have modified the discrete formulation using elements of the continuous distribution technique — this was done to limit numerical diffusion in the growth solutions. In the discrete formulation, we calculate the rate of volume addition (by condensation) to the particles in a certain size bin, and transfer some of these particles to the next largest size bin to account for this volume accretion. An accurate estimate of the total volume added to particles of all sizes is obtained by evaluating the growth integral

$$\frac{d\mathcal{V}}{dt} = \sum_i \frac{d\mathcal{V}_i}{dt} = \sum_i \int_{r_i}^{r_{i+1}} 4\pi r^2 n_{i,i+1}(r) g(r) dr \qquad (37)$$

where $\mathcal{V}$ is the total particulate volume per unit volume of air ($\mu m^3\ cm^{-3}$) and $n_{i,i+1}$ is a continuous particle size distribution (particles $cm^{-3}\ \mu m^{-1}$). In equation (37), we have divided the total particle size range (in our model) into radial intervals extending between bin centers; for example, from r_i to r_{i+1} (ignoring the small radial segments at the beginning and the end of the size range). We transfer particles from bin i to bin i+1 according to the rate that volume is added in the size interval r_i to r_{i+1}, that is, according to the magnitude of $d\mathcal{V}_i/dt$.

We approximate $n_{i,i+1}$ in each size interval by fitting it with a power law distribution,

$$n_{i,i+1}(r) = \mathring{n}_{i,i+1} \left(\frac{r_i}{r}\right)^{a_{i,i+1}} \tag{38}$$

During a time step at a given height, the constants $\mathring{n}$ and a in equation (38) are calculated using the initial particle bin concentrations n^{ℓ}_{ik} and $n^{\ell}_{i+1,k}$ in the following way; we adjust $\mathring{n}$ and a to simultaneously fit the total particle *surface areas* in bins i and i+1. Thus, we compute two integrals of the form,

$$4\pi r_i^2\ n^{\ell}_{ik} = \int_{\text{bin } i} 4\pi r^2 \mathring{n} \left(\frac{r_i}{r}\right)^a dr \tag{39}$$

and solve these for $\mathring{n}$ and a. Once $n_{i,i+1}(r)$ is determined, the rate of volume growth between bins i and i+1 is given by the $d\mathcal{V}_i/dt$ integral in equation (37), and the rate of particle transfer from bin i to bin i+1 by

$$\left.\frac{\partial n}{\partial t}\right)_{\substack{\text{growth} \\ i \to i+1}} = \frac{1}{V_i}\frac{d\mathcal{V}_i}{dt} \equiv \frac{n_i}{\tau_i} \tag{40}$$

If we adopt a constant average growth rate, $\bar{g}_i$, for the particles in the size interval r_i to r_{i+1}, we find from relations (37) to (39) that

$$\left.\begin{aligned} \frac{1}{\tau^{\ell}_{ik}} &= \bar{g}^{\ell}_{ik}\ \frac{3}{r_i}\left(\frac{2}{3}\right)^{\gamma^{\ell}_{ik}} \\ \gamma^{\ell}_{ik} &= \frac{\ell n\left(n^{\ell}_{ik}/n^{\ell}_{i+1,k}\right)}{\ell n\ 2} - \frac{2}{3} \end{aligned}\right\} \tag{41}$$

The use of $\bar{g}$ introduces a very small numerical dispersion into the particle growth solutions. We have imposed a constraint on the value of τ_i by choosing the maximum of the numbers (1) and (n_i/n_{i+1}) to evaluate γ_i in equation (41). We have done this to enhance the computational stability in the small particle size range.

The net rate of change of the particle concentration in bin i due to growth is the difference between the rates at which particles of size $i-1$ are entering bin i and particles of size i are leaving. Therefore, to complete our development of the discrete aerosol growth equation, we can combine the (logical) implicit numerical analogues of equation (40) for the size bins $i-1$ and i to obtain

$$\left.\frac{\partial n_{ik}^{\ell}}{\partial t}\right)_{\text{growth}} = \frac{n_{i-1,k}^{\ell+1}}{\tau_{i-1,k}^{\ell}} - \frac{n_{ik}^{\ell+1}}{\tau_{ik}^{\ell}} \tag{42}$$

There are similar growth equations for the core volume moments u and ε.

As we will show later, our treatment of particle growth effectively inhibits the artificial "numerical" diffusion (or rapid growth) of small droplets into large-size classes in our model solutions. Other workers have also addressed this problem (e.g., ref. 115), but their correction schemes are often difficult to apply or involve high-order nonimplicit differencing techniques. In the case of stratospheric aerosols, we always expect to have relatively smooth and continuous particle size distributions. Hence, the requirements on the growth solutions are less stringent than, for example, in a cloud-physics model where very steep size gradients exist, and so our correction scheme can be correspondingly simpler.

According to our previous discussion, the rate of volume addition to all of the droplets at height level k at time ℓ is given by

$$\frac{d\mathcal{V}_k^{\ell}}{dt} = \sum_i \frac{V_i n_{ik}^{\ell+1}}{\tau_{ik}^{\ell}} \tag{43}$$

In our finite difference solution, equation (43) — which becomes the numerical analog of equations (33) and (35) when transformed into H_2SO_4 molecule units — is used to couple the condensation of sulfuric acid vapor on particle surfaces to its gas phase photochemistry.

Our treatment of droplet evaporation is somewhat different from that of droplet growth. In this case, we calculate the time that it would take a droplet to evaporate to its average core size,

$$\tau_{ci} = \int_{r_i}^{r_{ci}} \frac{dr}{g} = \frac{r_i - r_{ci}}{|\bar{g}|_i} \tag{44}$$

where r_c is the average core radius. We use this time constant to estimate the rate at which droplets are being converted into activated cores (and therefore, condensation nuclei). The conversion rate turns out to be

$$\left(\frac{\partial n_{ik}^{\ell}}{\partial t}\right)_{evap.} = \frac{|\bar{g}_{i-1,k}^{\ell}|}{r_i}\left[1 - \left(f_{ik}^{\ell}\right)^{1/3}\right]^{-1} n_{ik}^{\ell+1} \tag{45}$$

where we have selected an average evaporation rate, $|\bar{g}_{i-1}|$, appropriate for the particle size increment to the next smallest size category (one-half of the droplet volume would be evaporated in this interval) and where f_{ik}^{ℓ} is the core volume fraction for the droplets, n_{ik}^{ℓ}. We have assumed that, in a short time interval, a few "average" droplets in a size bin evaporate all the way to their cores — rather than that all of the droplets in the bin evaporate to smaller size droplets. Moreover, we have assumed that, on the average, the sizes of individual droplet cores do not affect the overall rate of volume evaporation. Accordingly, we write the average loss rate of solution volume due to evaporation as:

$$\frac{d\mathcal{V}_k^{\ell}}{dt} = -\sum_i V_i\left(1 - f_{ik}^{\ell}\right)\left(\frac{\partial n_{ik}^{\ell}}{\partial t}\right)_{evap.} \tag{46}$$

Equation (46), which is analogous to equation (43), is used to calculate the net rate of release of H_2SO_4 molecules during droplet evaporation. It is obvious that our evaporation scheme is designed to conserve the number of cores and their total volume, as well as the mass of sulfuric acid, for a collection of evaporating droplets.

A more detailed evaporation scheme would allow droplets to evaporate into smaller size bins, carrying along the smaller cores and releasing the largest ones as condensation nuclei. Under stratospheric conditions, however, any acid solution droplets that are transported into a region where evaporation occurs will usually disappear very rapidly. In addition, since we do not know the exact size distribution of the cores within the droplets, it is difficult to determine accurately the fraction of the droplets that would release cores during an incremental decrease in the droplet size. Because a detailed evaporation treatment is too involved, we utilize the core volume moments, u_{ij}^{ℓ} and ε_{ik}^{ℓ}, to estimate the core size distribution and use this approximate distribution as a guide in placing evaporated cores into appropriate condensation nuclei size bins (see appendix B). In the numerical formulation of evaporation, as outlined in appendices B and C, we calculate the rates of production of various sizes of condensation nuclei from evaporating droplets — the $\hat{P}_{ik}^{\ell}$ for equation (32) — using the droplet evaporation rate from equation (45) and the core size distribution described in appendix B.

Since the vapor pressure of a droplet increases with decreasing radius (Kelvin effect), an environment which is only marginally supersaturated with H_2SO_4 may have the large particles growing while the small ones are evaporating. Under these conditions, special care must be taken in handling the particle growth rates for the size bins where the transition from growth to evaporation occurs.

The Numerical Solution for Particle Coagulation

Coagulation must be treated approximately in a numerical model because of the complexity of the integrals describing this process (see the discussion in appendix B). At the beginning of the subsection entitled The Numerical Treatment of Particle Growth, we mentioned three possible techniques which might be used to calculate particle coagulation rates: one technique is based on a discrete particle size spectrum and the other two employ continuous particle size distributions. For coagulation, these three numerical schemes lead to finite-difference equations having the same general form. Even so, the two techniques which assume continuous size distributions can have problems related to particle number and volume conservation. Actually, all three solutions give about the same results for the average rates of particle coagulation. Since the discrete formulation is much simpler to use, however, we have adopted it here; later we demonstrate that the discrete technique is also quite precise.

For each pair (i,j) of particle size bins in our model, a coagulation kernel is calculated at each height using the equations referred to in the subsection entitled Water Vapor Growth:

$$K_{ijk} \equiv K(r_i, r_j, z_k) = K_{jik} \tag{47}$$

The coagulation kernel is symmetric in the size indices i and j. The data tabulated in appendix A indicate that the coagulation kernels can vary up to 40% between adjacent size bins. Therefore, our numerical solutions of coagulation effects may contain some additional numerical dispersion due to our use of these average kernels.

In our discrete numerical formulation, we consider coagulation to be an interaction process between pairs of particles whose sizes are limited to a finite set of discrete values. Thus, instead of analyzing the continuous coagulation integrals, we proceed directly to a discrete analog of those integrals. Kritz (ref. 26) was one of the first workers to adopt geometrically increasing size bins to study discrete particle coagulation; this approach leads to some interesting numerical interpretations of the coagulation process. First consider the loss rate of particles of size i by coagulation with all other size droplets. Clearly, whenever a particle i collides with and adheres to a larger particle, particle i disappears from its own bin; the rate of disappearance is (suppressing the time and altitude variables):

$$\left.\frac{\partial n_i}{\partial t}\right)_{\substack{\text{coag.} \\ i,j>i}} = -K_{ij} n_i n_j \tag{48}$$

For encounters with smaller particles, however, the rate of removal of one i droplet from a size bin would require several sticking collisions with the smaller particles to add enough volume to make a particle of the next larger size; in fact, it would require V_i/V_j collisions. This is an interpretation of coagulation as a discrete growth mechanism. On the other hand, if we

consider the intermediate size coagulated particle composed of droplets i and j, we can subdivide it into a fraction V_j/V_i of an i+1 droplet and a fraction $(1 - V_j/V_i)$ of an i droplet. That is, a coagulation event which increases the volume of an i droplet by less than a discrete size increment can be interpreted as transferring only a fraction of the i droplet to the next size bin, while preserving particle number and volume in the process. In either case, the net rate of loss of droplets i by coagulation with smaller droplets is

$$\left.\frac{\partial n_i}{\partial t}\right)_{\substack{\text{coag.} \\ i,j \leqslant i}} = -K_{ij} n_i n_j (V_j/V_i) \tag{49}$$

For self-encounters, the kernel K_{ii} is not multiplied by a "symmetry" factor since the effect of counting self-collisions twice is already compensated in equation (49). Combining equations (48) and (49), the total loss rate of droplets i by coagulation is

$$\left.\frac{\partial n_i}{\partial t}\right)_{\substack{\text{coag.} \\ \text{loss}}} = -n_i L_i(\text{coag.})$$

$$= -n_i \left[\sum_{j \leqslant i} K_{ij} n_j (V_j/V_i) + \sum_{j>i} K_{ij} n_j \right] \tag{50}$$

Before proceeding, we point out that the coagulation terms all contain products of aerosol concentrations; we cannot easily solve the nonlinear finite-difference equations that result when each of the concentrations is evaluated implicitly at the time, $\ell+1$. Accordingly, we make the concentration products "implicitly" linear by evaluating n_i at $\ell+1$ and n_j at ℓ. (This mixing of time dependencies actually results in a more precise numerical solution than one which evaluates the coagulation rate at the beginning or the end of a computational step.) In finite difference form, the coagulation loss rate in equation (50) becomes,

$$\left.\frac{\partial n_{ik}^{\ell}}{\partial t}\right)_{\substack{\text{coag.} \\ \text{loss}}} = -n_{ik}^{\ell+1} L_{ik}^{\ell}(\text{coag.})$$

$$= -n_{ik}^{\ell+1} \left[\sum_{j \leqslant i} K_{ijk} n_{jk}^{\ell} (V_j/V_i) + \sum_{j>i} K_{ijk} n_{jk}^{\ell} \right] \tag{51}$$

The rate of production of particles $i+1$ by coagulation must equal the rate of loss of particles i in collisions with particles $j \leqslant i$; conversely, it must also equal the sum of the rates of loss of particles $j \leqslant i$ in collisions with particles i weighted by the volume factors V_j/V_i to account for the actual number of collisions which would be required to form a particle $i+1$. As before, an equivalent argument is based on the formation of an intermediate size coagulated droplet $i+j$ of which a fraction V_j/V_i is assigned to bin $i+1$. Following our convention for "implicitness," we can numerically calculate the coagulation production rate of particles $i+1$ as an average of the coagulation loss rates for particles i and for particles $j \leqslant i$, namely,

$$\left.\frac{\partial n^{\ell}_{i+1,k}}{\partial t}\right)_{\substack{\text{coag.}\\ \text{prod.}}} = P^{\ell}_{i+1,k}(\text{coag.}) \tag{52}$$

$$= \frac{1}{2} \sum_{j \leqslant i} K_{ijk}(V_j/V_i)\left(n^{\ell+1}_{ik} n^{\ell}_{jk} + n^{\ell}_{ik} n^{\ell+1}_{jk}\right)\theta_{ij}$$

with

$$\theta_{ij} = \begin{cases} 1 & i \neq j \\ \frac{1}{2} & i = j \end{cases} \tag{53}$$

The θ_{ij} factor is necessary to eliminate double summing when self-coagulation terms are evaluated. Equation (52) is balanced "implicitly" and, in conjunction with equation (51), conserves discrete droplet volume exactly.

We can include the effects of coagulation between condensation nuclei and aerosol droplets in our formulation once we make the following assumptions: (1) that nuclei are lost and droplets are formed during the coagulation process; (2) that the nucleus-droplet coagulation kernels are identical to those for droplet-droplet collisions (ignoring differences in the sticking efficiencies and particle densities); and (3) that each nucleus contributes its entire volume to the resulting droplet core. With these guidelines, we can derive the relations:

$$\left.\frac{\partial \hat{n}^{\ell}_{ik}}{\partial t}\right)_{\substack{\text{coag.}\\ \text{loss}}} = -\hat{r}^{\ell+1}_{ik} \sum_{\{\text{all } j\}} K_{ijk} n^{\ell}_{jk} \tag{54}$$

$$\left.\frac{\partial n^{\ell}_{ik}}{\partial t}\right)_{\substack{\text{coag.}\\ \text{loss}}} = -n^{\ell+1}_{ik}\left[\sum_{j \leqslant i} K_{ijk} \frac{V_j}{V_i}\left(n^{\ell}_{jk} + \hat{n}^{\ell}_{jk}\right) + \sum_{j > i} K_{ijk}\left(n^{\ell}_{jk} + \hat{n}^{\ell}_{jk}\right)\right] \tag{55}$$

$$\left.\frac{\partial n_{ik}^{\ell}}{\partial t}\right)_{\substack{\text{coag.}\\ \text{prod.}}} = \hat{n}_{ik}^{\ell+1} \sum_{j<i} K_{ijk}\left(1 - \frac{V_j}{V_i}\right) n_{jk}^{\ell} \tag{56}$$

$$\left.\frac{\partial n_{i+1,k}^{\ell}}{\partial t}\right)_{\substack{\text{coag.}\\ \text{prod.}}} = \frac{1}{2} \sum_{j\leq i} K_{ijk}\left(\frac{V_j}{V_i}\right)\left(n_{ik}^{\ell+1}\, n_{jk}^{\ell} + n_{ik}^{\ell} n_{jk}^{\ell+1} + n_{ik}^{\ell+1}\hat{n}_{jk}^{\ell}\right.$$

$$\left. + n_{ik}^{\ell}\hat{n}_{jk}^{\ell+1} + \hat{n}_{ik}^{\ell+1} n_{jk}^{\ell} + \hat{n}_{ik}^{\ell} n_{jk}^{\ell+1}\right)\theta_{ij} \tag{57}$$

Particle coagulation at any altitude must conserve the total particle volume. To check this in our equations, we compute, at altitude level k,

$$\left.\frac{\partial \mathscr{V}_k}{\partial t}\right)_{\text{coag.}} = \sum_i V_i \left(\frac{\partial n_{ik}}{\partial t} + \frac{\partial \hat{n}_{ik}}{\partial t}\right)_{\substack{\text{coag.}\\ \text{prod. + loss}}} \tag{58}$$

Accounting for the possible coagulation of particles out of the largest size bin, we can show, after some algebra, that the sum on the right is, as required, identically zero.

The effect of coagulation on the evolution of droplet core volume moments is discussed in appendix B. The resulting coagulation equations have the same general structure as those for the droplets. The radial boundary conditions for droplet growth, evaporation, and coagulation are described in appendix C.

The Numerical Treatment of Particle Transport

The sedimentation and diffusion terms in the aerosol continuity equation are handled as follows. The composite particle flux from equation (24) is numerically evaluated midway between altitude levels, for example, as

$$\phi^{SD}_{i,k+(1/2)} = -\frac{1}{h}\left(\frac{D_k D_{k+1}}{\gamma_k \gamma_{k+1} \mu_{ik} \mu_{i,k+1}}\right)^{1/2}\left(\gamma_{k+1}\mu_{i,k+1} n^{\ell+1}_{i,k+1} - \gamma_k \mu_{ik} n^{\ell+1}_{ik}\right) \tag{59}$$

Then we calculate the flux divergence,

$$\left.\frac{\partial n_{ik}^{\ell}}{\partial t}\right)_{\substack{\text{sed. +}\\ \text{diff.}}} = -\frac{1}{h}\left[\phi^{SD}_{i,k+(1/2)} - \phi^{SD}_{i,k-(1/2)}\right] \tag{60}$$

In equation (59), the expression for $D/\gamma\mu$ is a logarithmic interpolation to the midaltitude point. One can see by inspection that our transport formulation for sedimentation and diffusion conserves particle mass exactly in a vertical column (accounting for the boundary fluxes).

Some Additional Numerics

Water vapor growth, expressed by equations (28) and (29), can be analyzed in the same way as growth due to acid vapor condensation. If we calculate the rate of volume addition to the droplets in size bin i due to water vapor growth, using the assumption of a discrete particle size spectrum, and if we adopt a relation similar to equation (40) to describe the growth process, we can estimate the rate of particle transfer from bin i to bin $i+1$ using the time constant

$$\frac{1}{\tau^{H\ell}_{ik}} = \left[D \frac{d}{dz} \ell n(\rho W)\right]^{\ell}_{k} \left\{(1 - f_i) \frac{\partial}{\partial z} \ell n[\gamma\mu_i (1 - f_i) n_i]\right\}^{\ell}_{k} \left(\frac{2}{3}\right)^{\gamma^{\ell}_{ik}} \qquad (61)$$

where γ, defined in equation (41), limits numerical diffusion effects. The finite difference equivalent of equation (61), which we use in our model, except at the boundaries, is

$$\frac{1}{\tau^{H\ell}_{ik}} = \frac{D_k}{2h} \ell n\left(\frac{\rho_{k+1} W_{k+1}}{\rho_{k-1} W_{k-1}}\right)\left(1 - f^{\ell}_{ik}\right)\frac{1}{2h} \ell n \left[\frac{\gamma_{k+1}\mu_{i,k+1}\left(1 - f^{\ell}_{i,k+1}\right)n^{\ell}_{i,k+1}}{\gamma_{k-1}\mu_{i,k-1}\left(1 - f^{\ell}_{i,k-1}\right)n^{\ell}_{i,k-1}}\right]\left(\frac{2}{3}\right)^{\gamma^{\ell}_{ik}} \qquad (62)$$

The corresponding water vapor growth rate terms for u and ε are very similar to equation (62).

In connection with aerosol growth processes and our numerical analogs of them, we note that we have not written a separate continuity equation to keep track of the total mass of sulfuric acid within the aerosol solution droplets. Rather, we have carefully conserved the total droplet volume and core volume (and, hence, the acid solution volume) during each aerosol interaction. For proper H_2SO_4 conservation, this requires the inclusion of water vapor growth effects in our solutions. Because the water vapor growth effect is always small, however, we only need an approximate numerical representation for it — one such as equation (62) affords. In our model, we have also ignored water vapor growth in the upper and lower boundary layers ($k = 1$ and 30) and in regions where droplets are evaporating. The latter omission is justifiable because according to our model, aerosol droplets do not undergo large vertical displacements as they are evaporating (the evaporation rates above the aerosol layer are quite large).

The heterogeneous nucleation and washout rates in equations (16) and (30), respectively, can, quite simply, be replaced by their appropriate average values for each size-altitude bin; for example, $R^{N}_{ik} n^{\ell+1}_{ik}$. The particle

concentration in each case is evaluated implicitly at time $\ell+1$, which happens to couple the condensation nuclei and aerosol droplet continuity equations; a technique to solve the coupled equations simultaneously is given in appendix C. The heterogeneous nucleation rate R^N_{ik} is 1×10^{-6} sec^{-1} whenever the sulfuric acid supersaturation ratio $n_a/n_a{}^o$ is greater than 1 in the model; otherwise it is zero. The droplet washout rate is specified in equation (13).

Recapitulating our previous development, we can write the continuity equation for an evolving aerosol system in finite-difference form as,

$$\frac{n^{\ell+1}_{ik} - n^{\ell}_{ik}}{\tau} = R^N_{ik}\hat{n}^{\ell+1}_{ik} - R^W_{ik}n^{\ell+1}_{ik} - \left(\frac{1}{\tau^{\ell}_{ik}} + \frac{1}{\tau^{H\ell}_{ik}}\right)n^{\ell+1}_{ik} + \left(\frac{1}{\tau^{\ell}_{i-1,k}} + \frac{1}{\tau^{H\ell}_{i-1,k}}\right)n^{\ell+1}_{i-1,k}$$

$$+ P^{\ell}_{ik}(\text{coag.}) - n^{\ell+1}_{ik}L^{\ell}_{ik}(\text{coag.}) - \frac{1}{h}\left[-\frac{1}{h}\left(\frac{D_kD_{k+1}}{\gamma_k\gamma_{k+1}\mu_{ik}\mu_{i,k+1}}\right)^{1/2}\right.$$

$$\times\left(\gamma_{k+1}\mu_{i,k+1}n^{\ell+1}_{i,k+1} - \gamma_k\mu_{ik}n^{\ell+1}_{ik}\right) + \frac{1}{h}\left(\frac{D_kD_{k-1}}{\gamma_k\gamma_{k-1}\mu_{ik}\mu_{i,k-1}}\right)^{1/2}$$

$$\left.\times\left(\gamma_k\mu_{ik}n^{\ell+1}_{ik} - \gamma_{k-1}\mu_{i,k-1}n^{\ell+1}_{i,k-1}\right)\right] \qquad (63)$$

where we have replaced $\partial n/\partial t$ on the left-hand side of equation (14) by its numerical equivalent. There are similar equations for the condensation nuclei concentration and the core volume moments. Some details of a computer algorithm to solve these equations are given in appendix C.

MODEL VALIDATIONS AND SIMULATIONS

In this section we discuss, first, the numerical validation tests used to evaluate the accuracy and behavior of our model finite difference algorithms and, second, the ambient stratospheric aerosol simulations made for comparison to observational data. We have also summarized in tables 2 through 4 all of the major assumptions involved in the construction of our model.

Numerical Validation Tests

To validate the physical aerosol mechanisms as they are formulated in our model, several simple numerical calculations have been made. In each case, all aerosol processes except one are shut off and, under these controlled conditions, the resulting model prediction is compared to an "exact" analytical solution.

To obtain useful analytical solutions of the aerosol continuity equations (31) and (32), certain simplifying assumptions can be made. For example, at a fixed altitude in the sulfate layer we can consider the steady-state continuity equation (31) in the form

$$\frac{d}{dr}[g(r)n(r)] + \frac{n(r)}{\tau_R(r)} = P(r) \tag{64}$$

where τ_R(sec) is the local aerosol residence time – including the effects of sedimentation, diffusion, and coagulation – and P (droplets cm^{-3} sec^{-1}) is the local aerosol production rate, due to nucleation and coagulation, with possible contributions from other sources such as aircraft engines. The solution of equation (64) is

$$n(r) = n(r_o)\frac{g(r_o)}{g(r)}\exp\left(-\int_{r_o}^{r}\frac{dr'}{g\tau_R}\right) + \frac{1}{g(r)}\int_{r_o}^{r} dr''P(r'')\exp\left(-\int_{r''}^{r}\frac{dr'}{g\tau_R}\right) \tag{65}$$

An especially simple solution of equation (65) results when we set $P = 0$ and ignore the dependence of g and τ_R on particle radius; that is,

$$n(r) = n(r_o)\exp[-(r - r_o)/r_m] \tag{66}$$

where

$$r_m = g\tau_R \tag{67}$$

is the characteristic radius for this exponential size distribution. The predicted average particle size, in this case, is determined by the average radial growth that occurs during the droplet's residence time in the upper atmosphere.

A numerical aerosol growth experiment is illustrated in figure 8. In this calculation the number of particles in the first size bin is fixed (1 particle), a constant growth rate g of 0.5 μm yr^{-1} is specified, and all other aerosol interactions are deactivated except for an assumed removal process with an exponential lifetime τ_R of 0.2 yr. The corresponding numerical and theoretical steady-state particle distributions for these conditions are presented as curves at time $t = 0$ in figure 8; the analytical solution is represented by equations (66) and (67). The difference between the two solutions can be roughly interpreted as a 5% underestimate of the particle growth rate in the numerical simulation. This result should be compared to another model prediction obtained without a correction for numerical diffusion in the particle growth rates. In this instance, the large (~2.5 μm) particle concentrations were overestimated by several orders of magnitude. Numerical diffusion normally occurs because at each time step some of the particles in each size bin are allowed to grow across the entire bin. We have suppressed

numerical diffusion by limiting the number of these "fast-growing" particles – by carefully calculating the rate at which volume is being added to each bin (see A Numerical Representation of the Aerosol Continuity Equations).

When the droplet growth rate is doubled in our growth experiment, the ensuing development of the particle size distribution is that shown in figure 8. Our model solution for the time-dependent problem requires an average of only about 30 time steps per year. Note that the agreement between the analytical and numerical solutions is quite good, except for the very small systematic underestimate of the growth rate.

The results of the growth experiment clearly demonstrate that "numerical" diffusion is not polluting the large particle size range with artificially grown droplets in our model. We have also checked to see that the number of particles is conserved exactly during the growth process.

Figures 9 and 10 show the results of a particle coagulation experiment in which all of the other aerosol processes have been deactivated. Starting with one particle in the first size bin, we follow its coagulation history with our numerical coagulation scheme. Time is expressed in units of the characteristic coagulation time, τ_o (e.g., see ref. 116) and the experiment is continued for 10 time units. The coagulation time scales of importance to stratospheric aerosol problems are usually much less than 10 τ_o, since τ_o can be as long as several months in the lower stratosphere. For our calculation, only 20 equi-spaced time steps are taken for each unit of τ_o. By comparison to the exact solution of Smoluchowski (e.g., ref. 116), the model predictions in figure 9 are excellent. The data in figure 10 illustrate the corresponding development of the coagulation size spectrum and show that it is also in very good agreement with the exact Smoluchowski spectrum even after a long relaxation period. (The particle distributions in figure 10 are not *size* distributions, but are *bin-population* distributions for our geometric size bins. Accordingly, one of our size bins may contain a number of Smoluchowski bins – see fig. 7 – a fact we have taken into account in computing the equivalent Smoluchowski populations.)

To test our numerical formulation of sedimentation and diffusion, we have made the calculation shown in figure 11. In this experiment the atmosphere is assumed to have a constant scale height of 10 km, and both the settling velocity and diffusion coefficients are made inversely proportional to the air concentration. A point source of particles is placed at 20 km, and the aerosol concentration at 12 km is forced to be a very small value. All other particle interactions are turned off.

Analytical solutions for this problem can be obtained using a simplified version of the particle continuity equation (31) with only sedimentation and diffusion of a monodispersed aerosol, but with an added source of particles, Q (particles cm^{-3} sec^{-1}). The solution of the resulting steady-state equation gives the particle concentration profile,

$$n(z) = n(z_o) \frac{\gamma(z_o)}{\gamma(z)} \frac{\mu(z_o)}{\mu(z)} + \int_{z_o}^{z} \frac{\phi_p(z')}{D(z')} \frac{\gamma(z')\mu(z')}{\gamma(z)\mu(z)} dz' \qquad (68)$$

ϕ_p is the net (downward) particle flux (particles cm^{-2} sec^{-1}) which is related to the particle source Q by

$$\phi_p(z) = - \int_{z}^{\infty} Q(z')dz' \qquad (69)$$

For a point source of particles at a height z_p the particle mixing ratio $n\gamma$ decreases exponentially above z_p with a scale height D/v_s where v_s is the settling velocity. The analytical solutions for our settling experiment are plotted in figure 11 along with the model predictions for two different diffusion rates and two assumed particle sizes. Obviously, the numerical model gives a very accurate representation of one-dimensional aerosol transport processes.

Note in figure 11 that the vertical profile of the large (1.0 μm) particles is very sensitive to the vertical diffusion rate. Large particles might therefore be a useful tracer of vertical atmospheric motions. On the other hand, the steep vertical gradients in the large particle concentration profiles can lead to numerical diffusion errors in their solutions. In another experiment, where sedimentation and diffusion fluxes were calculated separately (i.e., without utilizing the combined flux of equation (24)), the predicted 1.0-μm particle concentrations at 30 km were overestimated by more than an order of magnitude. Obviously, our use of a combined particle flux (defined by eq. (24)) results in an overall diffusion-like transport process in which numerical diffusion effects are minimal.

The vertical dispersion of a narrow layer of aerosol particles due to the eddy diffusion coefficient in figure 3 is illustrated in figure 12. Starting with a concentration of the 100 particles cm^{-3} in the 2-km-thick altitude interval centered at 20 km, the particles are transported to other heights only by diffusion. We have verified that the diffusion process exactly conserves the total number of particles. Notice that the stratospheric residence time of the aerosol due to diffusion is about 2 to 3 years in this model, although it is obviously a function of the assumed eddy diffusion profile.

We have also checked the accuracy of the numerical algorithms in our model in other ways: by confirming that the coagulation process exactly conserves core mass and particle volume, that the overall atmospheric budget of sulfur atoms in gases and particles and of core material in nuclei and droplets correctly balances, and that the total number of nuclei and droplets is properly accounted for.

Numerical Model Simulations

We have made steady-state model predictions of the properties of the ambient stratospheric aerosol layer; these predictions of its characteristics are compared to experimental data in a series of figures (figs. 13 to 17). To make our calculations, we have used the aerosol model exactly as it is described in the preceding text. The values of the physical parameters and the techniques of numerical solution are those given in earlier sections of this paper and in the appendices.

Interestingly, even though we have not attempted to "tune" our model by varying any of the "adjustable" physical parameters — and there are many of them — the predictions for the five aerosol characteristics shown in figures 13 to 17 are reasonably good. We should also point out that there are many uncertainties in our calculations, as the comments in tables 2 through 4 indicate. Moreover, natural atmospheric variability and inhomogeneity make it difficult to compare steady-state, one-dimensional model predictions with a limited number of observational points. Nevertheless, the overall structure of the stratospheric aerosol layer is well established, and a one-dimensional model can be a useful diagnostic tool for studying the general properties of the layer. In NASA TP-1363, we present a detailed analysis of our model predictions in relation to the observed characteristics of the aerosol layer and the known physical processes of aerosol particles. In NASA TP-1363, we also give the results of a comprehensive study of the sensitivity of our model predictions to the uncertainties in the model parameters. Therefore, we will conclude this paper with only a brief description of the model calculations shown in figures 13 to 17.

The sulfate mass mixing ratios plotted in figure 13, for example, indicate that the model gives roughly the same amount of sulfate mass in the aerosol layer as has been observed. This result suggests that the stratospheric sulfur balance in our aerosol model is probably close to reality.

Predicted and measured total particle mixing ratios in the stratosphere are shown in figure 14. The scatter in the experimental data could be indicative of atmospheric variability, which might be partly related to the rate of vertical particle transport in this case; for Junge's data, the scatter is probably experimental. The steady-state model predictions presented here are believed to represent an average state for the ambient aerosol layer. However, we plan to study the effects of variability on the observable characteristics of the layer with our time-dependent model at a later date.

Figure 15 illustrates that our calculated concentrations of large particles (radii > 0.15 μm) are in accord with a number of stratospheric *in situ* measurements. Figure 16 shows that the concentration ratios of the large particles (those with radii > 0.15 μm to those with radii > 0.25 μm) are also in agreement with observations. In both cases, there is a substantial range of measured values, with the model calculation being generally representative of the data.

The computed stratospheric particle size distributions at 16 and 20 km are compared to several empirical size distributions in figure 17. The model reproduces the observed stratospheric aerosol zold size spectrum quite well.

To validate an aerosol model by comparing its predictions with atmospheric observations requires a diversified and high-quality data base. Unfortunately, existing aerosol data are not completely satisfactory for this purpose. In NASA TP-1363, therefore, we utilize our model to explore the possible experimental studies which might be most helpful to atmospheric scientists attempting to understand the origin and composition of the aerosol layer.

CONCLUSIONS

We have developed a new time-dependent, one-dimensional model of the terrestrial sulfate aerosol layer. Our model treats atmospheric photochemistry and aerosol physics in detail and includes the interaction between gases and particles explicitly. We have demonstrated that the numerical algorithms in our model are quite precise and have shown that the simulated aerosol physics generates a particle layer with most of the observed properties. In NASA TP-1363, we discuss at length the sensitivity of the calculated sulfate layer properties to changes in a large number of aeronomic and aerosol parameters.

Our model can predict almost all of the observable aerosol characteristics, including the height and shape of the layer, the total mass and number mixing ratios, the large particle mixing ratios, the small-to-large particle ratios, the acid solution droplet composition and size distributions, and the droplet core volumes. Moreover, it can simultaneously predict several measurable aeronomical quantities, such as the abundances of gaseous sulfur compounds in air, the vertical profiles of neutral trace constituents like methane and nitrous oxide, and the stratospheric residence times of gases and particles. As a result, the model calculations are highly constrained by data and are therefore useful for experimentation in parameter sensitivity.

Our aerosol model may be used in any one of several different computational modes: as a steady-state model to study average long-term aerosol characteristics or to perform aerosol sensitivity tests; as a time-dependent model to investigate perturbations of the sulfate layer (man-made or natural), short-time scale variability of the layer, or aerosol aging; or as a limited physical model, after some simple engineering alterations, to look at individual aerosol processes such as coagulation or growth, or to estimate the removal rates of particulate matter from the stratosphere. Our aerosol simulation has one severe limitation — it does not account for the horizontal spreading of gases and particles. We plan to correct this deficiency by developing a two-dimensional version of the present model based upon an existing two-dimensional model of stratospheric trace gases (e.g., see refs. 120 and 121). In the meantime we expect to apply our one-dimensional model to some unresolved aerosol-related problems including: the identification of the mechanisms that form stratospheric aerosol particles from gases and nuclei and which determine their eventual size spectrum; a clarification of the role of volcanoes and other sulfur sources in maintaining the sulfate layer; and an

estimation of the effect of man-made emissions of sulfur gases and solid particulates on the ambient aerosol layer.

Ames Research Center
National Aeronautics and Space Administration
Moffett Field, California 94035, November 29, 1978

APPENDIX A

PHYSICAL AEROSOL PARAMETERS

In this appendix we have tabulated values for several of the aerosol parameters discussed in the third section of this report, Physical Aerosol Processes. For sulfuric acid-water solution droplets of about 0.3 μm radius, table 5 lists the solution density, the equilibrium H_2SO_4 vapor concentration over the solution, and the weight percentage of H_2SO_4 in the solution at the altitude levels used in our model, up to a height of 40 km. The atmospheric temperatures in table 5 are taken from reference 96 for midlatitude spring/fall conditions and the water vapor concentrations from figure 4. Table 6 gives the values of the aerosol growth "kernel" g_{oa} (defined by eq. (3)) for the entire range of particle sizes used in our model and for altitudes up to 40 km. For brevity, only every third particle size has been selected for table 6 (and tables 7 and 8 as well). Droplet coagulation kernels at a height of 16 km are listed in table 7, and aerosol settling velocities are presented in table 8.

APPENDIX B

AEROSOL DROPLET CORES: THEIR SIZE DISTRIBUTION AND EFFECT ON AEROSOL BEHAVIOR

If we consider a collection of aerosol droplets that have identifiable cores, we can categorize the droplets by their total volume $v(\mu m^3)$ and their core volume $w(\mu m^3)$, where $w \leq v$. Likewise, we can define the droplet size distribution $\eta(v,w,t)$, where $\eta\, dv\, dw$ is the concentration of droplets per cubic centimeter of air whose volumes v lie in the range, v to $v + dv$, and whose core sizes w lie in the interval, w to $w + dw$, at time t; the units of η are particles $cm^{-3}\ \mu m^{-3}\ \mu m^{-3}$. (Note that the spatial dependence of η is suppressed and that particle volume rather than particle radius is used as a size coordinate. Because the transformation between volume and radius is straightforward, v and r are easily interchangeable size parameters in our equations.)

The aerosol variables employed in the text can be obtained from η by integration over core sizes:

$$n(v,t) = \int_o^v dw\ \eta(v,w,t) \tag{B1}$$

$$u(v,t) = \int_o^v dw\ w\ \eta(v,w,t) \tag{B2}$$

$$\varepsilon(v,t) = \int_o^v dw\ w^2 \eta(v,w,t) \tag{B3}$$

These equations define the total core volume "moments" u and ε.

We can readily formulate a continuity equation for the droplet distribution η; it will contain a rate term(s) for each physical aerosol process in our model. By taking the appropriate core volume moments of the η continuity equation, we can derive the continuity equations for n, u, and ε. The solutions of these equations are discussed at length in the text. Calculated values of u and ε are used to roughly characterize the droplet core size distribution; the manner in which this is done will be described shortly.

In the η continuity equation, we can show that the mathematical operators associated with particle growth, sedimentation, diffusion and washout all commute with the core volume moment integrals. As a result, the equivalent continuity equation terms for η, n, u, and ε are all similar, and the discussion of the n terms in the text can readily be generalized. However, we do have to consider more carefully the aerosol processes which are core dependent: that is, coagulation, which redistributes cores; water vapor growth, which depends on core fractions; and droplet evaporation, which is limited by core size.

DROPLET COAGULATION

As a starting point for our analysis of aerosol coagulation, we write the coagulation equation for droplets with cores,

$$\frac{\partial \eta(v,w,t)}{\partial t} = \frac{1}{2}\int_0^v dv' K(v', v - v') \int_0^{v'} dw' \eta(v',w',t)\eta(v - v', w - w', t)$$

$$- \eta(v,w,t) \int_0^{\infty} dv' K(v,v') \int_0^{v'} dw' \eta(v',w',t) \qquad \text{(B4)}$$

where K is the coagulation kernel. The limits on the dw' integration in the first term of equation (B4) must, in general, be modified to satisfy the following constraints on the core volumes:

$$\left.\begin{aligned} w' &\leqslant w \\ w - w' &\leqslant v - v' \end{aligned}\right\} \qquad \text{(B5)}$$

Equation (B4) is a generalization of the well-known integral equation describing particle coagulation. The 1/2 factor in the first term of equation (B4) arises because the integration over the entire range of dv' is found to count each pair of particle collisions exactly twice when one carries out the dw' integral indicated.

Taking the first three core volume moments (i.e., 1, w, w^2) of equation (B4), the time derivative and coagulation loss integral reduce to:

$$\frac{\partial}{\partial t}\begin{bmatrix} n(v,t) \\ u(v,t) \\ \varepsilon(v,t) \end{bmatrix} = -\begin{bmatrix} n(v,t) \\ u(v,t) \\ \varepsilon(v,t) \end{bmatrix} \int_0^{\infty} dv' K(v,v') n(v',t) \qquad \text{(B6)}$$

The coagulation production term, however, contains the core integrals,

$$\int_0^v dw \int_0^{v'} dw' w^m \eta(v',w',t)\eta(v - v', w - w', t) \qquad \text{(B7)}$$

with $m = 0,1,2$. Transforming the iterated integral (B7) to the variables $\{w';w'' = w - w'\}$ and using the fact that the physical limits on w' and w'' are 0 to v' and $v - v'$, respectively, expression (B7) becomes

$$\int_0^{v'} dw' \int_0^{v-v'} dw''(w' + w'')^m \eta(v',w',t)\eta(v - v', w'', t) \qquad \text{(B8)}$$

In this form, the core integrations can be factored, and the resulting coagulation production integrals for the core volume moments of interest are:

$$\frac{1}{2}\int_0^v dv'\, K(v',v-v') \begin{cases} n(v',t)n(v-v',t) \\ u(v',t)n(v-v',t) + u(v-v',t)n(v',t) \\ \varepsilon(v',t)n(v-v',t) + 2u(v',t)u(v-v',t) \\ \qquad + \varepsilon(v-v',t)n(v',t) \end{cases} \tag{B9}$$

The form of expressions (B9) indicates that we have to treat the coagulation terms for u and ε with special care in our numerical formulation (the coagulation terms for n are already developed in the text). Interestingly, the core volume moment equations are not coupled to higher order moments, and we can solve them without recourse to a closure approximation.

In a finite difference scheme which is based on a discrete set of droplet sizes, there is some ambiguity about the fate of the cores in coagulating droplets. Since our particle volumes double between size bins, several small droplets must, in general, coalesce to produce a droplet of the next largest discrete size; the resulting core is then composed of all the individual coagulated cores. However, a simpler, and more logical interpretation of core coagulation — which is also consistent with our discrete numerical treatment of droplet coagulation — takes into account only the rates at which pairs of particles are coagulating. In most cases, droplets of sizes i and $j \leq i$ coalesce into a particle whose volume $V_i + V_j$ is intermediate between the discrete sizes V_i and V_{i+1}. The average core volume (denoted here by W) in this intermediate droplet is given by

$$W = \frac{u_i}{n_i} + \frac{u_j}{n_j} \tag{B10}$$

In our droplet coagulation scheme, we divide such an intermediate size coagulated droplet into two fractional droplets of sizes i and $i+1$ (while conserving the total droplet volume and number — see the subsection, The Numerical Solution for Particle Coagulation, in the main body of the text). However, we now want to also specify that the average core volume fraction f for each of the droplet fragments should be the same as for the intermediate droplet. That is, we require

$$f = \frac{W}{V_i + V_j} = \frac{W_i}{V_i} = \frac{W_{i+1}}{V_{i+1}} \tag{B11}$$

where W_i and W_{i+1} are the volumes of the cores assigned to the fractional droplets. The requirement of a constant core volume fraction during coagulation is a constraint that can be justified by the following thought experiment. Assume that we have an initial ensemble of droplets, all with the same core fraction. Then, as the ensemble evolves by coagulation, every droplet must always have that same core fraction. Equation (B11) automatically satisfies this condition.

The rate of coagulation of the droplets i and j is $K_{ij}n_in_j$, but only a fraction, $\gamma_{ij} = V_j/V_i$, of a large droplet (i+1) will be formed by each coagulation. Accordingly, the rate of core volume transfer to the droplets of size i+1 is the product of W_{i+1}, $K_{ij}n_in_j$ and γ_{ij}, or

$$P_{i+1}(u)\Big|_{coag.} = \sum_{j\leq i} K_{ij}\left(\frac{2\gamma_{ij}}{1+\gamma_{ij}}\right)(u_in_j + u_jn_i)\theta_{ij} \qquad (B12)$$

where $\theta = 1$ except when $j = i$, in which case $\theta = 1/2$ (again, see The Numerical Solution for Particle Coagulation). Equation (B12) is the discrete analog of the core volume integral (B9). During coagulation, a fraction, $1 - \gamma_{ij}$, of an i droplet is also formed. This partly offsets the loss of the original i droplet which coagulated, but its core has been modified somewhat. The net core volume change in bin i is

$$P_i(u) - L_i(u) = \sum_{j\leq i} K_{ij}\left[\left(\frac{1-\gamma_{ij}}{1+\gamma_{ij}}\right)(u_in_j + u_jn_i) - u_in_j\right]$$

$$= \sum_{j\leq i} K_{ij}\left[\left(\frac{1-\gamma_{ij}}{1+\gamma_{ij}}\right)u_jn_i - \frac{2\gamma_{ij}}{1+\gamma_{ij}}u_in_j\right] \qquad (B13)$$

Equation (B13) shows that, because of core rearrangement, the coagulation of droplets i and j leads to the transfer of core volume from droplets j to droplets i at the rate

$$\Delta P_i(u)\Big|_{coag.} = \sum_{j\leq i} K_{ij}\left(\frac{1-\gamma_{ij}}{1+\gamma_{ij}}\right)u_jn_i \qquad (B14)$$

Moreover, core rearrangement also alters the net rate at which droplets i lose core volume by direct coagulation; without rearrangement, the direct loss rate (the u_i term in eq. (B13)) would be $K_{ij}\gamma_{ij}u_in_j$. For the smaller droplets j, however, the direct core loss rate (eq. (B6)) is unchanged and there is no core rearrangement. By summing the core volume production and loss terms for the droplets j, i, and i+1, it can be shown that the total core volume will be conserved during coagulation.

Our coagulation scheme attempts to follow the evolution of the cores within a collection of droplets of discrete size. Because of the finite width of the droplet size bins, it is reasonable to assume that collisions between the particles in a small bin and those in a large bin will affect the distribution of the cores in the larger bin; that is, that some of the collisions will produce droplets with a modified core structure within the boundaries of the larger bin. Our numerical approach to droplet coagulation, as outlined above, is actually a discrete representation of the exact coagulation integral

(B9) — one that is limited, however, by the lack of a clear definition of the droplet size distribution in each finite size bin.

The effect of coagulation on the second core volume moment ε is calculated in a manner similar to that used to calculate the first core volume moment u; that is, for which we utilized equations (B10) and (B11) to derive (B12) and (B13). Now, though, we require that subdivided droplets have a constant average second core volume moment fraction $\overline{f^2}$,

$$\overline{f^2} \equiv \frac{\varepsilon_i/n_i + 2(u_i/n_i)(u_j/n_j) + \varepsilon_j/n_j}{(V_i + V_j)^2} = \frac{\overline{W_i^2}}{V_i^2} = \frac{\overline{W_{i+1}^2}}{V_{i+1}^2} \tag{B15}$$

where $\overline{W_i^2}$ and $\overline{W_{i+1}^2}$ are the core volume second moments assigned to the subdivided droplets. Equation (B15), combined with (B11), results in a fixed relative core volume variance for the droplets that are fractionated from intermediate-size coagulated particles. This assumption leads directly to the second core volume moment coagulation production rates:

$$P_{i+1}(\varepsilon)\Big|_{\text{coag.}} = \sum_{j<i} K_{ij} \frac{4\gamma_{ij}}{(1 + \gamma_{ij})^2} (\varepsilon_i n_j + 2u_i u_j + \varepsilon_j n_i)\theta_{ij} \tag{B16}$$

and

$$\Delta P_i(\varepsilon)\Big|_{\text{coag.}} = \sum_{j<i} K_{ij} \left[\frac{1 - \gamma_{ij}}{(1 + \gamma_{ij})^2}\right] (\varepsilon_j n_i + 2u_j u_i) \tag{B17}$$

We also have the net core volume second moment loss rate for droplets of size i due to coagulation,

$$L_i(\varepsilon)\Big|_{\text{coag.}} = -K_{ij} \left[\frac{\gamma_{ij}(3 + \gamma_{ij})}{(1 + \gamma_{ij})^2}\right] \varepsilon_i n_j \tag{B18}$$

The core volume moment coagulation terms ((B12), (B13), and (B16)-(B18)) can be put in a semi-implicit numerical form similar to that of the droplet coagulation terms in the subsection, The Numerical Solution for Particle Coagulation; this can be done so that core volume is conserved exactly, and so that the core volume product $u_i u_j$ in the second moment equations (B16) and (B17) is not implicitly coupled to the first moment equation (this allows a simultaneous finite-difference solution for n, u, and ε).

For the coagulation of condensation nuclei with aerosol droplets, the related coagulation terms for u and ε are similar to those already given, except that for nuclei, $u_i = n_i V_i$ and $\varepsilon_i = n_i V_i^2$. Moreover, the coagulation of a nucleus with a droplet is assumed to form only a larger droplet. We will not write out all of the lengthy numerical coagulation expressions here.

DROPLET WATER VAPOR GROWTH

Droplet cores have a definite role in limiting the extent of water vapor growth that occurs when droplets move between physical environments. Equation (8) in the main body of the report indicates that a droplet with a fixed core size will move along a trajectory in $v - z$ space such that

$$\phi_v = \frac{dv}{dz}\,\phi_z \tag{B19}$$

where the ϕ's are particle fluxes. In the aerosol continuity equation, the calculation of the total particle flux divergence in $v - z$ space leads to

$$\left.\frac{\partial n(v,w,z,t)}{\partial t}\right|_{\substack{\text{transport +}\\ H_2O \text{ growth}}} = -\frac{\partial \phi}{\partial z} - \frac{\partial}{\partial v}\left(\frac{dv}{dz}\,\phi\right) \tag{B20}$$

where ϕ now represents just the vertical particle flux, which is defined by equation (24) in the text (but now has the units, particles cm^{-2} sec^{-1} μm^{-3} μm^{-3}). For a given droplet core size, the volume divergence term in equation (B20), which describes water vapor growth, can be written as

$$\left.\frac{\partial n(v,w,z,t)}{\partial t}\right|_{\substack{H_2O\\ \text{growth}}} = -\frac{\partial}{\partial v}\left\{-v\left[\frac{d}{dz}\,\ell n(\rho W)\right]\left(\phi - \frac{w}{v}\,\phi\right)\right\} \tag{B21}$$

Integrating equation (B21) over all the core sizes, we obtain:

$$\left.\frac{\partial n(v,z,t)}{\partial t}\right|_{\substack{H_2O\\ \text{growth}}} = -\frac{\partial}{\partial v}\left\{-v\left[\frac{d}{dz}\,\ell n(\rho W)\right]\left[\phi(n) - \frac{\phi(u)}{v}\right]\right\} \tag{B22}$$

where $\phi(u)$ is the vertical core volume flux (μm^3 cm^{-2} sec^{-1} μm^{-3}).

The corresponding results for u and ε are easily derived. and are:

$$\left.\frac{\partial u(v,z,t)}{\partial t}\right|_{\substack{H_2O\\ \text{growth}}} = -\frac{\partial}{\partial v}\left\{-v\left[\frac{d}{dz}\,\ell n(\rho W)\right]\left[\phi(u) - \frac{\phi(\varepsilon)}{v}\right]\right\} \tag{B23}$$

and

$$\left.\frac{\partial \varepsilon(v,z,t)}{\partial t}\right|_{\substack{H_2O\\ \text{growth}}} = -\frac{\partial}{\partial v}\left\{-v\left[\frac{d}{dz}\,\ell n(\rho W)\right]\left[\phi(\varepsilon) - \frac{\phi(\pi)}{v}\right]\right\} \tag{B24}$$

where π is the third core volume moment.

Obviously, we require a closure relation for π to solve these equations. In our model, we only require a value for ε in the regions of the atmosphere where droplets are evaporating; that is, high in the stratosphere where water-vapor growth effects are small (because the product ρW is nearly constant with height there). To be consistent with the core evaporation routine that is outlined in the following section, we achieve closure by assuming a log-normal core size distribution (see eq. (B26) below) which leads to an approximation for π,

$$\pi = \frac{n\varepsilon^3}{u^3} = \varepsilon v \frac{\overline{(f^2)}^2}{f^3} \tag{B25}$$

Equation (B25) may be substituted into equation (B24).

DROPLET EVAPORATION

When droplets evaporate they release their cores. In equation (45) we determine the rate at which cores of all sizes evaporate from droplets of size i; let us call this rate q_i (cores cm^{-3} sec^{-1}). We assume that all cores regardless of size are released at the same rate; hence, the size distribution of any collection of incrementally evaporated cores is the same as that of the cores left in the droplets. To describe the sizes of the cores inside the droplets of size i, we have chosen a particular log-normal probability distribution,

$$\psi_i(w)dw = \psi_{oi} w^{-3/2} \exp\left[\frac{-\ell n^2(w/W_i)}{2\ \ell n^2\ \sigma_i}\right] dw \tag{B26}$$

where ψ_{oi} is a normalization constant, W_i is the average size of the cores in the droplets, and σ_i is the core volume variance given by

$$2\ \ell n^2\ \sigma_i = 4\ \ell n\left(\frac{n_i \varepsilon_i}{u_i^2}\right) \tag{B27}$$

The cores that are evaporating from droplets of size i must be allotted to condensation nuclei volume bins, $m \leq i$. Our geometric size bins have equal log-volume spacing. Accordingly, we can estimate the relative probability that an evaporated core is of size m by using

$$\psi_{im} = \psi_{oi} V_m^{-1/2} \exp\left[\frac{-\ell n^2(V_m/W_i)}{2\ \ell n^2\ \sigma_i}\right] \tag{B28}$$

We want to conserve the number and volume of cores exactly during evaporation, so we proceed as follows. We divide the accessible core bins into large and

small sizes using the average core volume W_i as a demarcation point; that is, we determine m_{io} where

$$V_{m_{io}} \leq W_i < V_{m_{io}+1} \tag{B29}$$

Then we renormalize the probability distributions for the large and small core sizes independently,

$$\psi_{im} \Rightarrow \begin{cases} \psi_{im} \Big/ \sum_{m=1}^{m_{io}} \psi_{im}, & m \leq m_{io} \\ \psi_{im} \Big/ \sum_{m=m_{io}+1}^{i} \psi_{im}, & m > m_{io} \end{cases} \tag{B30}$$

and calculate the average large and small core volumes W_{Li} and W_{Si}, respectively, as, for example,

$$W_{Si} = \sum_{m=1}^{m_{io}} V_m \psi_{im} \tag{B31}$$

These volumes satisfy the inequality,

$$W_{Si} \leq W_i < W_{Li} \tag{B32}$$

Next, we define the volume fractions,

$$\begin{aligned} \nu_{Li} &= \frac{W_i - W_{Si}}{W_{Li} - W_{Si}} \\ \nu_{Si} &= 1 - \nu_{Li} \end{aligned} \tag{B33}$$

which we use with the renormalized probabilities ψ_{im} to compute the condensation nuclei production rates:

$$\Delta\hat{P}_m^{(i)} = \begin{cases} q_i \nu_{Si} \psi_{im}, & m \leq m_{io} \\ q_i \nu_{Li} \psi_{im}, & m > m_{io} \end{cases} \tag{B34}$$

Finally, we sum over all evaporating droplet sizes i to obtain the total nuclei production rates in each size category m.

To test the accuracy of our core evaporation algorithm, we have made several model calculations in which coagulation is omitted, and the gravitational settling velocity is made independent of particle size. Under these conditions the nucleation, growth, sedimentation, diffusion, rainout, and evaporation of droplets should not affect the size distribution of the total ensemble of cores at each altitude; that is, if we take the droplets at any height and evaporate them, the resulting collection of cores, when combined with the surrounding condensation nuclei, should have the same size distribution as the condensation nuclei at the ground. Accordingly, the predicted size spectrum of the condensation nuclei in the evaporation regime above the aerosol layer should reproduce the nuclei size distribution at the ground.

The results of our calculations for several different assumed condensation nuclei distributions at the ground are given in figure 18. The model predictions are obviously in excellent agreement with the expected values. In the monodispersed case, less than one core in 10^{13} has leaked outside the original 0.1-μm size bin. Curve "d" of figure 18 shows the effects of coagulation and differential sedimentation on the core size distribution. On the average, droplet coagulation leads to bigger cores in the small size range, while gravitational settling effectively depletes the cores in the large-size range.

APPENDIX C

A SOLUTION OF THE AEROSOL FINITE DIFFERENCE EQUATIONS

In this appendix we outline a numerical scheme to solve the finite difference continuity equations (63), which describe the evolution of aerosol particle concentrations. Some general comments about this scheme are in order. The equations for $n_{ik}^{\ell+1}$ (or $u_{ik}^{\ell+1}$ or $\varepsilon_{ik}^{\ell+1}$) as they are developed in the text, contain only the implicit concentrations of the smaller size acid droplets and of the same size condensation nuclei. The equations for the condensation nuclei contain nucleation, coagulation, and transport terms, as well as a production term due to droplet evaporation. If we treat this latter term as a source of condensation nuclei, a source that is fixed at the beginning of a time step, we can decouple the nuclei equations from the droplet and core volume moment equations. In this case, the solution strategy at each time step is to first solve the condensation nuclei continuity equation and then solve, in the order of increasing particle sizes, the aerosol droplet and core volume moment equations simultaneously, utilizing the nuclei concentrations already calculated to evaluate implicitly nucleation and coagulation terms. The rates of production of nuclei by droplet evaporation can then be computed for the start of the next time-step cycle using the implicit core volume moments, $u^{\ell+1}$ and $\varepsilon^{\ell+1}$, to determine the evaporated core size spectrum.

An alternative scheme is a sequential solution of the aerosol continuity equations, in which the variables are solved in the order $\hat{n}$-n-u-ε. The sequential approach has an advantage in that it allows more symmetry to be used in the implicit finite difference terms, particularly those terms describing core coagulation and water vapor growth, but it has a disadvantage in that it is more lengthy and costly.

The finite-difference equations for aerosol droplet concentrations (or for condensation nuclei concentrations or core volume moments) may all be written in the general form:

$$A_{ik} n_{i,k+1}^{\ell+1} + B_{ik}^{\ell} n_{ik}^{\ell+1} + C_{ik} n_{i,k-1}^{\ell+1} = D_{ik}^{\ell} \tag{C1}$$

(where D_{ik}^{ℓ} is not to be confused with a diffusion coefficient). Our solution of these equations is based on the fact that for a given size category i the system of equations (C1) can be represented by a tridiagonal matrix coupling together the aerosol number densities at different altitude levels k. We solve for the aerosol number densities by inverting the matrix (e.g., ref. 122). First, we define a relationship which couples the concentrations at adjacent altitude levels,

$$n_{ik}^{\ell+1} = E_{ik}^{\ell} - F_{ik}^{\ell} n_{i,k+1}^{\ell+1} \tag{C2}$$

Next, using equations (C1) and (C2), we derive the recursion formulas,

$$E_{ik}^{\ell} = \frac{D_{ik}^{\ell} - C_{ik}E_{i,k-1}^{\ell}}{B_{ik}^{\ell} - C_{ik}F_{i,k-1}^{\ell}}$$

$$F_{ik}^{\ell} = \frac{A_{ik}}{B_{ik}^{\ell} - C_{ik}F_{i,k-1}^{\ell}} \qquad \text{(C3)}$$

The lower boundary conditions are applied to determine E_{i1} and F_{i1} which, together with equations (C3), are used to calculate the E and F values at the higher altitude levels, $k > 1$. The upper boundary conditions are combined with the computed values of E and F for that level to determine $n_{i\kappa}^{\ell+1}$ (where $k = \kappa$ denotes the uppermost model level). Finally, working downward, the $n_{ik}^{\ell+1}$ are calculated in descending order using equation (C2) and the known E and F coefficients.

The lower boundary condition in our model is a fixed concentration of condensation nuclei in each size bin and a removal flux of aerosol droplets. In the former case, we have

$$E_{i1}^{\ell} = \hat{n}_{io}$$

$$F_{i1}^{\ell} = 0 \qquad \text{(C4)}$$

where $\hat{n}_{io}$ is the fixed nuclei abundance.

For aerosol droplets, on the other hand, we define an escaping flux,

$$\phi_{io} = \phi_{i1}^{S} - v_B n_{i1}^{\ell+1} \qquad \text{(C5)}$$

The first component of ϕ_{io} is a sedimentation flux, and the second is a surface recombination flux (nominally, $v_B = 1$ cm sec^{-1} in our calculations). The flux given by equation (C5) can be substituted into the aerosol continuity equation (63) to derive the appropriate values of E_{i1}^{ℓ} and F_{i1}^{ℓ} for the droplets.

At the upper boundary of the model, we specify zero fluxes for all of the particles.

In our calculations we assume that there are no particles smaller than our smallest size bin, and hence there is no growth or coagulation into the smallest size bin. We also prevent particles from growing or coalescing out of the largest size bin, although this mass flow would be negligible anyway.

The finite-difference aerosol equations are connected to the gaseous photochemical equations by H_2SO_4 condensation and evaporation; the mathematical connection is made through equations (34) and (35). The numerical analogs of the sulfuric acid production and loss rates in equation (35) are formally related to equations (43) and (46). A model calculation normally proceeds as follows: For each time step, the evolving H_2SO_4 vapor concentrations are computed using our photochemistry module which includes sulfuric acid condensation and evaporation rates based on the aerosol droplet concentrations at the start of the step. The new H_2SO_4 concentrations are then used to calculate the aerosol droplet formation and growth rates, and the continuity equations for the aerosol droplets, condensation nuclei, and core volume moments are solved over the same time interval. The numerical cycle is repeated until the desired simulated time has elapsed.

REFERENCES

1. Junge, Christian E.; Chagnon, Charles W.; and Manson, James E.: Stratospheric Aerosols. J. Meteorol., vol. 18, no. 1, Feb. 1961, pp. 81-108.

2. Lamb, H. H.: Volcanic Dust in the Atmosphere, with a Chronology and Assessment of its Meteorological Significance. R. Soc. London Phil. Trans. A, vol. 266, no. 1178, July 1970, pp. 425-533.

3. Pollack, James B.; Toon, Owen B.; Sagan, Carl; Summers, Audrey; Baldwin, Betty; and Van Camp, Warren: Volcanic Explosions and Climatic Change: A Theoretical Assessment. J. Geophys. Res., vol. 81, no. 6, Feb. 1976, pp. 1071-1083.

4. Pollack, James B.; Toon, Owen B.; Summers, Audrey; Baldwin, Betty; Sagan, Carl; and Van Camp, Warren: Stratospheric Aerosols and Climatic Changes. Nature, vol. 263, no. 5578, Oct. 1976, pp. 551-555.

5. Cadle, R. D.; and Grams, G. W.: Stratospheric Aerosol Particles and Their Optical Properties. Rev. Geophys. Space Phys., vol. 13, no. 4, Aug. 1975, pp. 475-501.

6. Cadle, Richard D.; Crutzen, P.; and Ehhalt, Dieter: Heterogeneous Chemical Reactions in the Stratosphere. J. Geophys. Res., vol. 80, no. 24, Aug. 1975, pp. 3381-3385.

7. Käselau, K. H.; Fabian, P.; and Röhrs, H.: Measurements of Aerosol Concentration up to a Height of 27 km. Pure and Appl. Geophys., vol. 112, 1974, pp. 877-885.

8. Laby, Jean; Rosen, J. M.; and Hofmann, D. J.: Stratospheric Aerosol Measurements. III: Optical Model Calculations. J. Atmos. Sci., vol. 33, no. 2, Feb. 1976, pp. 304-314.

9. Hofmann, D. J.; Rosen, J. M.; Pepin, T. J.; and Pinnick, R. G.: Stratospheric Aerosol Measurements. I: Time Variations at Northern Mid-Latitudes. J. Atmos. Sci., vol. 32, no. 7, July 1975, pp. 1446-1456.

10. Hofmann, D. J.; Rosen, J. M.; Kiernan, J. M.; and Laby, Jean: Stratospheric Aerosol Measurements. IV: Global Time Variations of the Aerosol Burden and Some Considerations. J. Atmos. Sci., vol. 33, no. 8, Sept. 1976, pp. 1782-1788.

11. Rosen, J. M.; Hofmann, D. J.; and Laby, Jean: Stratospheric Aerosol Measurements. II. The Worldwide Distribution. J. Atmos. Sci., vol. 32, no. 7, July 1975, pp. 1457-1462.

12. Ferry, Guy V.; and Lem, Homer Y.: Aerosols at 20 kilometers Altitude. Second International Conference on the Environmental Impact of Aerospace Operations in the High Atmosphere, July 8-10, 1974; published by the American Meteorological Society, Boston, Mass., pp. 27-33.

13. Bigg, E. K.: Stratospheric Particles. J. Atmos. Sci., vol. 32, no. 5, May 1975, pp. 910-917.

14. Lazrus, A. L.; and Gandrud, B. W.: Stratospheric Sulfate Aerosol. J. Geophys. Res., vol. 79, no. 24, Aug. 1974, pp. 3424-3431.

15. Castleman, A. W., Jr.; Davis, Richard E.; Munkelwitz, H. R.; Tang, I. N.; and Wood, William P.: Kinetics of Association Reactions Pertaining to H_2SO_4 Aerosol Formation. Proceedings of the Symposium on Chemical Kinetics Data for the Upper and Lower Atmosphere, Int. J. Chem. Kin. Symposium, vol. 1, 1975, pp. 629-40.

16. Pepin, T. J.; and McCormick, M. P.: Observations of Stratospheric Aerosols from the Apollo-Soyuz Test Project (A.S.T.P.), Proceedings of the Symposium on Radiation in the Atmosphere, H.-J. Bolle, ed., at IAMAP Radiation Symposium, Garmisch-Partenkirchen, Germany, Aug. 1976, Science Press, Princeton, N.J., pp. 151-152.

17. Russell, Philip B.; and Hake, Richard D., Jr.: The Post-Fuego Stratospheric Aerosol: Lidar Measurements, with Radiative and Thermal Implications. J. Atmos. Sci., vol. 34, no. 1, Jan. 1977, pp. 163-177.

18. Fernald, F. G.; and Schuster, B. G.: Wintertime 1973 Airborne Lidar Measurements of Stratospheric Aerosols. J. Geophys. Res., vol. 82, no. 3, Jan. 1977, pp. 433-437.

19. Hofmann, D. J.; and Rosen, J. M.: Balloon Observations of the Time Development of the Stratospheric Aerosol Event of 1974-1975. J. Geophys. Res., vol. 82, no. 9, Mar. 1977, pp. 1435-1440.

20. Friedlander, S. K.: Theoretical Considerations for the Particle Size Spectrum of the Stratospheric Aerosol. J. Meteorol., vol. 18, no. 6, Dec. 1961, pp. 753-759.

21. Martell, E. A.: The Size Distribution and Interaction of Radioactive and Natural Aerosols in the Stratosphere. Tellus, vol. 18, no. 2-3, 1966, pp. 486-498.

22. Hunten, D. M.: Residence Times of Aerosols and Gases in the Stratosphere. Geophys. Res. Lett., vol. 2, no. 1, Jan. 1975, pp. 26-28.

23. Hofmann, D. J.; Carroll, D. E.; and Rosen, J. M.: Estimate of the Contribution of the Space Shuttle Effluent to the Natural Stratospheric Aerosol. Geophys. Res. Lett., vol. 2, no. 3, Mar. 1975, pp. 113-116.

24. Cadle, R. D.; Kiang, C. S.; and Louis, J.-F.: The Global Dispersion of the Eruption Clouds from Major Volcanic Eruptions. J. Geophys. Res., vol. 81, no. 18, June 1976, pp. 3125-3132.

25. Cadle, R. D.; Fernald, F. G.; and Frush, C. L.: Combined Use of Lidar and Numerical Diffusion Models to Estimate the Quantity and Dispersion of Volcanic Eruption Clouds in the Stratosphere: Vulcán Fuego, 1974, and Augustine, 1976. J. Geophys. Res., vol. 82, no. 12, Apr. 1977, pp. 1783-1786.

26. Kritz, Mark Alan: Formation Mechanisms of the Stratospheric Aerosol. Ph.D. dissertation, Yale University, 1975.

27. Burgmeier, J. W.; and Blifford, I. H., Jr.: A Reinforced Coagulation-Sedimentation Model for Stratospheric Aerosols. Water, Air, and Soil Poll., vol. 5, no. 2, Dec. 1975, pp. 133-147.

28. Rosen, J. M.; Hofmann, D. J.; and Singh, S. P.: A Steady-State Stratospheric Aerosol Model. J. Atmos. Sci., vol. 35, no. 7, July 1978, pp. 1304-1313.

29. Rosen, J. M.; and Hofmann, D. J.: Balloonborne Measurements of Condensation Nuclei. J. Appl. Meteor., vol. 16, no. 1, Jan. 1977, pp. 56-62.

30. Scott, W. D.; Lamb, D.; and Duffy, D.: The Stratospheric Aerosol Layer and Anhydrous Reactions Between Ammonia and Sulfur Dioxide. J. Atmos. Sci., vol. 26, no. 4, July 1969, pp. 727-733.

31. Friend, James P.; Leifer, Robert; and Trichon, Morris: On the Formation of Stratospheric Aerosols. J. Atmos. Sci., vol. 30, no. 3, Apr. 1973, pp. 465-479.

32. Davis, D. D.; and Klauber, Gary: Atmospheric Gas Phase Oxidation Mechanisms for the Molecule SO_2. Proceedings of the Symposium on Chemical Kinetics Data for the Upper and Lower Atmosphere, Int. J. Chem. Kin. Symposium, Vol. 1, 1975, pp. 543-556.

33. Crutzen, Paul J.: The Possible Importance of CSO for the Sulfate Layer of the Stratosphere. Geophys. Res. Lett., vol. 3, no. 2, Feb. 1976, pp. 73-76.

34. Hamill, P.: The Time Dependent Growth of H_2O-H_2SO_4 Aerosols by Heteromolecular Condensation. J. Aerosol Sci., vol. 6, no. 6, Nov. 1975, pp. 475-482.

35. Harrison, Halstead; and Larson, Timothy: The Oxidation of SO_2 in the Stratosphere. J. Geophys. Res., vol. 79, no. 21, July 1974, pp. 3095-3097.

36. Harker, Alan B.: The Formation of Sulfate in the Stratosphere Through the Gas Phase Oxidation of Sulfur Dioxide. J. Geophys. Res., vol. 80, no. 24, Aug. 20, 1975, pp. 3399-3401.

37. Toon, O. B.; Turco, R. P.; Hamill, P.; Kiang, C. S.; and Whitten, R. C.: The NASA-Ames Research Center Stratospheric Aerosol Model. II. Sensitivity Studies and Comparison with Observations. NASA TP-1363, 1979.

38. Butcher, Samuel S.; and Charlson, Robert J.: An Introduction to Air Chemistry. Academic Press, 1972, pp. 103-106.

39. Bach, Wilfrid: Global Air Pollution and Climatic Change. Rev. Geophys. Space Phys., vol. 14, no. 3, Aug. 1976, pp. 429-474.

40. Peyton, T. O.; Steele, R. V.; and Mabey, W. R.: Carbon Disulfide, Carbonyl Sulfide. Literature Review and Environmental Assessment. Stanford Res. Inst. Report 68-01-2940, Menlo Park, Calif., 1976. (Available from National Technical Information Services as PB-257947/2.)

41. Friend, James P.: The Global Sulfur Cycle. Chemistry of the Lower Atmosphere, S. I. Rasool, ed., Plenum Press, 1973, pp. 177-201.

42. Lovelock, J. E.; Maggs, R. J.; and Rasmussen, R. A.: Atmospheric Dimethyl Sulfide and the Natural Sulphur Cycle. Nature, vol. 237, no. 5356, June 1972, pp. 452-453.

43. Maroulis, Peter J.; and Bandy, Alan R.: Estimate of the Contribution of Biologically Produced Dimethyl Sulfide to the Global Sulfur Cycle. Science, vol. 196, no. 4290, May 1977, pp. 647-648.

44. Lovelock, J. E.: CS_2 and the Natural Sulphur Cycle. Nature, vol. 248, no. 5449, Apr. 1974, pp. 625-626.

45. Cadle, Richard D.: Volcanic Emission of Halides and Sulfur Compounds to the Troposphere and Stratosphere. J. Geophys. Res., vol. 80, no. 12, Apr. 1975, pp. 1650-1652.

46. Westenberg, A. A.; and deHaas, N.: Rate of the Reaction $OH + H_2S \rightarrow SH + H_2O$ Over an Extended Temperature Range. J. Chem. Phys., vol. 59, no. 12, Dec. 1973, pp. 6685-6686.

47. Kellogg, W. W.; Cadle, R. D.; Allen, E. R.; Lazrus, A. L.; and Martell, E. A.: The Sulfur Cycle. Science, vol. 175, no. 4022, Feb. 1972, pp. 587-599.

48. Dana, M. Terry; Hales, Jeremy M.; and Wolf, M. A.: Rain Scavenging of SO_2 and Sulfate from Power Plant Plumes. J. Geophys. Res., vol. 80, no. 30, Oct. 1975, pp. 4119-4129.

49. Stedman, D. H.; Chameides, W. L.; and Cicerone, R. J.: The Vertical Distribution of Soluble Gases in the Troposphere. Geophys. Res. Lett., vol. 2, no. 8, Aug. 1975, pp. 333-336.

50. Hidy, G. M.: Removal Processes of Gaseous and Particulate Pollutants. Chemistry of the Lower Atmosphere, S. I. Rasool, ed., Plenum Press, 1973, pp. 121-176.

51. Breeding, R. J.; Lodge, J. P.; Pate, J. B.; Sheesley, D. C.; Klonis, H. B.; Fogle, B.; Anderson, J. A.; Englert, T. R.; Haagenson, P. L.; McBeth, R. B.; Morris, A. L.; Pogue, R.; and Wartburg, A. F.: Background Trace Gas Concentrations in the Central United States. J. Geophys. Res., vol. 78, no. 30, Oct. 1973, pp. 7057-7064.

52. Graedel, T. E.; Kleiner, B.; and Patterson, G. C.: Measurements of Extreme Concentrations of Tropospheric Hydrogen Sulfide. J. Geophys. Res., vol. 79, no. 30, Oct. 1974, pp. 4467-4473.

53. Levy, Hiram, II: Photochemistry of the Troposphere. In Advances in Photochemistry, vol. 9, 1974, pp. 369-524. J. N. Pitts, George S. Hammond, and Klaus Gollnick, eds., John Wiley and Sons, New York.

54. Cox, R. A.; and Penkett, S. A.: The Photo-Oxidation of Sulfur Dioxide in Sunlight. Atmos. Env., vol. 4, no. 4, July 1970, pp. 425-433.

55. Jaeschke, W.; Schmitt, R.; and Georgii, H.-W.: Preliminary Results of Stratospheric SO_2-Measurements. Geophys. Res. Lett., vol. 3, no. 9, Sept. 1976, pp. 517-519.

56. Hanst, Philip L.; Speller, Lester L.; Watts, Donald M.; Spence, John W.; and Miller, Matthew F.: Infrared Measurements of Fluorocarbons, Carbon Tetrachloride, Carbonyl Sulfide, and Other Atmospheric Trace Gases. Air Pollution Control Assn. J., vol. 25, no. 12, Dec. 1975, pp. 1220-1226.

57. Sandalls, F. J.; and Penkett, S. A.: Measurements of Carbonyl Sulphide and Carbon Disulphide in the Atmosphere. Atmos. Env., vol. 11, no. 2, 1977, pp. 197-199.

58. Wood, William P.; and Heicklen, Julian: The Photooxidation of Carbon Disulfide. J. Phys. Chem., vol. 75, no. 7, Apr. 1971, pp. 854-860.

59. Rodhe, Henning: Measurements of Sulfur in the Free Atmosphere over Sweden 1969-1970. J. Geophys. Res., vol. 77, no. 24, Aug. 1972, pp. 4494-4499.

60. Stoiber, Richard E.; Leggett, David C.; Jenkins, Thomas F.; Murrmann, Richard P.; and Rose, William I., Jr.: Organic Compounds in Volcanic Gas from Santiaguito Volcano, Guatemala. Bull. Geol. Soc. Am., vol. 82, no. 8, Aug. 1971, pp. 2299-2302.

61. Molina, Mario J.; and Rowland, F. S.: Stratospheric Sink for Chlorofluoromethanes: Chlorine Atom-Catalyzed Destruction of Ozone. Nature, vol. 249, no. 5460, June 1974, pp. 810-812.

62. Davis, D. D.; Kelmm, R. B.; and Pilling, M.: A Flash Photolysis-Resonance Fluorescence Kinetics Study of Ground-State Sulfur Atoms: I. Absolute Rate Parameters for Reaction of $S(^3P)$ with $O_2(\Sigma)$. Int. J. Chem. Kin., vol. 4, no. 4, July 1972, pp. 367-382.

63. Schofield, Keith: Evaluated Chemical Kinetic Rate Constants for Various Gas Phase Reactions. J. Phys. Chem. Ref. Data, vol. 2, no. 1, 1973, pp. 25-84.

64. Davis, D. D.: A Kinetics Review of Atmospheric Reactions Involving H_xO_y Compounds. Can. J. Chem., vol. 52, no. 8, Apr. 1974, pp. 1405-1414.

65. Payne, W. A.; Stief, L. J.; and Davis, D. D.: A Kinetics Study of the Reactions of HO_2 with SO_2 and NO. J. Am. Chem. Soc., vol. 95, no. 23, Nov. 1973, pp. 7614-7619.

66. Moortgat, G. K.; and Junge, C. E.: The Role of the SO_2 Oxidation for the Background Stratospheric Sulfate Layer in the Light of New Reaction Rate Data. Pure and Appl. Geophys., vol. 115, no. 4, 1977, pp. 759-774.

67. Westenberg, A. A.; and deHaas, N.: Atom-Molecule Kinetics Using ESR Detection. V. Results for O + OCS, O + CS_2, O + NO_2 and H + C_2H_4. J. Chem. Phys., vol. 50, no. 2, Jan. 1969, pp. 707-719.

68. Golomb, D.; Watanabe, K.; and Marmo, F. F.: Absorption Coefficients of Sulfur Dioxide in the Vacuum Ultraviolet. J. Chem. Phys., vol. 36, no. 4, Feb. 1962, pp. 958-960.

69. Warneck, P.; Marmo, F. F.; and Sullivan, J. O.: Ultraviolet Absorption of SO_2: Dissociation Energies of SO_2 and SO. J. Chem. Phys., vol. 40, no. 4, Feb. 1964, pp. 1132-1136.

70. Chou, C. C.; Ruiz, H. V.; Moe, K.; and Rowland, F. S.: UV Absorption Cross Sections for OCS. Dept. of Chemistry, University of California (Irvine), 1976.

71. Breckenridge, W. H.; and Taube, Henry: Ultraviolet Absorption Spectrum of Carbonyl Sulfide. J. Chem. Phys., vol. 52, no. 4, Feb. 1970. pp. 1713-1715.

72. Atkinson, R.; and Pitts, J. N., Jr.: Rate Constants for the Reaction of $O(^3P)$ Atoms with SO_2(M=N_2O) over the Temperature Range 299-392 K. Chem. Phys. Lett., vol. 29, no. 1, Nov. 1974, pp. 28-30.

73. Westenberg, A. A.; and deHaas, N.: Rate of the Reaction $O + SO_2 + M \rightarrow SO_3 + M$. J. Chem. Phys., vol. 63, no. 12, Dec. 1975, pp. 5411-5415.

74. Krezenski, David C.; Simonaitis, R.; and Heicklen, Julian: The Reactions of $O(^3P)$ with Ozone and Carbonyl Sulfide. Int. J. Chem. Kin., vol. 3, no. 5, Sept. 1971, pp. 467-482.

75. Inn, Edward C. Y.: Absorption Coefficients for HCl in the Region 1400-2200Å. J. Atmos. Sci., vol. 32, no. 12, Dec. 1975, pp. 2375-2377.

76. Ackerman, M.: Ultraviolet Solar Radiation Related to Mesospheric Processes. ESLAB/ESRIN Symposium on Mesospheric Models and Related Experiments, G. Fiocco, ed., Reidel Publ. Co. (Dordrecht, Holland), 1971, pp. 149-159.

77. Donovan, R. J.; Kirsch, L. J.; and Husain, D.: Rate of the Reaction of $S(3P^4\ ^1D_2)$ with OCS. Nature (London), vol. 222, no. 5199, June 1969, pp. 1164-1165.

78. Atkinson, R.; Perry, R. A.; and Pitts, J. N., Jr.: Rate Constants for the Reaction of OH Radicals with COS, CS_2, and CH_3SCH_3 Over the Temperature Range 299-430 K. Chem. Phys. Lett., vol. 54, no. 1, Feb. 1978, pp. 14-18.

79. Calvert, J. G.; and McQuigg, R. D.: The Computer Simulation of the Rates and Mechanisms of Photochemical Smog Formation. Proceedings of the Symposium on Chemical Kinetics Data for the Upper and Lower Atmosphere, vol. 1, 1975, pp. 113-154.

80. Farlow, N. H.; Snetsinger, K. G.; Lem, H. Y.; Hayes, D. M.; and Trooper, B. M.: Nitrosyl Sulfuric Acids in Stratospheric Aerosols. Trans. Am. Geophys. Union (EOS), vol. 58, 1977, p. 1148.

81. Crutzen, Paul J.: Photochemical Reactions Initiated by and Influencing Ozone in Unpolluted Tropospheric Air. Tellus, vol. 26, no. 1-2, 1974, pp. 47-57.

82. Davis, D. D.; Smith, G.; and Klauber, G.: Trace Gas Analysis of Power Plant Plumes via Aircraft Measurements: O_3, NO_x, and SO_2 Chemistry. Science, vol. 186, no. 4165, Nov. 1974, pp. 733-736.

83. Graedel, T. E.: Sulfur Dioxide, Sulfate Aerosol and Urban Ozone. Geophys. Res. Lett., vol. 3, no. 3, Mar. 1976, pp. 181-184.

84. Kuhn, P. M.; Mastenbrook. H. J.; Sissenwine, N.; and Weickmann, W.: Water Vapor. The Natural Stratosphere of 1974 (CIAP monograph 1), E. R. Reiter, E. Bauer, and S. C. Coroniti, eds., U.S. Department of Transportation, Washington, D.C., 1975, pp. 346-374.

85. Eggleton, A. E. J.; and Penkett, S. A.: Oxidation of Sulfur Dioxide in Cloud and Fog Droplets by Atmospheric Ozone and Hydrogen Peroxide. Paper presented at IAGA/KAMAP Joint Assembly, Seattle, Wash., Aug. 22-Sept. 3, 1977.

86. Turco. R. P.: Photodissociation Rates in the Atmosphere Below 100 km. Geophys. Surveys, vol. 2, no. 2, Apr. 1975, pp. 153-192.

87. Turco, R. P.; and Whitten, R. C.: A Comparison of Several Computational Techniques for Solving Some Common Aeronomic Problems. J. Geophys. Res., vol. 79, no. 22, Aug. 1974, pp. 3179-3185.

88. Turco, R. P.; and Whitten, R. C.: Chlorofluoromethanes in the Stratosphere and Some Possible Consequences for Ozone. Atmos. Env., vol. 9, no. 12, Dec. 1975, pp. 1045-1061.

89. Turco, R. P.; and Whitten, R. C.: The NASA-Ames Research Center One- and Two-Dimensional Stratospheric Models, Part I. The One-Dimensional Model. NASA TP 1002, 1977.

90. Turco, R. P.; and Whitten, R. C.: A Note on the Diurnal Averaging of Aeronomical Models. J. Atmos. Terr. Phys., vol. 40, no. 1, Jan. 1978, pp. 13-20.

91. Johnston, Harold S.; Kattenborn, David; and Whitten, Gary: Use of Excess Carbon 14 Data to Calibrate Models of Stratospheric Ozone Depletion by Supersonic Transports. J. Geophys. Res., vol. 81, no. 3, Jan. 1976, pp. 368-380.

92. Wofsy, Steven C.; and McElroy, Michael B.: On Vertical Mixing in the Upper Stratosphere and Lower Mesosphere. J. Geophys. Res., vol. 78, no. 15, May 1973, pp. 2619-2624.

93. Davis, D. D.; Heaps, W.; and McGee, T.: Direct Measurements of Natural Tropospheric Levels of OH via an Aircraft-Borne Tunable Dye Laser. Geophys. Res. Lett., vol. 3, no. 6, June 1976, pp. 331-333.

94. Krueger, Arlin J.; and Minzner, Raymond A.: A Midlatitude Ozone Model for the 1976 U.S. Standard Atmosphere. J. Geophys. Res., vol. 81, no. 24, Aug. 1976, pp. 4477-4481.

95. Sissenwine, N.; Grantham, D. D.; and Salmela, H. A.: Humidity up to the Mesopause. Air Force Surveys in Geophysics 206, Air Force Cambridge Research Laboratories Report 68-0550, Bedford, Mass., 1968.

96. U.S. Standard Atmosphere Supplements. U.S. Government Printing Office, Washington, D.C., 1966.

97. Brownlee, D. E.; Blanchard, M. B.; Cunningham, G. C.; Beauchamp, R. H.; and Fruland, R.: Criteria for Identification of Ablation Debris from Primitive Meteoric Bodies. J. Geophys. Res., vol. 80, no. 35, Dec. 1975, pp. 4917-4924.

98. Hamill, Patrick; Kiang, C. S.; and Cadle, R. D.: The Nucleation of H_2SO_4-H_2O Solution Aerosol Particles in the Stratosphere. J. Atmos. Sci., vol. 34, no. 1, Jan. 1977, pp. 150-162.

99. Farlow, Neil H.; Hayes, Dennis M.; and Lem, Homer Y.: Stratospheric Aerosols: Undissolved Granules and Physical State. J. Geophys. Res., vol. 82, no. 31, Oct. 1977, pp. 4921-4929.

100. Rosen, J. M.: The Boiling Point of Stratospheric Aerosols. J. Appl. Meteor., vol. 10, no. 5, Oct. 1971, pp. 1044-1046.

101. Cadle, R. D.; and Kiang, C. S.: Stratospheric Aitken Particles. Rev. Geophys. Space Phys., vol. 15, no. 2, May 1977, pp. 195-202.

102. Toon, Owen B.; and Pollack, James B.: A Global Average Model of Atmospheric Aerosols for Radiative Transfer Calculations. J. Appl. Meteor., vol. 15, no. 3, Mar. 1976, pp. 225-246.

103. Hamill, Patrick; Toon, O. B.; and Kiang, C. S.: Microphysical Processes Affecting Stratospheric Aerosol Particles. J. Atmos. Sci., vol. 34, no. 7, July 1977, pp. 1104-1119.

104. Hoppel, W. A.: Growth of Condensation Nuclei by Heteromolecular Condensation. J. Rech. Atm., vol. 9, no. 4, Oct.-Dec. 1976, pp. 167-180.

105. Toon, Owen B.; and Pollack, James B.: Physical Properties of the Stratospheric Aerosols. J. Geophys. Res., vol. 78, no. 30, Oct. 1973, pp. 7051-7056.

106. Fuchs, N. A.; and Sutugin, A. G.: Highly Dispersed Aerosols. Topics in Current Aerosol Research. Vol. 2, G. M. Hidy and J. R. Brock, eds., Pergamon Press (Oxford), 1971, pp. 1-60.

107. Shugard, W. J.; and Reiss, H.: Transient Nucleation in H_2O-H_2SO_4 Mixtures: A Stochastic Approach. J. Chem. Phys., vol. 65, no. 7, Oct. 1976, pp. 2827-2840.

108. Gmitro, John I.; and Vermeulen, Theodore: Vapor-Liquid Equilibria for Aqueous Sulfuric Acid. AIChE J., vol. 10, no. 5, Sept. 1964, pp. 740-746.

109. International Critical Tables of Numerical Data: Physics, Chemistry and Technology. E. W. Washburn, ed., McGraw-Hill, 1928.

110. Okuyama, Masataka; and Zung, Joseph T.: Evaporation-Condensation Coefficient for Small Droplets. J. Chem. Phys., vol. 46, no. 5, Mar. 1967, pp. 1580-1585.

111. Fuchs, N. A.: (R. E. Daisley and M. Fuchs, Transl.) The Mechanics of Aerosols. Pergamon Press (New York), 1964.

112. Smithsonian Meteorological Tables. Smithsonian Institution Publication 4014, Washington, D.C., 1951.

113. Kasten, Fritz: Falling Speed of Aerosol Particles. J. Appl. Meteor., vol. 7, no. 5, Oct. 1968, pp. 944-947, 6th rev. ed. prepared by Robert J. List, 1951.

114. Binder, K.; and Stauffer, D.: Statistical Theory of Nucleation, Condenstaion, and Coagulation. Adv. Phys., vol. 25, no. 4, 1976, pp. 343-396.

115. Young, Kenneth C.: A Numerical Simulation of Wintertime Orographic Precipitation. Part I. Description of Model Microphysics and Numerical Techniques. J. Atmos. Sci., vol. 31, no. 7, Oct. 1974, pp. 1735-1748.

116. Hidy, G. M.; and Brock, J. R.: The Dynamics of Aerocolloidal Systems. Pergamon Press, New York, 1970, Chapter 10.

117. Podzimek, J.; Haberl, J. B.; and Sedlacek, W. A.: Recent Measurements of Aitken Nuclei in the Lower Stratosphere. In Proceedings of the Fourth Conference on the Climatic Impact Assessment Program, eds. T. M. Hard and A. J. Broderick, U.S. Dept. of Transportation DOT-TSC-OST-75-38, 1975.

118. Cadle, R. D.; and Langer, Gerhard: Stratospheric Aitken Particles near the Tropopause. Geophys. Res. Lett., vol. 2, no. 8, Aug. 1975, pp. 329-332.

119. Pinnick, R. G.; Rosen, J. M.; and Hofmann, D. J.: Stratospheric Aerosol Measurements. III. Optical Model Calculations. J. Atmos. Sci., vol. 33, no. 2, Feb. 1976, pp. 304-314.

120. Borucki, W. J.; Whitten, R. C.; Watson, V. R.; Woodward, H. T.; Riegel, C. A.; Capone, L. A.; and Becker, T.: Model Predictions of Latitude-Dependent Ozone Depletion due to Supersonic Transport Operations. AIAA J. vol. 14, no. 12, Dec. 1976, pp. 1738-1745.

121. Whitten, R. C. ; Borucki, W. J.; Watson, V. R.; Shimazaki, T.; Woodward, H. T.; Riegel, C. A.; Capone, L. A.; and Becker, T.: The NASA Ames Research Center One- and Two-Dimensional Stratospheric Models. Part II. The Two-Dimensional Model. NASA TP-1003, Sept. 1977.

122. Ames, William F.: Numerical Methods for Partial Differential Equations. Barnes and Noble, New York, 1969, p. 52.

TABLE 1.- REACTIONS OF SULFUR COMPOUNDS

	Reaction	Rate coefficients[a]	Reference
R1	$S + O_2 \rightarrow SO + O$	2.2×10^{-12}	62
R2	$SO + O_2 \rightarrow SO_2 + O$	$3.0\times10^{-13}\ e^{-2800/T}$	63
R3	$SO + O_3 \rightarrow SO_2 + O_2$	$2.5\times10^{-12}\ e^{-1050/T}$	63
R4	$SO + NO_2 \rightarrow SO_2 + NO$	1.5×10^{-11}	63
R5	$SO_2 + O + M \rightarrow SO_3 + M$	$3.4\times10^{-32}\ e^{-1130/T}$ (M = N_2)	64[b]
R6	$SO_2 + HO_2 \rightarrow SO_3 + OH$	$1.0\times10^{-13}\ e^{-1410/T}$	65[c]
R7	$SO_2 + OH + M \rightarrow HSO_3 + M$	$8.2\times10^{-13}/(7.0\times10^{17} + [M])$ (M = N_2, 220 K)	66[d]
R8	$HSO_3 + OH \rightarrow SO_3 + H_2O$	1×10^{-11}	*e*
R9	$SO_3 + H_2O \rightarrow H_2SO_4$	9.1×10^{-13}	15
R10	$OCS + O \rightarrow SO + CO$	$3.0\times10^{-11}\ e^{-2270/T}$	67[f]
R11	$SO_2 \rightarrow$ washout	$3.8\times10^{-6}\ \frac{(13 - z)}{13}$ $z \leq 13$ km 0 $z > 13$ km	*g*
R12	$HSO_3 \rightarrow$ washout	$R_{12} = R_{13}$	*h*
R13	$H_2SO_4 \rightarrow$ washout	$2.3\times10^{-5}\ \frac{(13 - z)}{13}$ $z \leq 13$ km 0 $z > 13$ km	*i*
J_1	$SO_2 + h\nu \rightarrow SO + O$	1.9(-13)[j], 3.1(-10), 2.3(-8), 4.1(-7), 2.7(-6), 8.5(-6), 1.8(-5), 2.6(-5), 3.3(-5)	68 69
J_2	$OCS + h\nu \rightarrow S + CO$	1.5(-14)[j], 1.9(-11), 1.4(-9), 3.0(-8), 2.8(-7), 1.4(-6), 5.0(-6), 1.1(-5), 1.7(-5)	70 71
J_3	$H_2SO_4 + h\nu \rightarrow SO_2 +$ products	8.5(-16)[j], 1.6(-12), 1.3(-10), 2.4(-9), 1.5(-8), 4.4(-8), 8.6(-8), 1.3(-7), 1.6(-7)	*k*

[a-k] See footnotes on following page.

FOOTNOTES FOR TABLE 1

[a]Rate coefficient units are sec^{-1} for unimolecular, cm^3 sec^{-1} for bimolecular, and cm^6 sec^{-1} for termolecular processes.

[b]Atkinson and Pitts (ref. 72) have obtained a similar rate constant, 9.2×10^{-32} $e^{-(1000 \pm 200)/T}$ cm^6 sec^{-1}, for M = N_2O, and Westenberg and deHaas (ref. 73), a value of 1.1×10^{-31} $e^{-(1400 \pm 50)/T}$ cm^6 sec^{-1} for M = He.

[c]The rate constant measured at room temperature is 9×10^{-16} cm^3 sec^{-1}; we have assumed a prefactor of 1×10^{-13} cm^3 sec^{-1} and the corresponding activation energy. Reaction R6 is much less important than reaction R7 in the aerosol layer.

[d]The rate constant value is based on a review of the available measurements, principally those by Castleman et al. (ref. 15). The observed pressure dependence has been simulated by a two-state reaction mechanism.

[e]An estimated value; complemented by R9, reaction R8 is proposed to replace a complex, but as yet undetermined, photoreaction sequence starting with HSO_3 and presumably leading to sulfuric acid vapor production.

[f]Krezenski et al. (ref. 74) have obtained a similar rate coefficient of 1.6×10^{-11} $e^{-2250/T}$ cm^3 sec^{-1}.

[g]The assumed SO_2 washout rate is based on an estimated low-altitude residence time of about 3 days (refs. 41, 47, 53).

[h]Equal washout rates for HSO_3 and H_2SO_4 are assumed.

[i]The H_2SO_4 washout rate is based on an assumed 0.5 day residence time near the surface.

[j]Twenty-four hour average photodissociation rates (sec^{-1}) are given for altitudes of 10, 15, 20, 25, 30, 35, 40, 45, and 50 km, respectively. The number 1.9(-13) $\equiv$ 1.9×10^{-13}.

[k]The H_2SO_4 photoabsorption spectrum is assumed to be the same as the HCℓ spectrum, with cross section data taken from reference 75. Ultraviolet decomposition of H_2SO_4 in the upper stratosphere is assumed to lead to SO_2 production.

TABLE 2.- A SUMMARY OF THE MAJOR AERONOMIC ASSUMPTIONS MADE IN THIS STUDY

Assumption (parameters)	Parameter uncertainty[a]	Physical effects
Fixed atmospheric temperature and density profiles (air temperature and density)	These parameters vary with season and geographical location but can be changed in the model accordingly. Large perturbations such as stratospheric warmings may also occur.	Changes in temperature can affect the H_2SO_4 supersaturation ratio and hence the height of the top of the aerosol layer. For small excursions in temperature and density, the effect on chemical reaction rates is negligible.
Parameterized one-dimensional transport by diffusion (diffusion coefficient)	About a factor of 2-3	The height of the equivalent tropopause level in the model, which directly affects the predicted height of the aerosol layer, is defined largely by the diffusion profile minimum. The diffusion coefficient also affects the transport rate of SO_2 and OCS to, and the removal rate of aerosol from, the stratosphere.
Reaction of OH with SO_2 as the rate limiting step in SO_2 oxidation (overall SO_2 oxidation rate)	Unknown, but probably unimportant	If the H_2SO_4 formation time were very long (~ years, compared to weeks for the OH reaction) the distribution of the sulfur gases and the height and shape of the aerosol layer would be changed significantly.

[a]The parameter uncertainty factors quoted in this table are our estimates based on our evaluation of information currently available.

TABLE 2.- CONTINUED

Assumption (parameters)	Parameter uncertainty[a]	Physical effects
Fast reaction of SO_3 with H_2O to form H_2SO_4 (rate constant for $SO_3 + H_2O$)	The observed rate constant is fast, but for this type of reaction it could conceivably be orders of magnitude slower.	Probably small, unless the rate were very slow, $<10^{-17}$ cm^3 sec^{-1}.
An H_2SO_4 photolysis rate equal to that of HCL (H_2SO_4 photodissociation coefficient)	An order of magnitude	Little effect, except possibly at the top of the aerosol layer where H_2SO_4 evaporates from droplets.
Omission of heterogeneous chemical interactions, including the condensation of HSO_3 on particles (heterogeneous reaction rates)	For the overall rate of SO_2 oxidation, unknown. For the overall chemical rates of destruction of species like O_3, N_2O_5, and $ClONO_2$, a factor of 2 in the extreme case.	Heterogeneous chemistry could speed SO_2 oxidation, which would have little consequence for our model. Surface effects on other gaseous constituents could be significant, but the influence on the aerosol would be second order.
Fixed vertical profiles of OH, HO_2, H_2O, NO_2, and O_3 (species concentrations)	Since the species profiles are calculated with a model including aerosol interactions, only the normal uncertainties associated with these species need to be considered. The most important uncertainties are in OH (± factor of 3) and H_2O (± factor of 2). After a volcano, the species profiles could be affected by the large amounts of emitted sulfur gases.	OH affects the rate of SO_2 oxidation, but for its probable range of values the effect would be small. H_2O partly controls the H_2SO_4 supersaturation in air and it could affect the top and bottom of the aerosol layer. In a volcanic plume, OH could be severely depleted by reaction with SO_2, and the aerosol formation rate slowed significantly.

TABLE 2.- CONCLUDED

Assumption (parameters)	Parameter uncertainty[a]	Physical effects
Ground-level abundances of OCS and SO_2 (concentrations of SO_2 and OCS)	The surface OCS concentration is probably uncertain by about 10-20%. SO_2 at the ground is uncertain by at least a factor of 3, and more so at the tropopause (there is only one preliminary observation).	OCS is responsible for a large fraction of the aerosol sulfate mass above the tropopause. The SO_2 contribution to the aerosol layer by vertical transport is roughly proportional to its concentration near the tropopause.
Omission of CS_2 as a source of stratospheric sulfur (deposition rate of sulfur in the stratosphere)	Unknown, but it probably results in less than a 20% uncertainty in the total rate of sulfur input to the stratosphere.	An additional source of stratospheric sulfur would increase the amount of sulfate mass in the aerosol layer. However, CS_2 concentrations in the upper troposphere and stratosphere are undetermined.
Washout lifetimes of about 3 days for SO_2, 0.5 day for H_2SO_4, and 1 day for aerosol particles near the ground (washout rate).	At least a factor of 2-3	For H_2SO_4 and aerosol, washout is an important sink. Without it, the aerosol layer would be much denser near the tropopause. SO_2 washout also controls its abundance at the tropopause.

TABLE 3.- A SUMMARY OF THE MAJOR AEROSOL PHYSICAL ASSUMPTIONS MADE IN THIS STUDY

Assumption (parameters)	Parameter uncertainty[a]	Physical effects
Omission of homogeneous nucleation (aerosol nucleation rate)	The homogeneous nucleation rate may be uncertain by several orders of magnitude for stratospheric conditions.	Previous work has shown that homogeneous nucleation, or nucleation onto ions, is probably not significant under normal stratospheric conditions.
A fixed heterogeneous heteromolecular nucleation rate of 10^{-6} sec^{-1} (heterogeneous nucleation rate)	A factor of 10 or more	Theory suggests that heterogeneous heteromolecular nucleation is fast. Our assumed rate, ± factor of 10, would have little effect on our results.
H_2SO_4-H_2O solution vapor pressures from reference 108 (H_2SO_4 and H_2O equilibrium vapor pressures)	An order of magnitude or more at some altitudes (based on the disagreement between theory and measurements)	In the aerosol layer, H_2SO_4 vapor supersaturations are large enough that a change by a factor of 10 in the H_2SO_4 vapor pressure has little consequence. The H_2SO_4 vapor pressure does affect the predicted height extent of the aerosol layer, and the importance of homogeneous nucleation.
Use of vapor pressure for pure H_2SO_4-H_2O solutions (H_2SO_4 and H_2O equilibrium vapor pressures)	A factor of 10 or more decrease in the H_2SO_4 vapor pressure might occur when certain materials are dissolved in solution	See discussion immediately above

[a]The parameter uncertainty factors quoted in this table are estimates based on our evaluation of information currently available.

TABLE 3.- CONTINUED

Assumption (parameters)	Parameter uncertainty[a]	Physical effects
Liquid, not frozen, stratospheric particles (aerosol phase)	Stratospheric aerosols are most probably solution or slurry droplets	Vapor condensation onto crystal surfaces would lead to modified particle growth rates. The related vapor pressures over the solid particles would, likewise, be different.
The condensation rate of H_2SO_4 vapor on droplets given by reference 106 (aerosol growth rate, H_2SO_4 sticking coefficient)	At low altitudes, the growth rate is probably uncertain by less than 50%. However, the H_2SO_4 sticking coefficient is unknown, and it may lie anywhere between 0.03 and 1.0, which makes high-altitude growth rates significantly more uncertain.	If the H_2SO_4 condensation rate is altered, the H_2SO_4 vapor concentration adjusts itself to maintain about the same net particle growth rate. Particle evaporation at high altitudes is affected in the same way.
Droplet cores are inactive and do not grow by absorption and reaction of trace gases (droplet core volume, solution reaction rates)	Unknown	Core growth can affect aerosol size distributions; its treatment requires detailed information about reactants and reactions which is not yet available.
Aerosol droplets are in local thermal equilibrium at the ambient air temperature (particle temperature)	Probably negligible	For stratospheric particles a change in thermal energy — due to the latent heat of condensation or evaporation, radiation absorption, or a change in ambient temperature — should be rapidly equilibrated by heat transfer with the surrounding air.

TABLE 3.- CONTINUED

Assumption (parameters)	Parameter uncertainty[a]	Physical effects
Coagulation kernels from reference 111 (coagulation kernels)	May be as large as a factor of 2 for some size ranges, but probably less than 20% overall — based on comparisons with experimental data. Atmospheric parameters such as temperature, density, and viscosity affect the kernel values.	Coagulation is an important sink for small particles near the tropopause level. Coagulation affects the total particle mixing ratio profile. Coagulation is an important growth mechanism in some size ranges.
Sedimentation velocities based on the Stokes-Cunningham formula (sedimentation velocity)	About 20% or less; the determining equation has been studied extensively and is not very sensitive to variability. Additional uncertainties are introduced with air density and viscosity data.	Sedimentation controls, to a large extent, the particle residence times in the stratosphere, especially at higher altitudes.
An inverse fourth power (r^{-4}) Aitken nuclei size distribution at the ground (Aitken nuclei concentration)	Probably an order of magnitude, particularly in the small and large size ranges. The r^{-4} distribution is one of many which can be fit to observational data.	Small Aitken nuclei are a major source of new aerosol particles in the stratosphere. Large Aitken nuclei contribute to the large particle concentration in the lower stratosphere.
One-dimensional particle transport by diffusion and sedimentation (net transport flux)	About a factor of 2. In addition, horizontal transport and inhomogeneities, as well as large scale stratospheric-tropospheric exchange, are not simulated by a one-dimensional model.	In a model, vertical particle diffusion is most important in the lower stratosphere, where the diffusive fluxes are most uncertain. Sedimentation and diffusion oppose each other at higher altitudes and establish the particle mixing ratios above the aerosol layer.

TABLE 3.- CONCLUDED

Assumption (parameters)	Parameter uncertainty[a]	Physical effects
An aerosol washout rate of about 1 day^{-1} near the ground and about 1 $week^{-1}$ near the tropopause (washout rate)	Factor of 2-3	Washout is an important sink for stratospheric particles reaching the troposphere. However, a factor of 2 change in washout rate has little effect on the sulfate layer except near the tropopause.
Omission of particle electric charge effects on aerosol growth and coagulation processes (growth and coagulation rates, particle charge)	This omission probably leads to very small uncertainties in the physical growth rates. Stratospheric particle charges are not well determined.	For growth, the condensation rate of polar molecules and their corresponding vapor pressures could be slightly altered. For coagulation, coulombic forces would probably not affect particle trajectories except for very small particles.

TABLE 4.- A SUMMARY OF THE MAJOR NUMERICAL APPROXIMATIONS MADE IN THIS STUDY

Approximation	Numerical uncertainty	Computational effects
Doubling of particle volume between model size bins	Some numerical dispersion may be introduced into particle coagulation and growth rates	Volume doubling gives a crude particle size resolution. Coagulating and growing particles must often be subdivided into two adjacent size bins.
A semi-implicit integration scheme	The major uncertainty arises in droplet growth and sedimentation processes. In these cases individual particles may eventually be dispersed over several grid points. For a smooth, continuous distribution of particles, however, the net spreading should not introduce a significant error.	The semi-implicit scheme leads to greater solution stability, but enhances numerical diffusion between grid points.
Boundary conditions: no mass flow through the model boundaries except at the ground where Aitken nuclei enter and aerosol droplets leave, and where sulfur gases originate	With the numerical boundaries at 0 and 58 km altitude and at about 0.009 and 2.9 μm radial size, most of the stratospheric aerosol is sufficiently isolated from the boundaries to prevent large uncertainties from propagating into the results. Other types of boundary condition uncertainties (e.g., Aitken nuclei concentrations and gas abundances) are discussed in tables 2 and 3.	Boundary conditions help to establish the net rates of mass flow for the model. They also partially determine the distributions of condensation nuclei and gaseous sulfur constituents in the upper troposphere and lower stratosphere.

TABLE 4.- CONCLUDED

Approximation	Numerical uncertainty	Computational effects
Treatment of particle growth and coagulation using discrete particle sizes	No more than 10 to 20% in growth and coagulation rates	Some numerical dispersion is introduced into the growth and coagulation rates. Otherwise there appears to be little effect on the model predictions.
A scheme to suppress numerical diffusion in the aerosol sedimentation and growth rates	Less than 10 to 20% in predicted particle height and size distributions based on modeling experiments	Artificial numerical diffusion affects the settling and growth rates of particles, especially the larger particles.
The technique used to solve stiff, coupled, nonlinear gaseous species continuity equations.	For steady-state calculations, less than 5%; for time-dependent calculations, less than 10%.	See published discussions of our chemistry model for more details.

TABLE 5.- PHYSICAL PROPERTIES OF A 0.3-μm RADIUS AQUEOUS SULFURIC ACID SOLUTION DROPLET IN THE ATMOSPHERE

Altitude, km	Air temperature, K	Water vapor concentration, molecules cm^{-3}	H_2SO_4-H_2O solution density, g cm^{-3}	H_2SO_4 equilibrium vapor concentration, molecules cm^{-3}	H_2SO_4 weight fraction in solution, percent
0	288	1.6 (17)	1.39	2.48 (5)	48
2	275	5.8 (16)	1.41	4.78 (4)	50
4	262	2.0 (16)	1.42	4.96 (3)	51
6	249	6.8 (15)	1.42	2.32 (2)	51
8	236	1.9 (15)	1.42	1.04 (1)	51
10	223	5.2 (14)	1.40	1.46 (-1)	49
12	219	1.0 (14)	1.52	7.98 (0)	61
14	216	1.7 (13)	1.62	1.93 (2)	69
16	216	1.3 (13)	1.63	3.78 (2)	70
18	216	1.0 (13)	1.65	6.79 (2)	72
20	217	7.8 (12)	1.67	1.98 (3)	73
22	219	5.9 (12)	1.69	9.54 (3)	75
24	221	4.4 (12)	1.71	4.17 (4)	77
26	223	3.3 (12)	1.73	1.63 (5)	79
28	225	2.5 (12)	1.75	5.79 (5)	80
30	227	1.9 (12)	1.76	1.83 (6)	81
32	230	1.4 (12)	1.78	8.22 (6)	83
34	234	1.1 (12)	1.79	4.37 (7)	84
36	239	8.3 (11)	1.81	2.81 (8)	86
38	245	6.3 (11)	1.83	1.88 (9)	89
40	250	4.8 (11)	1.84	7.64 (9)	91

TABLE 6.- CONDENSATION (GROWTH) KERNELS, g_{oa}, FOR H_2SO_4-H_2O SOLUTION DROPLETS IN AIR

Altitude, km \ Particle radii, μm	Condensation kernels (in units of 10^{-15} μm cm^3 $molecule^{-1}$ sec^{-1})[a]								
	0.01	0.02	0.04	0.08	0.16	0.32	0.64	1.28	2.56
0	15.0	14.5	13.6	11.9	9.09	5.99	3.49	1.88	0.976
2	13.8	13.5	12.8	11.5	9.15	6.29	3.77	2.07	1.08
4	13.2	13.0	12.5	11.4	9.45	6.79	4.22	2.36	1.25
6	13.1	12.9	12.5	11.7	10.0	7.55	4.90	2.82	1.51
8	12.7	12.6	12.3	11.6	10.3	8.17	5.56	3.31	1.81
10	13.0	12.9	12.7	12.2	11.1	9.17	6.58	4.08	2.28
12	9.59	9.53	9.41	9.13	8.55	7.40	5.64	3.70	2.14
14	7.90	7.87	7.79	7.63	7.29	6.58	5.31	3.75	2.29
16	7.68	7.66	7.61	7.50	7.26	6.76	5.80	4.36	2.82
18	7.50	7.48	7.45	7.37	7.21	6.86	6.15	4.93	3.41
20	7.28	7.27	7.24	7.19	7.08	6.84	6.33	5.38	3.98
22	7.02	7.01	6.99	6.96	6.88	6.72	6.37	5.67	4.50
24	6.80	6.79	6.78	6.75	6.70	6.59	6.35	5.85	4.93
26	6.61	6.61	6.60	6.58	6.54	6.47	6.31	5.96	5.26
28	6.45	6.45	6.64	6.43	6.41	6.35	6.24	6.00	5.49
30	6.33	6.33	6.33	6.32	6.30	6.26	6.18	6.02	5.65
32	6.20	6.20	6.19	6.19	6.17	6.15	6.09	5.98	5.72
34	6.08	6.08	6.08	6.07	6.06	6.04	6.01	5.92	5.75
36	5.95	5.95	5.95	5.94	5.94	5.92	5.90	5.84	5.72
38	5.80	5.80	5.80	5.80	5.79	5.78	5.76	5.72	5.64
40	5.67	5.67	5.67	5.67	5.67	5.66	5.65	5.62	5.56

[a]Values are given for every third particle size category in the model.

TABLE 7.- COAGULATION KERNELS FOR A SULFURIC ACID AEROSOL AT 16 km ALTITUDE
(The air temperature is 216 K and the air number density is 3.5×10^{18} molecules cm^{-3})

Droplet radii, μm	Coagulation kernel, cm^3 $particle^{-1}$ sec^{-1} [a]								
	0.01	0.02	0.04	0.08	0.16	0.32	0.64	1.28	2.56
0.01	1.87 (-9)[b]	3.14 (-9)	8.14 (-9)	2.50 (-8)	7.88 (-8)	2.29 (-7)	5.82 (-7)	1.32 (-6)	2.80 (-6)
0.02	[c]	2.60 (-9)	4.24 (-9)	1.02 (-8)	2.72 (-8)	6.92 (-8)	1.60 (-7)	3.47 (-7)	7.20 (-7)
0.04			3.33 (-9)	4.84 (-9)	9.71 (-9)	2.08 (-8)	4.41 (-8)	9.13 (-8)	1.86 (-7)
0.08				3.33 (-9)	4.03 (-9)	6.73 (-9)	1.27 (-8)	2.48 (-8)	4.92 (-8)
0.16					2.50 (-9)	2.69 (-9)	4.08 (-9)	7.24 (-9)	1.37 (-8)
0.32						1.64 (-9)	1.70 (-9)	2.48 (-9)	4.27 (-9)
0.64							1.10 (-9)	1.15 (-9)	1.64 (-9)
1.28								8.18 (-10)	8.77 (-10)
2.56									6.86 (-10)

[a] Values are given for every <u>third</u> particle size category in the model.
[b] 1.87 (-9) = 1.87×10^{-9}.
[c] The kernels are symmetric; i.e., $K(r_1,r_2) = K(r_2,r_1)$.

TABLE 8.- TERMINAL SEDIMENTATION VELOCITIES FOR ATMOSPHERIC AEROSOL PARTICLES

Altitude, km \ Particle radii, μm	Sedimentation velocity, cm sec^{-1} [a]								
	0.01	0.02	0.04	0.08	0.16	0.32	0.64	1.28	2.56
0	2.39 (-5) [b]	4.41 (-5)	9.57 (-5)	2.35 (-4)	6.68 (-4)	2.13 (-3)	7.83 (-3)	2.95 (-2)	1.30 (-1)
2	2.99 (-5)	5.52 (-5)	1.18 (-4)	2.80 (-4)	7.63 (-4)	2.41 (-3)	8.45 (-3)	3.15 (-2)	1.38 (-1)
4	3.77 (-5)	6.95 (-5)	1.46 (-4)	3.37 (-4)	8.79 (-4)	2.67 (-3)	9.12 (-3)	3.36 (-2)	1.47 (-1)
6	4.85 (-5)	8.87 (-5)	1.83 (-4)	4.11 (-4)	1.03 (-3)	2.97 (-3)	9.85 (-3)	3.57 (-2)	1.56 (-1)
8	6.33 (-5)	1.16 (-4)	2.36 (-4)	5.15 (-4)	1.24 (-3)	3.41 (-3)	1.08 (-2)	3.85 (-2)	1.66 (-1)
10	8.37 (-5)	1.52 (-4)	3.05 (-4)	6.51 (-4)	1.50 (-3)	3.94 (-3)	1.20 (-2)	4.15 (-2)	1.78 (-1)
12	1.12 (-4)	2.15 (-4)	4.34 (-4)	9.12 (-4)	2.04 (-3)	5.07 (-3)	1.45 (-2)	4.81 (-2)	1.87 (-1)
14	1.55 (-4)	3.08 (-4)	6.25 (-4)	1.30 (-3)	2.82 (-3)	6.65 (-3)	1.78 (-2)	5.58 (-2)	1.98 (-1)
16	2.11 (-4)	4.21 (-4)	8.51 (-4)	1.75 (-3)	3.73 (-3)	8.42 (-3)	2.12 (-2)	6.21 (-2)	2.09 (-1)
18	2.88 (-4)	5.76 (-4)	1.16 (-3)	2.37 (-3)	4.96 (-3)	1.09 (-2)	2.59 (-2)	7.07 (-2)	2.24 (-1)
20	3.92 (-4)	7.86 (-4)	1.59 (-3)	3.22 (-3)	6.66 (-3)	1.48 (-2)	3.25 (-2)	8.29 (-2)	2.45 (-1)
22	5.37 (-4)	1.08 (-3)	2.19 (-3)	4.43 (-3)	9.08 (-3)	1.91 (-2)	4.21 (-2)	1.01 (-1)	2.75 (-1)
24	7.30 (-4)	1.49 (-3)	3.00 (-3)	6.07 (-3)	1.24 (-2)	2.56 (-2)	5.51 (-2)	1.26 (-1)	3.19 (-1)
26	9.93 (-4)	2.04 (-3)	4.11 (-3)	8.30 (-3)	1.68 (-2)	3.46 (-2)	7.29 (-2)	1.61 (-1)	3.84 (-1)
28	1.35 (-3)	2.78 (-3)	5.62 (-3)	1.13 (-2)	2.29 (-2)	4.67 (-2)	9.71 (-2)	2.09 (-1)	4.78 (-1)
30	1.82 (-3)	3.78 (-3)	7.63 (-3)	1.54 (-2)	3.10 (-2)	6.30 (-2)	1.30 (-1)	2.74 (-1)	6.07 (-1)
32	2.44 (-3)	5.07 (-3)	1.03 (-2)	2.08 (-2)	4.19 (-2)	8.48 (-2)	1.73 (-1)	3.61 (-1)	7.79 (-1)
34	3.29 (-3)	6.59 (-3)	1.37 (-2)	2.82 (-2)	5.69 (-2)	1.15 (-1)	2.33 (-1)	4.80 (-1)	1.01
36	4.41 (-3)	8.83 (-3)	1.77 (-2)	3.78 (-2)	7.67 (-2)	1.55 (-1)	3.13 (-1)	6.39 (-1)	1.33
38	5.83 (-3)	1.17 (-2)	2.33 (-2)	4.95 (-2)	1.02 (-1)	2.05 (-1)	4.15 (-1)	8.43 (-1)	1.73
40	7.72 (-3)	1.54 (-2)	3.09 (-2)	6.43 (-2)	1.35 (-1)	2.73 (-1)	5.51 (-1)	1.11 (-1)	2.27

[a] Values are given for every third particle size category in the model.
[b] 2.39 (-5) = 2.39×10^{-5}.

Blank
Page

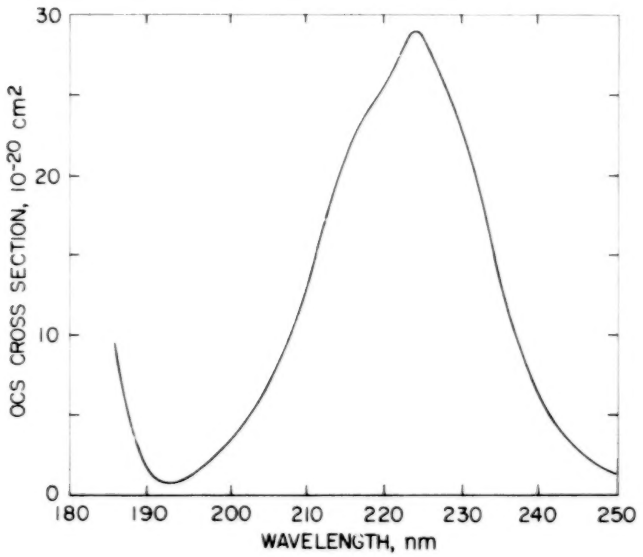

Figure 1.- Carbonyl sulfide photoabsorption cross sections. Below 226 nm the data are taken from reference 70 at 232 K, and above 226 nm from reference 71 at 300 K.

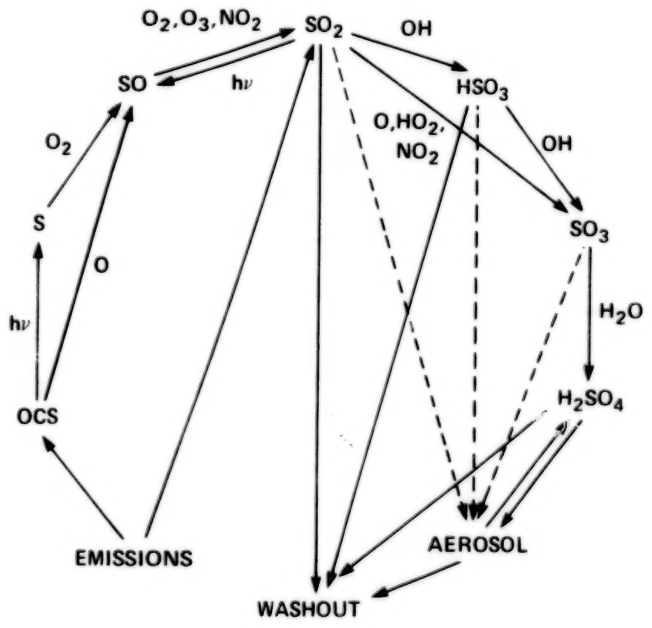

Figure 2.- Gas phase sulfur interactions that are included in our model. The dashed lines indicate possible heterogeneous reactions which are not treated.

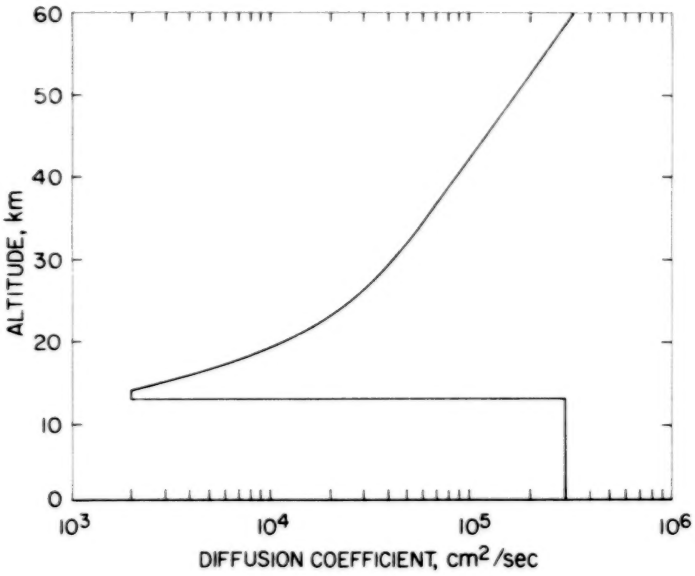

Figure 3.- Eddy diffusion coefficients in the lower atmosphere.

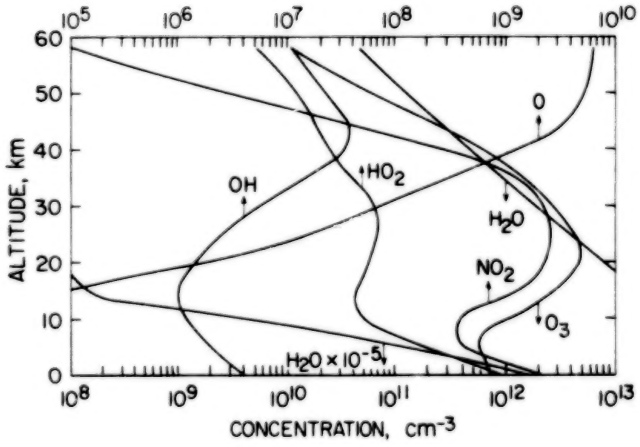

Figure 4.- Neutral species concentrations up to 58 km.

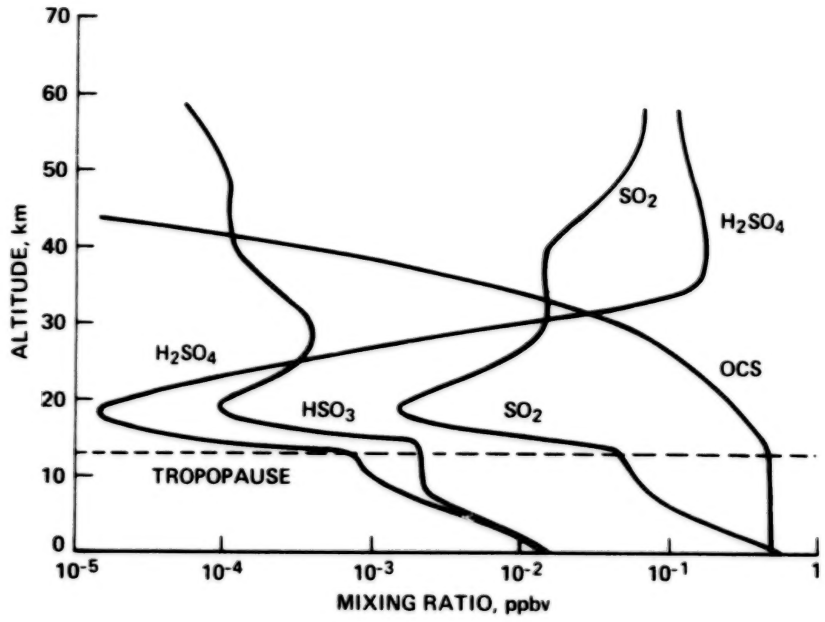

Figure 5.- Predicted sulfur compound mixing ratios in the atmosphere.

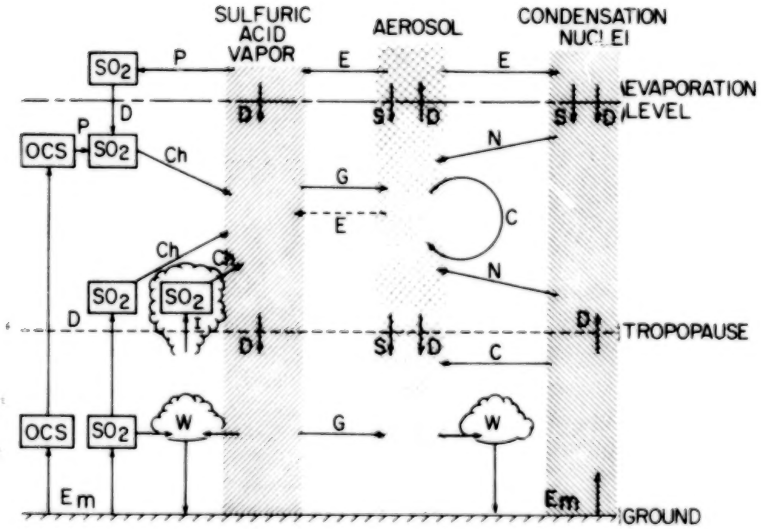

Figure 6.- A partial schematic outline of the physical and chemical interactions included in our one-dimensional model. C = coagulation, Ch = chemistry, D = diffusion, E = evaporation, Em = emission, G = condensation and growth, I = injection, N = nucleation, P = photolysis, S = sedimentation, W = washout and rainout.

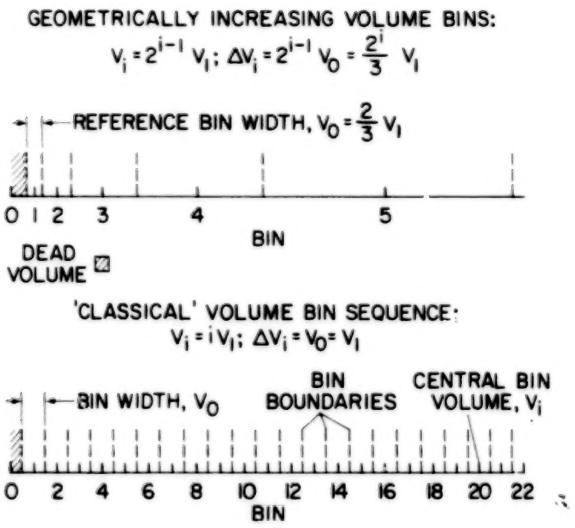

Figure 7.- Aerosol particle volume bin structures for numerical models.

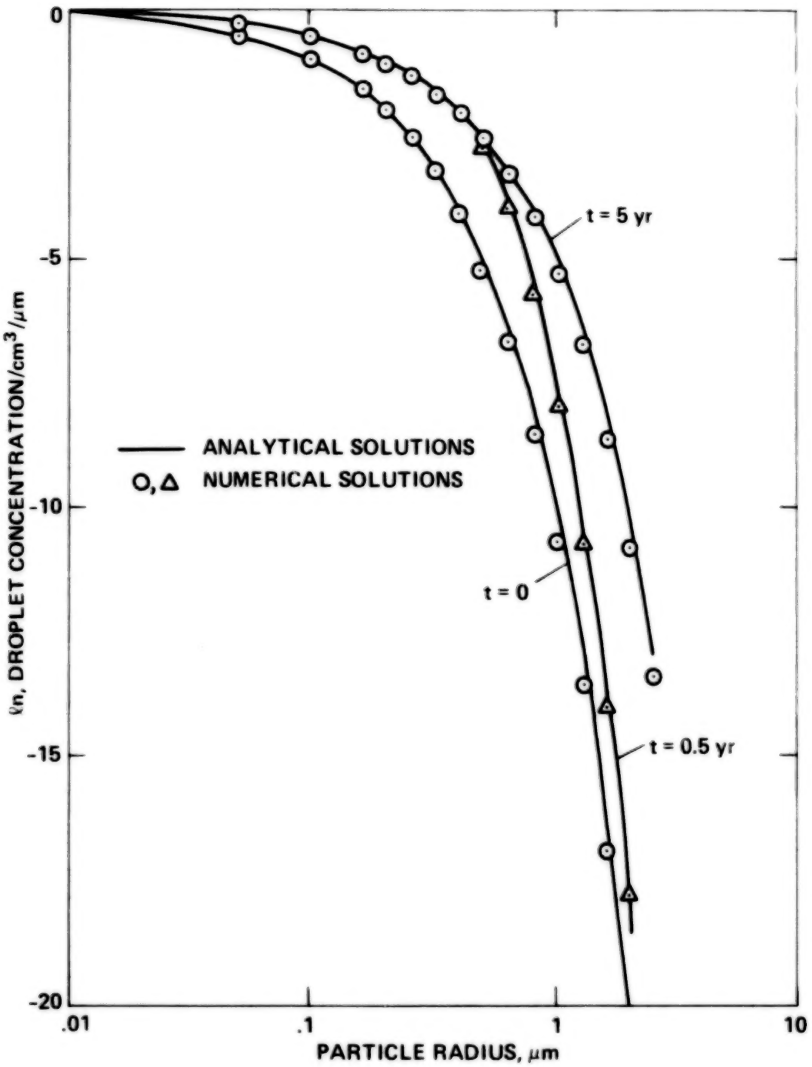

Figure 8.- Aerosol droplet growth. The evolution of a droplet size distribution following a change in the droplet growth rate is shown. Both analytical and numerical solutions are given. The conditions for the calculation are described in the text.

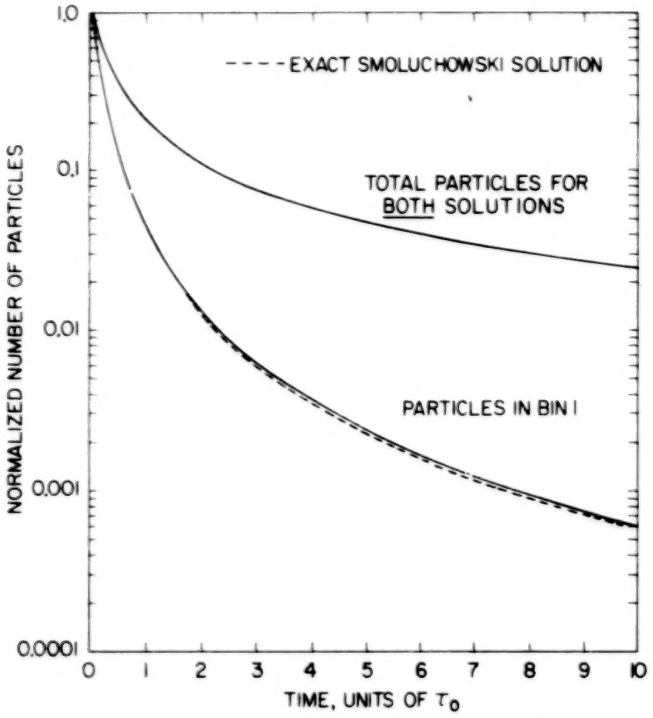

Figure 9.- Aerosol coagulation. Calculated transient decay curves are shown for the number of particles in the smallest model size bin, and for the total number of particles of all sizes, when one particle is initially placed in the smallest model bin. Time is measured relative to the characteristic coagulation time, τ_o. The exact solutions of Smoluchowski are shown for comparison.

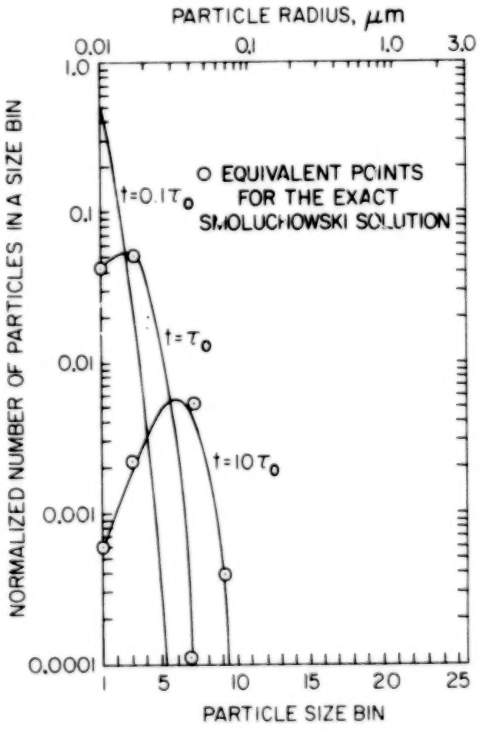

Figure 10.- The development of an aerosol size spectrum by coagulation. The conditions for the calculation are the same as for figure 9.

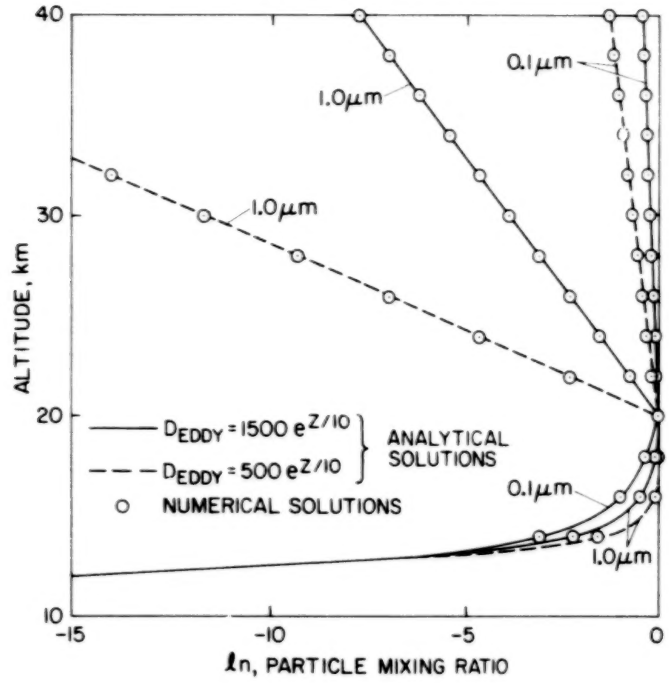

Figure 11.- Particle sedimentation and diffusion. The steady-state altitude distributions of 0.1 and 1.0 μm radius particles resulting from their continuous injection at 20 km are presented. Particle mixing ratios calculated for two different diffusion coefficients are shown. Theoretical and numerical solutions are both given for comparison. See the text for details.

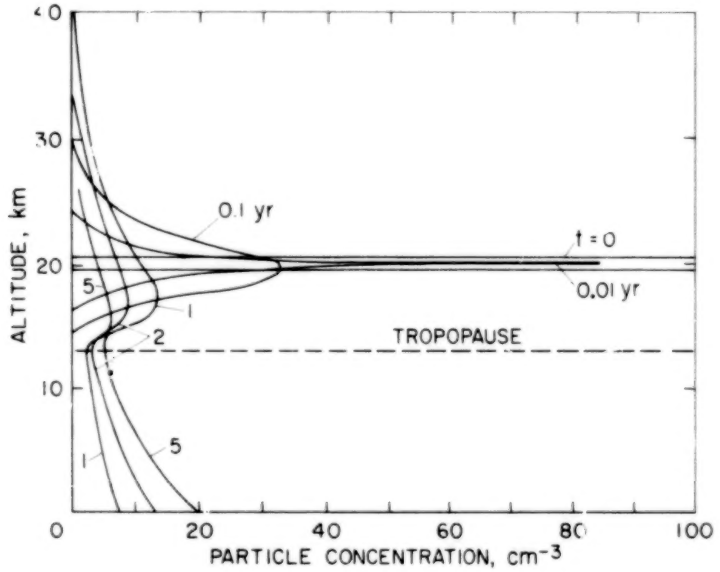

Figure 12.- Particle diffusion. The time-dependent diffusive transport of aerosol particles released at 20 km is shown. The initial particle concentration is 100 cm^{-3}. The diffusion coefficient is given in figure 3.

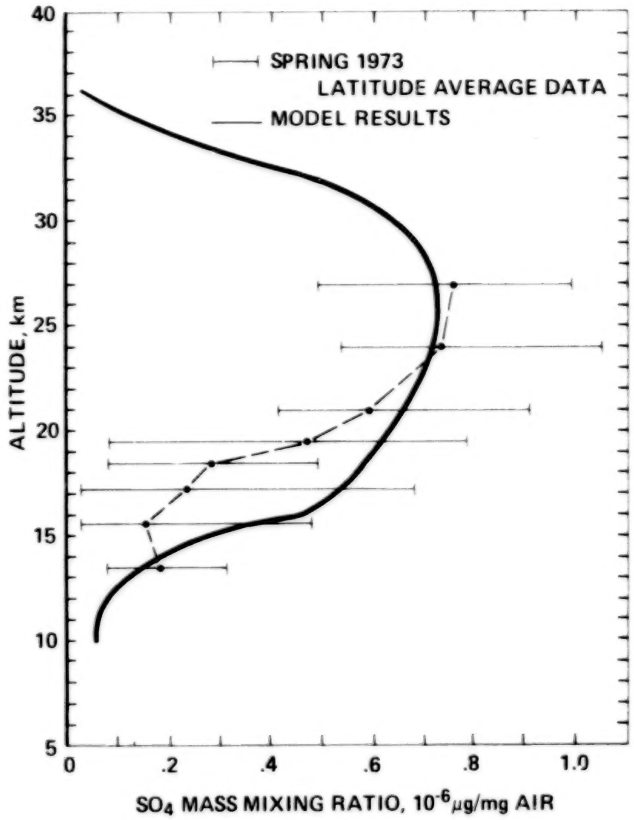

Figure 13.- Observed and calculated aerosol sulfate mixing ratios (µg $SO_4^{=}$/kg air). The observations (ref. 14) were made with filters, and have been averaged over latitude from pole to pole. The error bars give the extreme values found at individual latitudes.

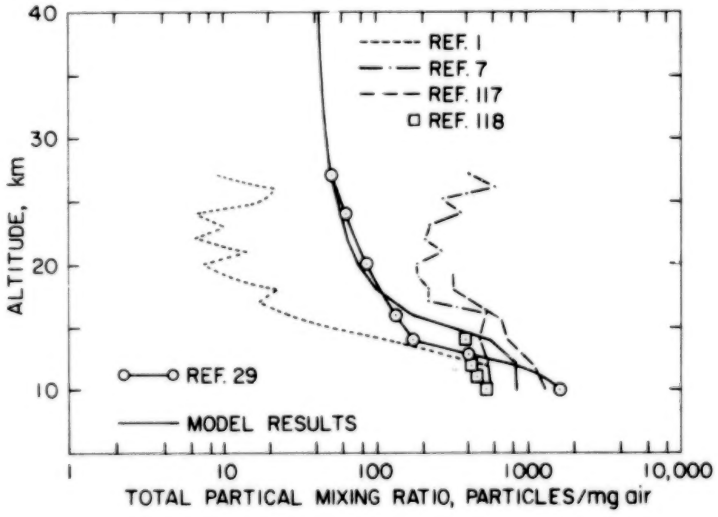

Figure 14.- Observed and calculated total particle number mixing ratios (particles/mg air). The data were obtained over a period of 15 years by various investigators using condensation chambers. The large spread in the data may be partly due to real differences in aerosol abundances and partly due to different sampling techniques.

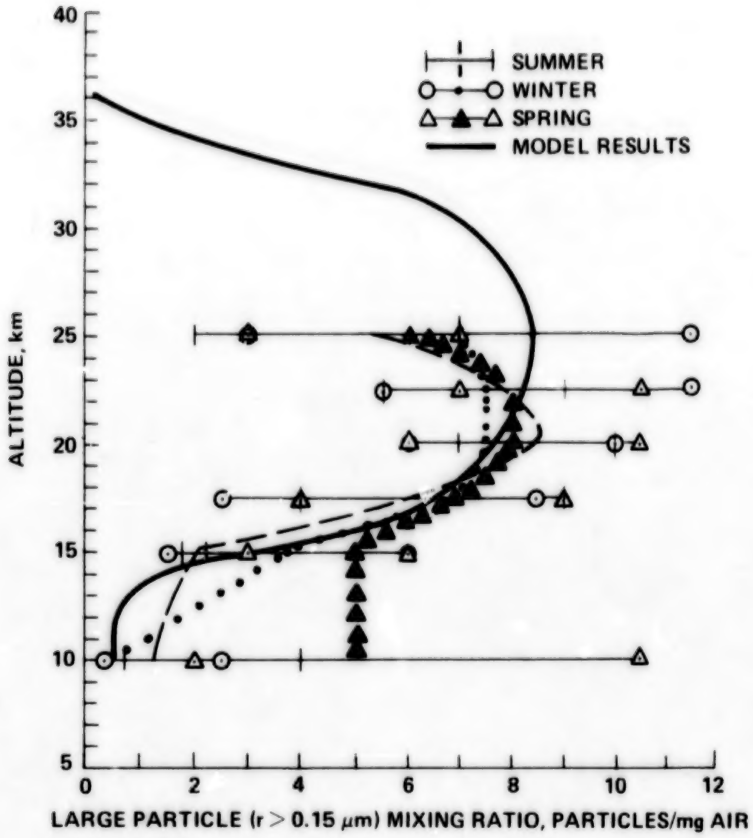

Figure 15.- Observed and calculated mixing ratios of particles with radii $\geq$0.15 μm. The observations (ref. 9) were made using a light-scattering particle counter. A large number of measurements were made over Wyoming; the mean value and a measure of the standard deviation are presented for different seasons.

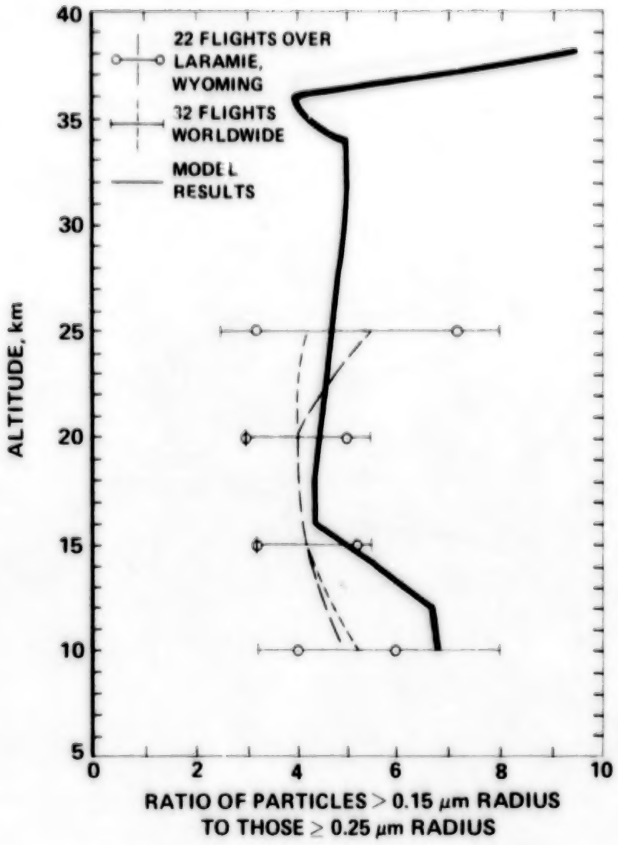

Figure 16.- Observed and measured concentration ratios of particles with radii $\geq$0.15 μm to those with radii $\geq$0.25 μm. The observations (ref. 119) were made with a light-scattering particle counter. Numerous flights were made over Wyoming and worldwide. The average value and a measure of the standard deviation are illustrated.

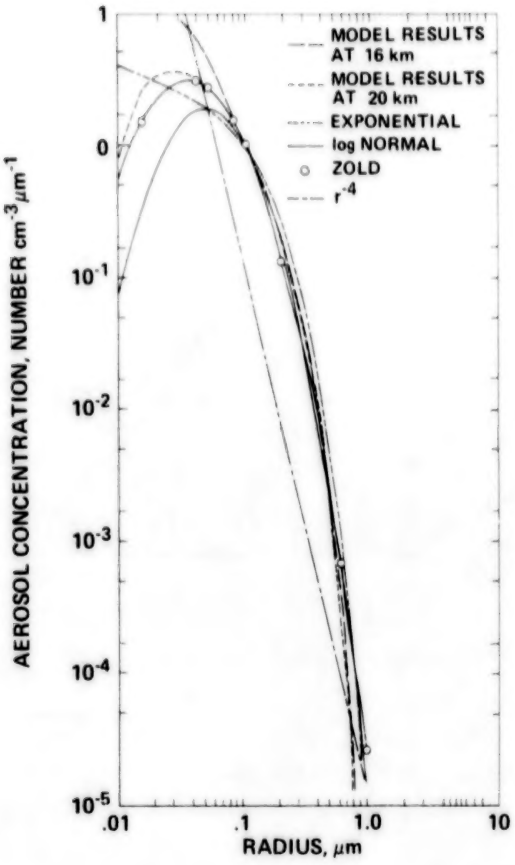

Figure 17.- Observed and calculated aerosol size distributions. The calculated distributions are for altitudes of 16 and 20 km. The observations are represented by three analytic functions that are based upon close fits to a variety of measured distributions (refs. 102 and 119). An r^{-4} size distribution, typical of tropospheric aerosol, is also shown for comparison.

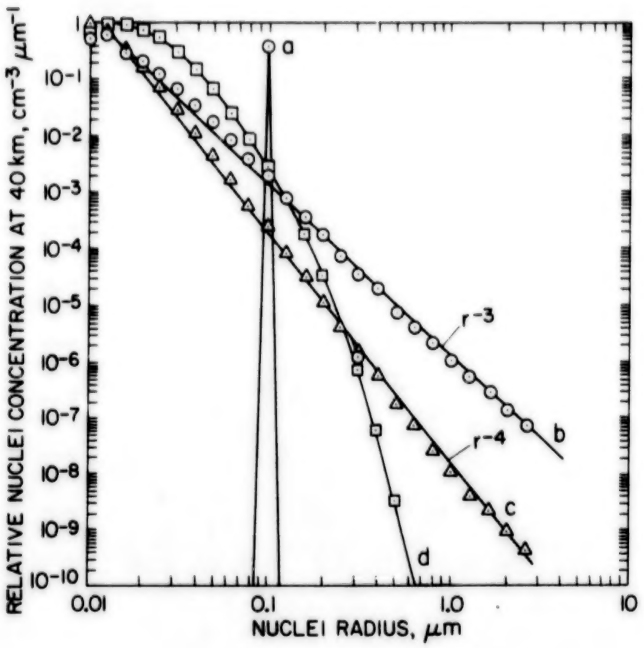

Figure 18.- Calculated condensation nuclei size spectra at 40 km altitude (above the model droplet evaporation level). The assumed condensation nuclei distributions at the ground are: (a) monodispersed 0.1 μm radius particles, (b) an r^{-3} size distribution, (c) and (d) an r^{-4} size distribution. The points within the symbols correspond to the numerical predictions; the curves have been added for clarity. Results (a) to (c) were obtained using the aerosol model without droplet coagulation or differential sedimentation. Result (d) is for the complete aerosol model.

1. Report No.	2. Government Accession No.	3. Recipient's Catalog No.
NASA TP-1362		

4. Title and Subtitle	5. Report Date
THE NASA-AMES RESEARCH CENTER STRATOSPHERIC AEROSOL MODEL. I. PHYSICAL PROCESSES AND COMPUTATIONAL ANALOGS	April 1979
	6. Performing Organization Code

7. Author(s)	8. Performing Organization Report No.
R. P. Turco,* P. Hamill,† O. B. Toon,† R. C. Whitten,† and C. S. Kiang‡	A-7532
	10. Work Unit No. 198-30-02

9. Performing Organization Name and Address	11. Contract or Grant No.
*R and D Associates, Marina del Rey, Calif. 90291 †NASA-Ames Research Center, Moffett Field, Calif. 94035 ‡National Center for Atmospheric Research, Boulder, Colo. 80303	
	13. Type of Report and Period Covered: Technical Paper

12. Sponsoring Agency Name and Address	14. Sponsoring Agency Code
National Aeronautics and Space Administration Washington, D.C. 20546	

15. Supplementary Notes

16. Abstract

A time-dependent one-dimensional model of the stratospheric sulfate aerosol layer is presented. In constructing the model, a wide range of basic physical and chemical processes are incorporated in order to avoid predetermining or biasing the model predictions. The simulation, which extends from the surface to an altitude of 58 km, includes the troposphere as a source of gases and condensation nuclei and as a sink for aerosol droplets. The size distribution of aerosol particles is resolved into 25 categories with particle radii increasing geometrically from 0.01 to 2.56 μm such that particle volume doubles between categories. In the model, sulfur gases reaching the stratosphere are oxidized by a series of photochemical reactions into sulfuric acid vapor. At certain heights this results in a supersaturated H_2SO_4-H_2O gas mixture with the consequent deposition of aqueous sulfuric acid solution on the surfaces of condensation nuclei. The newly formed solution droplets grow by heteromolecular heterogeneous condensation of acid and water vapors; the droplets also undergo Brownian coagulation, settle under the influence of gravity, and diffuse in the vertical direction. Below the tropopause, particles are washed from the air by rainfall. A set of continuity equations is derived which describes the temporal and spatial variations of aerosol droplets and condensation nuclei concentrations in air as well as the sizes of cores in droplets; numerical techniques to solve these equations accurately and efficiently are also developed. Calculations illustrate the behavior and precision of the computer algorithms. The model correctly predicts many of the observed properties of the sulfate layer, including its height, density, composition, and particle size spectra.

17. Key Words (Suggested by Author(s))	18. Distribution Statement
Stratosphere Pollution Aerosol Atmosphere modeling	Unlimited STAR Category - 47

19. Security Classif. (of this report)	20. Security Classif. (of this page)	21. No. of Pages	22. Price*
Unclassified	Unclassified	100	$5.00

*For sale by the National Technical Information Service, Springfield, Virginia 22161

NASA-Langley, 1979

END

Sept. 14, 1979